Preparation of Dexamethasone-loaded Biphasic Calcium Phosphate Nanoparticles/Collagen Porous Composite Scaffold for Bone Tissue Engineering

Ying Chen

February 2018

Preparation of Dexamethasone-loaded Biphasic Calcium Phosphate Nanoparticles/Collagen Porous Composite Scaffold for Bone Tissue Engineering

Ying Chen

Doctoral Program in Materials Science and Engineering

Submitted to the Graduate School of
Pure and Applied Sciences
in Partial Fulfillment of the Requirements
for the Degree of Doctor of Philosophy in
Engineering

at the
University of Tsukuba

Content

List of abbreviations

HA	Hydroxyapatite
CaP	Calcium phosphate
β-TCP	β-tricalcium phosphate
BCP	Biphasic calcium phosphate
NPs	Nanoparticles
Col I	Collagen type I
DEX	Dexamethasone
MSCs	Human mesenchymal stem cells
HUVECs	Human umbilical vascular endothelial cells
ECM	Extracellular matrix
FBS	Fetal bovine serum
DMEM	Dulbecco’s modified Eagle medium
BSA	Bovine serum albumin
OCN	Osteocalcin
PBS	Phosphate buffered saline
cDNA	Complementary DNA
DAB	Diaminobenzidine
HE	Hematoxylin and eosin
EDTA	Ethylene diamine tetraacetic acid
ALP	Alkaline phosphatase staining
ARS	Alizarin red S staining
IBSP	Bone sialoprotein 2
BMP-2	Bone morphogenic protein-2
Runx2	Runt-related transcription factor-2
FGF	Fibroblast growth factor
PDGF	Platelet derived growth factor
NC	Negative control
PC	Positive control
RT-PCR	Real-time polymerase chain reaction
VEGF	Vascular endothelial growth factor
KDR	Kinase insert domain receptor
GAPDH	Glyceraldehyde 3-phosphate dehydrogenase
DMEM	Dulbecco's modified eagle medium
DAPI	4',6-diamidino-2-phenylindole
CLSM	Confocal laser scanning microscopy
RT-PCR	Real-time polymerase chain reaction
ANOVA	Analysis of variance
MVD	Microvessel density
TEM	Transmission electron microscope
XRD	X-ray diffraction
DLS	Dynamic light scattering

Chapter 1

General introduction

1.1. Composition and function of bone

Bone is composed of living cells entrapped in an organic mineralized matrix. The cells in bone tissue contain osteoblasts (which are responsible for the formation and mineralization of bone), osteocytes, and osteoclasts (which are responsible for the resorption of bone). The detailed morphological characteristics and functions of these bone cells are shown in Table 1.1 . Bone matrix consists of organic components, mainly Type I collagen, and inorganic components, mainly hydroxyapatite (HA) and some other types of calcium and phosphate salts [1]. For the acellular part of bone tissue, over 30% of them are organic components, and about 70% of them are salts [3]. Collagen fibers provide bone tissue with the tensile strength, while the speckled crystals of HA provide bone with compressive strength [4].

Table 1.1 The living cells in bone and their characteristics and functions (Source: refs [5, 6]).

Cell type	Morphological characteristics	Function
Osteoblasts	Cuboidal in shape, polarized and located, with their precursors, at the bone surface, where they form a tight layer of cells	Synthesis and regulation of bone ECM deposition and mineralization Respond to mechanical stimuli
Osteocytes	Stellate shaped Possess fewer organelles than the osteoblasts	Calcification of the osteoid matrix Blood-calcium homeostasis Mechanosensor cells of the bone
Osteoclasts	Polarized cells Multinucleated cells	Bone resorption

90-95% of the organic matrix of bone is Type I collagen and the rest of the matrix is a homogenous liquid called matrix that is composed of non-collagenous proteins (e.g., osteopontin, osteocalcin and bone sialoprotein) and proteoglycans (e.g., chondroitin sulfate and hyaluronic acid and). For better understanding, Table 1.2 shows a brief introduction to the main organic components of the bone matrix [2, 7]. The collagen fibers consist of the repeating unit that impart tensile strength to bone, and are aligned in an overlapping manner that can prevent the shear stress. The bone mineral (the inorganic component of bone) is primarily composed of calcium and phosphate salts and the main component is HA (formula: $Ca_{10}(PO_4)_6(OH)_2$) [1]. The accurate composition of the matrix can vary with time and nutrition, and the ratio of calcium to phosphate varies between 1.3 and 2.0 (mass ratio). Some trace minerals such as the sodium, carbonate,

magnesium and potassium can also being found in the bone matrix [1]. The composition of human bone is summarized in Fig. 1.1.

Table 1.2. The composition of organic phase of the bone matrix (Source: refs [2, 5, 7]).

Bone extracellular matrix constituent	Functions and properties
Collagen I	Provides framework for skeletal structure; matrix calcification
Byglican Decorin	Proteoglycan; affect collagen fiber growth and diameter; involved in the process of matrix mineralization
Osteonectin	Glycoprotein; binds Ca^{2+} and collagen; nucleates hydroxylapatite
Thrombospondin	Glycoprotein; binds calcium, hydroxylapatite, osteonectin and other cell surface proteins; mediates cell adhesion in a RGD-independent fashion
Fibronectin	Osteoblast attachment to substrate
Osteopontin	Sialoprotein; constituent of cement line; involved in bone remodelling;
Bone Sialoprotein	Sialoprotein; constituent of cement line
Osteocalcin	Skeletal gla protein; late marker of osteogenic phenotype; involved in bone remodelling; it may also be involved in the control of mineralization trough its inhibition.

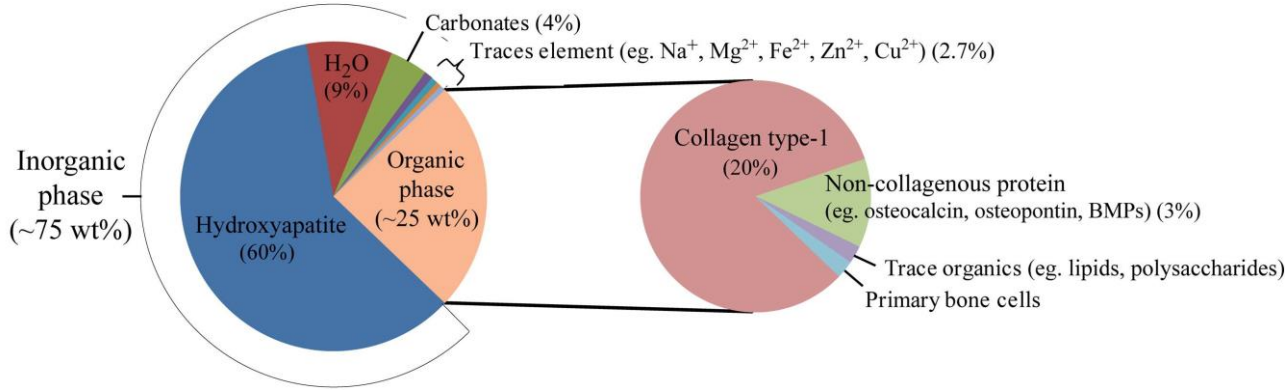

Fig. 1.1. Composition of human bone. Source: Chan et al. (2008) [1].

Bone tissue in adults has two forms of architecture [8]: trabecular bone (also known as cancellous or spongy bone) which is about 20% of the whole bone tissue, and compact bone (as known as cortical bone) which is about 80% of the whole bone tissue. Proportions of the two forms vary at different locations of the bone tissue. The compact bone is almost solid with only about 10% porosity. The compact bone can be further categorized into three different types: the short bones (ankle and wrist), the long bones (tibia and femur), and the flat bones (irregular bones and skull). The trabecular bone exhibits a higher porosity (ranging between 50–90%), with a modulus and ultimate compressive strength about 20 times lower than those of the compact bone [9]. The trabecular bone is arranged in a sponge-like morphology, with a honeycomb of various-sized branching bars, plates and rods named trabeculae. It's generally presented in metaphysis of long bones, covered by compact bone, and in the vertebral arches.

Bone tissue has a number of functions, including: a). Support: bones provide a framework for muscles and some other tissues. b). Movement: bones capacitate the body movements by serving as levers and attachment points of muscles. c). Protection: bones such as the rib cage and skull can prevent the internal organs from injuries. d). Hematopoiesis: the hematopoiesis (production of blood cells) happens in the red marrow in some bone cavities. e). Mineral storage: bones act as the reservoir for calcium and phosphate salts, and other essential minerals for diverse cellular activities. f). Energy storage: the lipids (e.g., fats) stored in the adipose cells of the yellow marrow can act as the energy reservoir.

1.2. Bone defects and bone repair

A bone defect is a lack of bone tissue where it should normally occur. Bone injury caused by congenital malformations, aging, osteoporosis, traumatic infections, tumors, traffic accidents and other reasons is one of the major diseases that threaten human health. Reconstruction of large bone defects and non-unions has long been a significant clinical challenge in orthopedics [10]. Even though bone is one of the few regenerative tissues, some defect size is beyond the body's self-healing capacity, so further intervention is required [11]. The critical size of bone defect depends on the cause and the location of the defect.

In modern medicine, there are three main ways to repair bone defects: autologous bone graft, allogeneic bone graft and artificial bone graft. Autologous and allogeneic bone grafts are still the most common solutions in clinical applications. The autologous bone grafts use bones from another parts of the patient themselves, so that there is no immune rejection therefore a good bone repair result can be obtained. The autologous bone grafts have been the gold standard for bone replacement for several decades also since it can provide osteoblasts and essential osteoinductive factors that is required for bone healing [9, 12]. They are generally extracted from the trabecular bone of the iliac crests of the patients, while the compact bones can also be used [13, 14]. Nevertheless, the autologous bone grafts would cause the secondary trauma to the patient's body and increase the risk of hemorrhage, infection and damage the structural integrity of the patient. Moreover, the limited sources of the autologous bone cannot be used for the repair of defect bone tissue in large size [15]. Allogeneic bone grafts can be divided into allografts and xenografts. Allografts use the bones taken from living or dead bodies of other people. This method has some shortages such the limited sources, the immunological rejection and the risk of disease-spreading. Xenografts use the animal bones for the transplantation, although it's easy to obtain the grafts, there are also some problems such as the immune rejection and disease transmission, therefore their applications have been greatly restricted [16, 17].

To overcome the disadvantages of the autologous and allogeneic bone grafts, more and more attention has been drawn to artificial bone grafts. The artificial bone materials are easy to get and their performances can be designed and controlled [18]. Synthetic biomaterials used in the repair of bone defects have been massively investigated over the past few decades. But until now, the applications of artificial bone grafts are still much less than the autologous and allogeneic bone grafts. The reason for the restricted application of the artificial bone grafts is that their physical, mechanical and biochemical properties cannot yet totally meet the requirements of bone repair. Therefore, enhancing the comprehension of the interaction between artificial bone materials and organisms, improving characteristics of artificial bone materials and making them better applied to repair bone defects are urgent problems in contemporary materials science. Among all the artificial bone substitutes, metals and ceramics are most widely investigated [19]. Nevertheless, they all have some limitations. For example, metals, although they can provide immediately with the mechanical support at the defect sites, they usually exhibit insufficient integration with the surrounding tissues and may fail due to the infection and the fatigue loading [20]. Ceramics, on the other hand, have quite low tensile strength and are very brittle, so they cannot be applied in locations of significant bending, torsion or shear stress [21]. It is therefore clear that an appropriate bone substitute is yet to be found which is urgently needed for full recovery of the patients. A possible solution for these problems may be in bone tissue engineering.

Bone tissue engineering is the strategy applying biotechnology in biomaterials to induce bone tissue regeneration, which is a complicated dynamic process that begins with cell migration and recruitment followed by cell proliferation, differentiation, matrix formation and finally the bone regeneration [22]. Three fundamental principles are included in bone tissue engineering, i.e., cells, bioactive molecules and scaffolds

which will gradually degrade and reabsorb as the tissue structures (Fig. 1.2) [23].

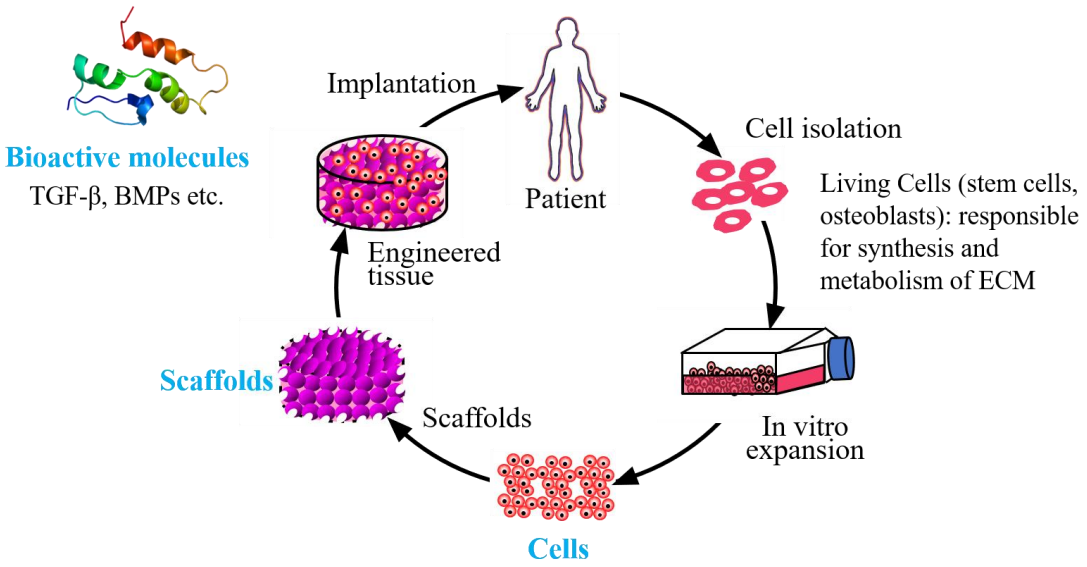

Fig. 1.2. Three fundamental principles in bone tissue engineering.

1.3. Principles of bone tissue engineering

1.3.1. Scaffolds-temporary matrices for bone growth

Every tissue is formed from (generally) many types of cells and a matrix. The matrix is a three-dimensional scaffold for cells *in vivo* and present a tissue-specific circumstance and structure [24]. In addition, it can serve as a reservoir of cytokines, growth factors, nutrients and water. For purpose of rebuilding functions or regenerating tissue, the scaffold, which would serve as the temporary matrix to initiate the cell proliferation as well as the deposition of the extracellular matrix (ECM) along with the bone regeneration, is needed [25, 26]. Furthermore, scaffold can also serve as the temporary matrix for the vascularization of the newly formed bone tissue [26, 27] and can take part in the remodeling process of bone tissue by releasing the differentiation or growth factors *in situ* in itself [28, 29].

Therefore, it's reasonable that a proper 3D scaffold is a crucial part for the tissue engineering approach. Whereas, it's considerable to recognize that the scaffold need to have many characteristics that are suitable for bone tissue engineering. An ideal scaffold not only requires to be with proper biocompatibility, biodegradability, porous structure and mechanical property, but also claims to be osteoconductive and osteoinductive [30, 31]. Scaffold with good osteoconductivity can stimulate the survival, migration and attachment of the osteogenic cells, while the osteoinductivity of the scaffold offers physical and chemical factors to promote the stem cells differentiate into osteoblastic lineage.

1.3.1.1. Requirements of scaffolds

The scaffolds need to meet the requirements as show below when they are applied in bone tissue engineering [25, 26, 32-34]:

a). Biocompatibility

The scaffolds should integrate sufficiently in host's tissues without causing an immunological rejection. The scaffold should be biocompatible with cells cultured within them and the living tissue around it. Scaffolds should enable cells to attach and proliferate well, as well as maintain the cell-specific functions. Scaffolds and their degradation products should not be cytotoxic to cells and surrounding tissues after implantation. The implanted scaffold should not adversely affect the functions of the organ and the whole body. Besides, the inflammatory response to the implant should be prevented, and the formation of fibrous capsules that separate the implant from the surrounding tissue should be avoided to allow integration of the implant with the surrounding tissue.

b). Biodegradability

As we know, goal of bone tissue engineering is to make host's own cells can ultimately substitute the tissue engineered construct (the implanted scaffold) over time then eventually form the new bone tissue. Scaffold and construct in bone tissue engineering should not be served as the permanent structures. Therefore, scaffolds need to be biodegradable thus the cells can produce the ECM by themselves *in situ* of the implants [35]. Biodegradability is usually an important factor because the scaffold should be preferentially absorbed by neighboring tissues without the need for a further surgical invasion and removal. Degradation rate of the scaffold must be in consistent with the rate of tissue regeneration. That is to say, when the cells are producing the ECM surrounding themselves, scaffold must ensure the structural integrity. Meanwhile, scaffold needs to ultimately decompose, remaining the newly regenerated tissue which can bear the mechanical load [36, 37].

c). Mechanical property

Ideally, the mechanical property of the scaffolds should be in accord with the anatomic sites where they are implanted. The strength of the scaffold must be sufficient to permit the surgical operation for the implantation. Although the mechanical property is very important for all the tissues, it offers certain specific challenges for the scaffolds used in orthopaedic applications. It’s one of the major challenges when design scaffold for bone tissue engineering that the scaffold needs to be with a sufficient mechanical property. When used in bone tissue engineering, the scaffold should remain competent mechanical stability to act properly from the initial implantation to end of the bone regeneration [38]. Another problem is that the remodeling rate of bone tissue varies with age. For the youths, the bone defects usually recover to point of the weight-bearing within 1.5 months, with the whole mechanical integrity recovering within one year. For elder people, the healing rate slows down. It also needs to be considered when design scaffold for the applications in bone tissue engineering.

Nevertheless, as the field evolves, one may argue that researchers have paid too much attention to manufacture the scaffolds with the similar mechanical property to natural bones. Lots of scaffolds with good mechanical properties have been produced, but not conducive to maintaining high porosity. Many other scaffolds, which have shown good *in vitro* results, have failed after *in vivo* implanted because of the lacking vascularization capabilities caused by the low porosity of the scaffolds. Therefore, the balance between the mechanical property and the porous structures allowing cellular penetration and neovascularization is crucial for the final success of the scaffold for bone tissue engineering [39, 40].

d). Porosity

Scaffold in bone tissue engineering must have highly porous structure with large ratio of the surface area to its volume, which facilitates cells to grow in as well as distribute homogeneously throughout the scaffold, as well as a better vascularization of the scaffold from the neighboring tissue. In addition, the scaffold should also exhibit sufficient micro porosity to allow for the ingrowth of the capillaries. Good interconnectivity and porosity are also crucial for the exact infiltration of the nutrients and oxygen, and also taking away the

metabolic waste resulted from the activity of the cells growing in the scaffolds. For the bone tissue engineering, this is of particular importance because high-rate mass transfer would occur resulting from the bone metabolic characteristics even under the *in vitro* cell culture conditions [41]. Moreover, the porosity would affect other characteristics of the scaffold (e.g., its mechanical property). In this case, the balance between the porosity and other properties of the scaffold should always be carefully considered.

e). Pore size

The pore size of the scaffold is another critical issue. If the size of the pores is too small, the pore occlusion would happen when seeding cells on the scaffold, which further inhibit the cellular penetration, vascularization of the inner regions of the scaffold, and the sufficient production of extracellular matrix (ECM). For bone tissue engineering purposes, it is widely accepted that the pore size should between 200 and 900 μm [34, 42]. Meanwhile, some researchers gave a different report [43]. Their studies supported the well-interconnected 3D scaffold with pores sizing between 1.2 and 2.0 mm would mostly facilitate the bone regeneration since the scaffold with those pores has obvious advantages due to the high ratio of surface to volume, which is beneficial for the in-growth of cells, blood vessels and tissues. Nevertheless, the large-sized macropores decreased the mechanical stability of the scaffold avoiding its usage in regions that need high mechanical property.

f). Surface properties

Both the topographical and biochemical properties of the scaffold surface would affect the cellular adhesion and proliferation [44, 45]. The topographical properties of the scaffold are of special importance where the research is about osteoconduction. Since osteoconductivity is the process that the osteogenic cells from the surrounding tissues migrate to surface of the scaffold [45], it's important that matrix of the scaffold is good for the migration after the scaffold implanted *in vivo*. Otherwise, when the cells begin the migration they will detach from the surface because of the wound contraction. It has been previously reported that the surface with higher roughness is better for cell attachment and migration than the smooth surface [46]. Chemical properties of scaffold surface are associated with the capacity of the cells to attach to scaffold and also the interactions with proteins.

g). Osteoconductivity

Osteoconductivity means the bones grow on the surface of a scaffold. An osteoconductive scaffold allows bone tissue to grow on its surface and down into the pores, pipes or channels [46]. The bone growing on the implant surface relies on role of the differentiated osteocytes. These cells might be from the pre-existing preosteoblasts or the osteoblasts which are activated by trauma or cells that are recruited from the primitive mesenchymal cells via osteogenesis [47]. Therefore, under the practical circumstance, osteoconductivity depends to a quite large extent on the osteoinductivity (which will be describe later). In addition, without sufficient blood supply, the growth process of bone tissue will not happen. Albrektsson et al. investigated the *in vivo* bone remodeling, concluding that full vascularization is a necessary condition for bone formation [48]. However, as far as the implant is concerned, osteoconductivity depends not only on the conditions of the bone repair, but also on the biological material used and its reaction. For some materials such as copper and silver, it is not possible for the osteoconductivity [49]; While for other materials such as the stainless steel which is of poor biocompatibility, and the materials of high biocompatibility such as the titanium, osteoconductivity has been found [50].

h). Osteoinductivity

Osteoinductivity of the scaffold means that the primitive, undifferentiated and pluripotent cells developed into the osteogenic lineage under the stimulation of scaffold [51]. Bone and the surrounding tissues contain many less differentiated cells, besides the differentiated bone cells including osteoblasts,

osteoclasts as well as the osteocytes. Those undifferentiated cells are most important for appropriate bone healing as they are able to be recruited to produce osteoprogenitors and to develop into differentiated bone cells over time [51] (Fig. 1.3). Undifferentiated mesenchymal cells could develop into the preosteoblast with the proper stimulus (osteoinductive cues), as a process which composes the bone induction. Many researchers have reported the osteoinductivity of some types of scaffolds in the last several decades [52, 53]. The bone tissue engineering scaffolds were implanted in anterior chamber of eyes or muscles, respectively, to prove the ectopic bone formation. The most reasonable way to prove one specific construct has osteoinductivity is to implant it in a ectopic position (e.g., muscle pouch, or subcutaneous implantation), and to analyze the possibility for new bone formation. Inducers also function naturally in the skeletal environment, but osteoinduction and osteoconduction are difficult to distinguish in situ. The osteoinductive agents also can function *in situ* of the bone defects, while it's hard to distinguish between osteoinductivity and osteoconductivity of the agent in an orthotopic site.

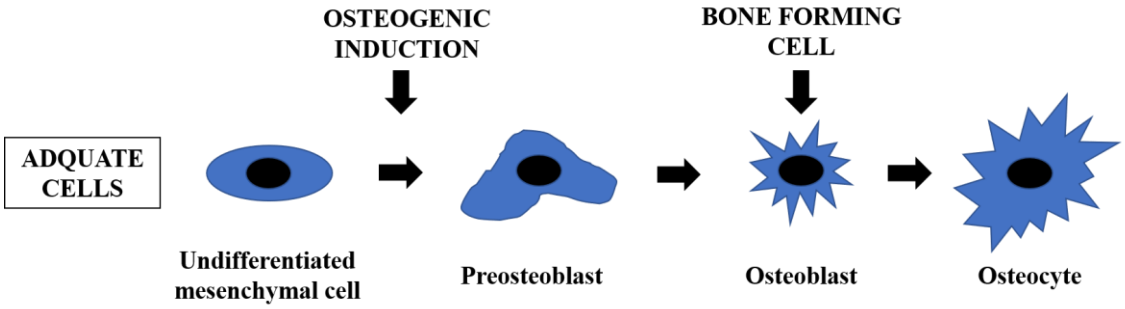

Fig. 1.3. After bone gets injured, both the undifferentiated and differentiated bone cells will be recruited to bone defect site. Most of the bone regeneration relys on the undifferentiated cells which can be developed into preosteoblasts.

Osteoinductivity is the enrichment of the undifferentiated cells and the further development of those cells to preosteoblasts. Osteoinductivity is a fundamental mechanism which happens commonly, e.g., in incorporation of implant and bone defect healing. Though the pre-existing osteoblasts can contribute to the formation of the new bone tissue, it is normally believed that these preexisting cells contribute to only a small proportion of the newly formed bone [54, 55]. According to the study of Frost et al. [16, 17], the bone defect initiates the succeeding remodeling by sensitizing diverse kinds of cells. At the same time, the injured site will release topical, biophysical and biochemical signals to guide cells to respond in an appropriate manner. Those signals are divided into two parts. One part of these messengers are responsible for guidance of the differentiation and organization of the cells, while the other part of these messengers can provide the mitogens. The initial part of the healing procedure involves osteoinduction, which begins shortly after the injury and is most effective during the first week.

1.3.1.2. Biomaterials used as bone tissue engineering scaffolds

For bone tissue engineering applications, choosing the suitable material for fabrication of the scaffold is of particular importance since the characteristics of the material will directly decide the properties of the scaffold [23]. To date, several materials have been proposed to use in bone tissue engineering from both natural sources and synthetic sources, among which the ceramics, metals and polymers have been most commonly used. Nevertheless, most of the ceramics and all the metals are not biodegradable, reducing the researchers' choices to biodegradable polymers and a small amounts of ceramics.

Ceramics have been commonly applied in biomedical engineering, bone replacement and bone regeneration [56]. They can come from natural sources (e.g., coral HA) or synthetic sources (e.g., β-tricalcium phosphate (β-TCP), synthetic HA) [57]. They have been applied in bone tissue engineering contributing to their attractive characteristics, mainly the nature of being osteoinductive and osteoconductive. Good outcomes regarding new bone formation were obtained in several works by applying the ceramics with or without bone tissue related cells [52, 58, 59]. Whereas these works showed some major limitations. First of all, they have low mechanical stability and very brittle, which avoid their applications in bone regeneration of large bone defects. In addition, the rate of degradation or dissolution is unpredictable *in vivo* due to the multiple factors such as the osteoclastic activity that occurs *in vivo*. The rate of degradation can cause problems because if the degradation rate of the scaffold is too quick, mechanical stability of the scaffold will be decreased. At the same time, the extracellular concentration of the calcium and phosphorous would be dramatically increased, which would lead to the cell death [60].

As another choose, the biodegradable polymers can be considered to be alternative materials for bone tissue engineering [26, 34]. These polymers can be categorized into two types: the natural type and the synthetic type.

Natural biodegradable polymers are the polymers derived from the natural sources (i.e., animal source or plants). Among them, the most commonly used natural polymers are collagen [42, 61], chitosan [62, 63], fibrinogen [64, 65], hyaluronic acid [66, 67], starch [68, 69] and poly (hydroxybutyrate)(PHB) [70, 71]. Major advantages of the natural polymers are the low immunological response, non-toxic degradation products, potential bioactive behavior, the ability to interact with host tissues, biochemical versatility, and the unlimited sources.

Synthetic biodegradable polymers are the biocompatible and biodegradable synthetic polymers most commonly used in the field of biomedical engineering. Their processability and biochemical versatility changes on the basis of their structures and natural properties, therefore it's impossible to directly compare the synthetic polymers and the natural polymers. Among all the synthetic polymers, the most generally used polymers are poly anhydride) [72, 73], poly (phosphazenes) [74, 75], poly (ε-caprolactone) [76, 77], poly (α-hydroxy acids)) [78, 79], poly (carbonate) [80, 81] and poly (propylene fumarate) [82-84].

1.3.1.3. Processing techniques

After choosing the proper material for preparation of scaffold, the next step is to choose or develop the appropriate processing techniques. To realize this and to ensure that all scaffold properties are met, the optimized processing method needs to generally reach the following criteria [33]: 1. The processing method should not adversely affect the material's properties (e.g., its chemical properties or biocompatibility). 2. The processing method should be consistent and accurate with reference to pore size, porosity, pore distribution, interconnectivity and mechanical property. When processed from the same processing method with the same parameters and conditions, different scaffold batches should have minimal changes in their characteristics. Over the years, to fabricate scaffold with sufficient properties for bone tissue engineering, numerous processing techniques have been developed such as solvent casting [85, 86], phase inversion [43, 87], freeze drying [88, 89], rapid prototyping technologies [90-92], melt based technologies [2, 93], high pressure based methods [94, 95] and fiber bonding [96, 97]. These processing techniques are described and discussed below.

Solvent casting (particulate leaching) may be the most well-known and commonly used method for fabrication of scaffolds for bone tissue engineering. Mikos et al. firstly described this method [98]. The method rests with dispersing calibrated inorganic (e.g., ice particulates, sodium tartrate, sodium chloride,

sodium citrate and effervescent salts) or organic (e.g., sucrose) particles in the polymer solution [85]. Further, the dispersive solution is casted or freeze-dried to make a scaffold with porous structure. Agrawal et al. developed the method with vibration in procedure of the polymer dissolution and the solvent evaporation. By this way, the ratio of porogen to polymer would be increased and the crystal deposition would be avoided [99]. The particulate leaching method was further developed by Murphy et al. by pouring the NaCl crystals to a mold and then exposed to 95% humidity for varied time so that the salt fusion could be obtained. The pore interconnectivity was increased by using this method [86]. The porous polymer matrix was finally produced after the salt particles were eventually leached out by the selective dissolution. The ratio of porogen to polymer determined the porosity while the size of porogen determined the size of the pores. By using the solvent casting method the fully interconnected scaffolds with high porosity (more than 90%) could be obtained [85, 86]. This technique has been applied in bone tissue engineering for preparation of porous scaffold from collagen, poly (lactide-co-glycolide) (PLGA) or poly (L-lactic acid) (PLLA) using ice particulates, dichloromethane or chloroform. The advantages of this method are that the pore size and the porosity of the prepared scaffolds can be independently controlled without use of any special equipments. Nevertheless, there are some limitations of this method. Since the porogen embedded in the polymer matrix needs to be removed completely, the thickness of the scaffold should to be limited within 2 mm. Furthermore, the agglomeration of the porogen in the polymer matrix might inhibit the formation of a homogeneous pore structure. If the organic solvents used in the fabrication procedure are not removed totally, the residuals may show cytotoxicity to the cells seeded on the scaffold and affect the efficiency of the bioactive molecules [100, 101].

Phase inversion is like the solvent casting method. Fig. 1.4a shows a PLGA scaffold prepared by using this technique. Instead of allowing solvent to evaporate which occurs in solvent casting method, the solution film is put in aqueous solution in the phase inversion method. This leads to a phase inversion that causes PLGA precipitation [43]. The major advantage of phase inversion method over the solvent casting is that it avoids crystal deposition and sample with thickness in excess of 3 mm can be produced. Scaffolds with morphologies similar with trabecular bone and higher interconnectivity were obtained by using this method [43, 87]. However, excluding improvement of the interconnectivity and thickness of the scaffolds, the other disadvantages presented in solvent casting remain in phase inversion method.

Freeze-drying process depends on a thermal phase separation technique, which happens when the temperature of the polymer solution (which was injected to the mold in advance) is deceased. After the phase-separation system becomes stable, by using the vacuum sublimation the solvent-rich phase is excluded and a polymeric foam leaves behind. Both natural and synthetic polymer scaffolds have been fabricated by using this method [89]. By controlling the freezing rate, pH and freezing temperature, the pore structure of the scaffolds can be controlled [102]. This method can result in rather highly porous scaffolds. However, the heterogeneity of polymer matrix of the scaffolds, the random pore structure, the low mechanical stability and the technical sensitivity (process parameters should be well controlled) are the main drawbacks of this method [103, 104].

Rapid prototyping (RP), also called *freeform fabrication (SFF)* has been developed for bone tissue engineering with the advances in processing technology and computer [90]. This method can design and prepare complicated 3D scaffolds using the data obtained from digitizers, computer based medical imaging, computer assisted design (CAD) systems or the other data makers. The RP methods employ the layered manufacturing technique, by which the 3D scaffolds are produced layer by layer through the processing of liquid, powder or solid sheet material stocks. The computer dominated fabrication procedures, customized design and anisotropic scaffold microstructures are the major superiorities for their applications in bone tissue engineering. The most commonly used methods in the field are respectively the 3D printing [105, 106], 3D plotting [107, 108], fused deposition modeling (FDM) [109, 110] and indirect RP approaches [90, 111].

The representative examples of scaffolds prepared by RP techniques are shown in Fig. 1.4 (c and d). RP techniques allow the produce of complex, customized scaffolds with accurate and consistent pore structure as well as mechanical properties under the minimal manual handling and various kinds of processing conditions. Drawbacks of the RP techniques include: 1. The pore size of the manufactured scaffold depends on the size of the stock material powder; 2. The pore closure of the scaffold caused by the stock material; 3. Organic solvents are used as the binders for polymers; 4. The inappropriate mechanical properties since the final structure of the scaffolds is the stack-up of multiple layers [90, 112].

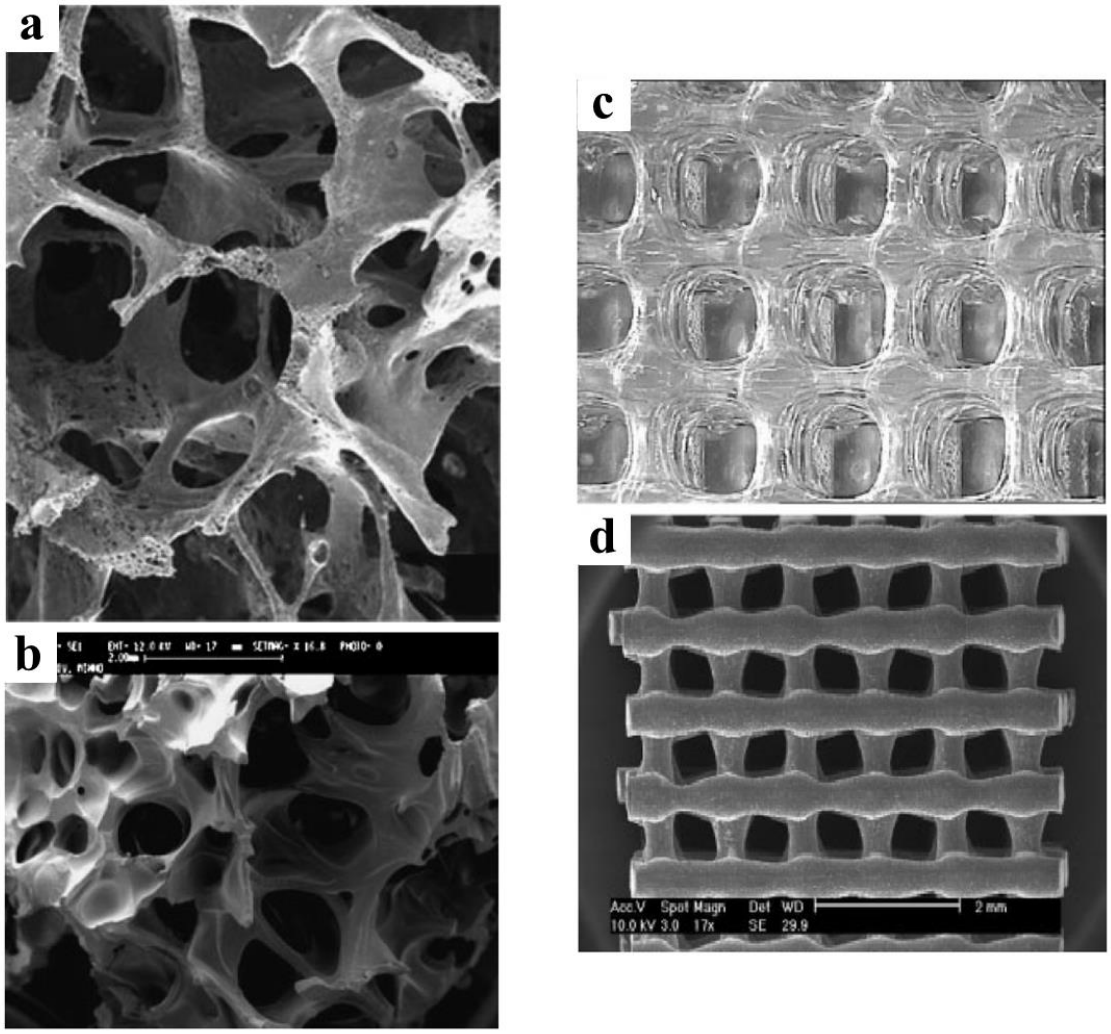

Fig. 1.4. a). PLGA scaffold (Osteofoam^{TM}) obtained by phase inversion. b). Starch-poly (lactic acid) (SPLA) scaffold prepared by using a method depended on extrusion with blowing agents. c). Chitosan scaffold prepared by a 3D plotting method. d). PCL/PEG scaffold prepared by Fused Deposition Modelling. Source: Salgado, A.J. et al. (2004) [2].

Melt based technique is another way to prepare scaffold for bone tissue engineering. One of such techniques is melt molding. In this method, the raw polymers are homogenously blended with the porogen materials in advance and then poured to molds, which are then heated above the glass transition temperature of the polymers. Afterwards, the porogen/polymer composites are immersed in the solvents for the selective dissolution of the porogens. By using this method the porous 3D scaffolds with different shapes are prepared

by just changing the geometries of the molds [33, 97]. In addition, by altering the size and amount of the porogen materials, the method can also regulate the pore size and porosity of the prepared scaffolds [113]. Other melt based techniques for processing scaffolds for bone tissue engineering are injection and extrusion molding. These methods are relied on the blends of the raw polymers with blowing agents. After being mixed well, the blends undergo injection into or extrusion from the molds. The blowing agents degrade during the processing, releasing carbon dioxide and water which create the porous structure of the polymeric scaffolds [114, 115]. Based on these techniques, the scaffolds with a proper porosity and interconnectivity, as well as the morphologies similar to those of the natural trabecular bone have been fabricated, as shown in Fig. 1.4 (b). Moreover, the mechanical properties (the compressive modulus and compressive strength) of these scaffolds are at the same level with the trabecular bone, and significantly higher than those of the scaffolds prepared by conventional techniques. In addition to good material properties from a material science perspective, the scaffolds also showed no cytotoxicity to cells, which facilitates the cell growth and deposition of extracellular matrix [68, 116]. The limitation of these methods is the restricted control of the pore distribution within the prepared scaffolds.

High pressure processing depends on the CO_2 saturation of the polymer discs by settling in the high-pressure CO_2 [33, 117]. By decreasing the CO_2 pressure to the ambient level, a thermodynamic instability is created resulting in the nucleation and expansion of the dissolved CO_2 therefore generating marcopores. Scaffolds prepared using this method have been proved to support the growth of bone cells, as well as the deposition and mineralization of the bone matrix. On the other hand, there are still some disadvantages of this method such as the non-porous surface, the closed pore structure and the low mechanical stability of the prepared scaffolds, which can show some inhibition to the growth of bone cells and tissues.

Fiber bonding is another scaffold processing method that fabricates the porous scaffold with variable pore size by weaving or knitting individual fibers into 3D patterns. Its major advantage is the large surface area of the prepared scaffolds which is good for both cell adhesion and the effective infiltration of nutrients [32, 118]. The porous 3D scaffold has been prepared by first aligning PGA fibers in the designed shape. Afterwards, the PGA fibers were immersed into a methylene chloride/PLLA solution [97]. After evaporation of the solvent, the PGA/PLLA composite scaffold was heated above the melting point of the two polymers. The PGA fibers are then physically connected at their cross-points by selective removal of the PLLA during cooling process. The main disadvantage of this technique are the immiscibility of the two polymers, the lack of control of pore size and porosity and the residues of solvent in the scaffold that can be detrimental to the cells and tissues [32].

1.3.2. Cells for bone tissue engineering

After choosing the proper material and techniques for preparation of scaffold, the next step is to choice a reliable cells source for bone tissue engineering. An desired cells source needs to be non-immunogenic and easily expandable to larger amount, as well as have the certain pattern of protein expression which is similar to the *in situ* tissue needed to repaired [119].

1.3.2.1. Osteoblasts

Due to the non-immunogenicity, the primary and most reasonable option of cell type for bone tissue

engineering is isolated osteoblasts from the biopsy obtained from patient (as the autologous cells) and then perform the restricted *in vitro* expansion. Nevertheless, this approach has some disadvantages: it takes time, quite small amount of the osteoblasts are useful after tissue dissociation and their rate of expansion is very low, restricting the cells amount available for seeding onto the scaffold. In addition, in some bone diseases, the osteoblasts cannot be suitable for the transplantation since the protein expression is below the anticipated value [120]. Another way to obtain the cells is by using the osteoblasts derived from the non-human donors (as the xenogeneic cells), which overcomes the limitation of low cell numbers. Nevertheless, the risk of transmission of infectious pathogens such as viruses, the immunogenicity of these cells and the ethical and social problems associated with them have inhibited the development of this method [120, 121].

To overcome the limitations of above-mentioned approaches, more and more attention has been drawn to stem cells. It has been a long time for the research of stem cells, and though some issues are yet to be answered, the use of the stem cells in bone tissue engineering can be regarded as a good alternative.

1.3.2.2. Stem cells

The stem cells are the undifferentiated cells remaining the high proliferative ability, being able to go through the self-renewal, multidirectional differentiation and thus the remodeling of the tissues [122]. Nevertheless, the stem cells have different extents of differentiation potential. The most primary stem cells are derived from zygote, more accurately from descendants of the very first divisions [123, 124]. Those cells are the totipotent cells due to their capacity of forming the embryo as well as the trophoblast of the placenta. After a few days, those cells became specialized, forming a hollow cell sphere, blastocysts and a bunch of cells named the Inner Cell Mass (ICM) (The embryo will be then derived from the ICM). The ICM cells, also called the embryonic stem cells (ES), are the pluripotent cells and are capable of differentiating into almost all cell types arisen by the three germ lines. In the end, the multipotent stem cells (also called adult stem cells, ASCs) are present in the fully differentiated tissues [125]. In theory, in contrast to ES, these cells produce only a restricted range of differentiation progeny associated with the embryo's origin of the tissue where they are located. Whereas, in fact, these cells are proved to show a higher extent of differentiation plasticity.

1.3.2.2.1. Embryonic Stem Cells

As mentioned above, the embryonic stem cells (ES) locate in the ICM of blastocyst. To date, the ES cells have been isolated from human, primates and rodents [126]. The ES cells have been proved to differentiate to hematopoietic cells, cardiomyocytes, endothelial cells, neurons, ectodermal cells, hepatocytes, islets and chondrocytes [127]. Buttery et al. demonstrated that the osteoblasts could be differentiated from ES cells at presence of one specific osteogenic differentiation inducer-dexamethasone [128]. Nevertheless, though the ES cells have great potential in the applications for tissue engineering, some problems are still needed to be solved. First of all, it is necessary to develop methods that allow for direct differentiation, selective differentiation and integration, and the somatic tissue-specific functions of ES cells upon transplantation [129]. Second, it has been ensured that the undifferentiated ES cells can increase the risk for teratocarcinomas and teratomas after *in vivo* implantation since their proliferative capability is unlimited. Therefore, it's an issue to ensure the ES-cell-derived somatic donor cells are not tumorigenic. The third problem needed to be solved is the immunological of the cells.

1.3.2.2.2. Adult Stem Cells

The stem cells located in the fully differentiated tissues are the so-called adult stem cells (ASCs) [130]. Until now the ASCs have been found in bone marrow [131], adipose [132], muscle [133], periosteum [133], skin [134] and brain [134]. In the field of bone tissue engineering, the stem cells resided in the bone marrow, called as the Mesenchymal Stem Cells (MSCs), are of particular interest. Caplan et al. reported that when these cells are placed under appropriate culture conditions, they can differentiate to cells with mesenchymal origin and form bone, tendon, muscle, adipose, cartilage and skin [135, 136]. In addition to the differentiation potential, the MSCs can also show other features. Bruder et al. reported that the extensive expansion of the MSCs can be obtained *in vitro* [137]. As described by Pittinger et al., the MSCs did not differentiate spontaneously as the increased number of passages [135, 136]. Besides, it was suggested that these cells showed immunosuppressive effects *in vivo* that made them available for allogeneic or xenogeneic transplantation [138]. Currently, for the applications in bone tissue engineering, the MSCs have shown more achievements than those of ES cells. The MSCs have been used in clinical trials of certain applications [139], while for ES cells it is still a long way from reaching this stage. Whereas, it has to be noted that the ES cells will be a huge cells source for bone tissue engineering once the related issues are solved.

1.3.3. Bioactive molecules

Bioactive molecules such as growth factors and small molecular-weight drugs are employed in tissue engineering to control cell functions as well as the formation of tissues. Growth factors are the most commonly used bioactive molecules that affect cell proliferation, differentiation and morphogenesis. Growth factors are usually proteins which are secreted by cells and act as the cell-signaling molecules [13]. Bonding of growth factors with their receptors triggers intracellular signaling which leads to diverse events such as promoting and/or preventing the cell migration, adhesion, proliferation, and differentiation via up- or downregulating the production of certain growth factors or receptors [121, 140]. Similar to other tissues, bone tissues also have plenty of growth factors. Among those, the bone morphogenetic proteins (BMPs), fibroblast growth factor (FGF), transforming growth factor beta (TGF-β), platelet derived growth factor (PDGF) and insulin growth factor I and II (IGF I/II) are most commonly used in the applications for bone tissue engineering [141, 142].

Here gives a brief introduction to the most commonly used growth factors in bone tissue engineering. First is the BMPs. BMPs are usually embedded in bone matrix which are usually expressed in the early stages of bone defect remodeling [143]. The key role of BMPs is to recruit MSCs to the healing site and then stimulate the differentiation of these MSCs to osteogenic lineage. It's not yet fully understood of the mechanisms by which the BMPs act on MSCs. While, it has been accepted that the BMP-2 has a significant function in expression of osteogenic markers such as the osteocalcin (OCN) and the alkaline phosphatase (ALP) via mitogens activated protein kinase (MAPK) pathway [144]. The BMPs may also be associated in the expression of nuclear transcription factor Cbaf-1/Runx2 [145].

Another widely used growth factor is TGF-β. The biological effects of TGF-β are diverse. The TGF-β has been found to facilitate the cell proliferation, hypertrophy and differentiation *in vitro* [146]. It has also been proved that TGF-β can block or initiate cell migration and differentiation. It enhances the collagen production and the proliferation of osteoblast-like cells *in vitro*. Moreover, TGF-β has been shown to increase the callus formation at the facture healing sites in some *in vivo* studies [147].

IGF genes are expressed by skeletal cells. Although IGF I and II have similar effects on bone

metabolism, IGF I has been approved to be more effective than IGF II [148]. After injury the IGFs can be found at the fracture site to stimulate the synthesis of collagen type I, as well as promote the deposition of the extracellular matrix [149]. Moreover, by reducing collagen synthesis or the expression of the stromal collagenase in osteoblasts, the IGFs can maintain the collagen integrity in the bone microenvironment [148].

In addition to the above-mentioned growth factors, other growth factors may also be employed in bone tissue engineering. Vascular endothelial growth factor (VEGF) is an angiogenic factor that is expressed in the vascularized tissues. It is commonly presented at fracture healing sites to regulate the vascularization by recruiting the endothelial cells to the sites. VEGF can also regulate the interaction between angiogenesis and osteogenesis at the fracture healing sites. Besides VEGF, the FGF-2 is another cytokine related to the process of bone remodeling.

The FGF-2 is associated with the delicate balance between the bone-forming cells and the bone-resorbing cells [150]. The FGF-2 can also enhance the neovascularization and stimulates the osteogenic phenotype by activating Cbaf-1/Runx2 nuclear transcription factors [142]. Moreover, the PDGF, which produced by osteoblasts, monocytes/macrophages or platelets, also plays a role in bone regeneration. It is also thought to stimulate the migration of MSCs towards the facture healing site [151].

Although up to now the protein growth factors are mostly common used, there are many shortages of growth factors such as the limited sources, the high price, short half-life, easy-lost activity and risk of tumors [152]. To solve those problems, some researchers has been trying to use single component, safe, stable and inexpensive low-molecular-weight bioactive molecules to substitute the role of protein growth factors. One of such low-molecular-weight bioactive molecules used in bone tissue engineering is dexamethasone (DEX). DEX is a kind of glucocorticoid with highly potent and long-acting property [153]. As an earliest known and readily available osteogenic inducer for MSCs, DEX plays a key role in controlling regulation of osteogenic marker genes [154]. Moreover, DEX has antiallergic, antitoxic, antishock, antipyretic and immunosuppressive properties and can inhibit secretion of pro-inflammatory cytokines, including IL-1β, IL-6, INF-γ and TNF-α [155]. MSCs cultured with continuous DEX treatment exhibited higher expression levels of osteogenic markers and higher positive rates of osteogenic colony formation than those without DEX treatment [156].

1.4. Bone tissue engineering strategies

Many efforts have been made to prepare the scaffolds for bone tissue engineering. To mimic extracellular matrix composition of bone, a variety of strategies have been considered, including usage of the components present in natural bone [10], controlling of pore structure and interconnectivity [157], construction of multiple scale architectures [158] and incorporation of growth factors [159]. For example, calcium phosphate (CaP) has been hybridized with polymers in the forms of tablets [160], blends [161], pastes [162] or cements [163]. However, these CaP/polymer composite scaffolds do not have appropriate pore structures for cell accommodation and migration. In particular, their pore interconnectivity is poor [164, 165].

To render scaffolds with good osteoinductivity, growth factors have been incorporated in the scaffolds. Nevertheless, the most commonly used growth factors such as bone morphogenetic proteins (BMPs) and transforming growth factor beta (TGF-β) are proteins and can easily lose their bioactivity during the preparation procedures [166]. To minimize denaturation and maintain their bioactivity, growth factors are generally introduced in scaffolds by physical adsorption. The release of physically adsorbed proteins always exhibits an initial burst and cannot last for a long period [167-169]. On the other hand, dexamethasone (DEX), as a low molecular weight osteoinductive factor, has drawn much attention for incorporation in scaffolds for bone tissue engineering because of its high stability even in tough chemical environment [170].

DEX and hydroxyapatite (HA) nanoparticles have been hybridized with gelatin and poly(L-lactide) to construct hydroxyapatite/DEX/PLLA/gelatin composite scaffold by electrospinning technique [171]. There are some limitations in this work. For instance, the PLLA/gelatin hybrid scaffold was prepared by electrospinning technique, which resulted in uneven distribution of nanofibers, the low thickness and low mechanical of the scaffold. Such scaffold cannot offer a proper 3D environment for cell proliferation, migration and differentiation. Besides, the PLLA were used in the dexamethasone (DEX) delivery system. As we know, the major concerns associated with biodegradable synthetic polymeric drug delivery systems are the acidic or degradation by-products that alter the drug activity, and even can adversely interact with the drug or tissue as they come in contact during circulation. Moreover, to load the DEX into the scaffold, the DEX was primarily dissolved in DMF then mixed with nanocomposite of PLLA and nHA. The DMF is with high cytotoxicity, so how to completely remove the organic solvent remains to be solved.

In another work, the DEX-loaded mesoporous silica nanoparticles have been deposited onto poly(L-lactic acid)/poly(ε–caprolactone) nanofibrous scaffold by electrophoretic deposition [172]. Besides the disadvantage of using synthetic polymers in the system as described above, there are some other drawbacks in this work. First, the prepared scaffolds showed very low interconnectivity, which was no good for the penetration of cells, nutrient, oxygen, growth factors and wastes flow through the scaffold [173, 174]. Second, to load the DEX to the MSNs-NH_2, the MSNs-NH_2 were soaked in the DEX solution. In other words, the DEX were just coated on surface of the MSNs-NH_2. The burst release of DEX showed at the first 5 days, and after 7 days there was almost no further release of DEX.

A dual delivery system of DEX and BMP-2 has been designed via co-electrospinning the blending solution that is composed of BMP-2-encapsulated bovine serum albumin nanoparticles, DEX and PCE copolymer [175]. In this work, besides the disadvantages of using synthetic polymer (PCE) and electrospinning technique as described above, the other drawbacks are as follows: First, to prepare the BMP-2-loaded chitosan-stabilized BSA nanoparticles (BNPs), the BMP-2 was primarily added to the BSA solution, then 40 mL ethanol was pumped into the 1% BSA solution. Then, 40 mL of chitosan solution (1 mg/mL, dissolved in 1% acetic acid solution) was added to the mixture, and ethanol was pumped into the mixture at 0.5 mL/min. The formed BNPs were collected by centrifugation and washed with 50/50 distilled water/ethanol (v/v) solution. As we know, BMP-2 is protein, which easily loses the bioactivity under some extreme conditions (ethanol, acidic solution) [176]. Considering BMP-2 is very expensive, the method for loading BMP-2 in this article is inappropriate since the BMP-2 was exposure to ethanol; Second, the BMP-2 showed a burst release. We know it's unsafe when exposing body to high dosages of growth factors and this might even increase the risks for tumors, therefore the clinical potential of the prepared nanofibers is limited; Third, the DEX-loaded nanofibers display a typical initial burst release of DEX due to the DEX located in the external surface formed by its dissolving out or phase separation at the nanofiber surface, and the DEX release only sustained for 8 days.

1.5. Motivation, objectives and outline

1.5.1. Motivation and objectives

Bone defect has become one of the big menaces in human daily life. Although bone is one of the few regenerative tissues in human body, its regenerative ability is limited. Some bone defects undergo incomplete fracture healing (nonunion fractures) and sometimes the defect size is beyond the body's healing capacity (critical size defects). Therefore, further intervention is required to treat these fractures and defects. At present, autologous

and allogenic bone grafts are the two main choices to replace the damaged bone. However, both of them have many problems such as limited autologous donor tissues, donor site morbidity and immunological rejection of allogenic grafts. Instead, a number of artificially synthesized biomaterials such as ceramics, alloys and polymers have been developed for the repair of bone defects. Although these biomaterials are osteoconductive, they generally do not have osteoinductive capacity. On the other hand, osteoinductive cues such as bone growth factors are able to induce bone formation, even in nonskeletal sites (e.g., muscle). Hence, combination of an osteoconductive biomaterial with osteoinductive cues is supposed to overcome the limitations of conventional bone graft biomaterials. Such composite biomaterials can have both osteoconductive and osteoinductive capacities and accelerate bone formation and regeneration when implanted.

Protein growth factors are most commonly used as osteoinductive cues. However, they havesome shortages such as limited sources, high price, short half-life and easily lost activity. One way to solve those problems is using stable and inexpensive low-molecular-weight molecules to substitute the role of protein growth factors. One of such low molecular weight molecules used for bone regeneration is dexamethasone (DEX). DEX is a kind of glucocorticoid with high potency and long-acting property. As one of the earliest known and readily available osteogenic inducers for mesenchymal stem cells (MSCs), DEX plays a key role in controlling expression of osteogenic marker genes. MSCs cultured with continuous DEX treatment exhibit higher expression level of osteogenic markers and a higher positive rate of osteogenic colony formation than those without DEX treatment. To date, several DEX delivery methods are available, ranging from systemic injection, eluting coating, and loading within biodegradable polymer carriers. Nevertheless, systemic injection has the obvious disadvantage of exposing the whole body to high dosage of the drug. Release of DEX from eluting coatings can neither last as long as the required period for biomedical application nor release appropriate dose in response to the dynamic change of the local biochemical environment.

Compared with biodegradable polymer carriers, calcium phosphate nanoparticles (CaP NPs) have been showing enormous potential as carriers of osteoinductive factors because CaP NPs are the inorganic component of natural bone. CaP NPs are biocompatible and biodegradable, which are essential properties for drug carriers. Furthermore, synthesis of CaP NPs is a straightforward precipitation process. Incorporation of drug molecules only requires molecules of interest be present during the particle formation. Hence, CaP NPs have been widely used as carriers for drugs, proteins, DNA and RNA. Therefore, in this study CaP NPs were used to load DEX and the DEX-loaded CaP NPs were hybridized with collagen sponges to prepare their composite scaffolds. The composite scaffolds were used for culture of human bone marrow-derived MSCs (hMSCs) to investigate their effects on osteogenic differentiation of hMSCs and bone regeneration.

1.5.2. Outline

The DEX loaded calcium phosphate nanoparticles/collagen scaffold were prepared for bone tissue engineering. The cell proliferation and osteogenic differentiation were checked in both *in vitro* and *in vivo* environments.

In Chapter 2, DEX was incorporated in biphasic calcium phosphate nanoparticles (BCP NPs) by immersion method and precipitation method to prepare DEX-loaded BCP NPs (DEX@BCP NPs). The release profile of DEX and their effects on the osteogenic differentiation of hMSCs were investigated. The parameter for preparation of the DEX@BCP NPs was optimized to obtain the final DEX@BCP NPs. The DEX@BCP NPs were used for cell culture of hMSCs to check their osteogenic differentiation.

In Chapter 3, the potential applications of the above prepared DEX@BCP NPs in bone tissue engineering were explored. Composition of natural bone is about 35% organic (primarily collagen type I) and 65% inorganic (nanocrystalline calcium phosphate, CaP). So, in this part, the DEX@BCP NPs were hybridized with porous

collagen sponge of which pore structure was controlled by using pre-sieved ice particulates as a porogen material. Potential of the DEX@BCP NPs/collagen composite scaffolds (DEX@BCP/Col) for osteogenesis was investigated both *in vitro* and *in vivo*.

In Chapter 4, the prepared DEX@BCP/Col were further developed for better angiogenesis and osteogenesis. In the previous research, we found that the DEX@BCP/Col scaffold showed the osteogenesis starting from the peripheral regions, and even after 12 weeks of subcutaneous implantation the osteogenesis of the central regions of the scaffolds was not sufficient. Because of the critical role of blood vessels on osteogenesis of tissue engineering scaffolds, lack of sufficient mature vascular networks should be responsible for the deficiency of the osteogenesis at the central regions of the DEX@BCP/Col. So, in this part, for simultaneous enhancement of angiogenesis and osteogenesis, DEX@BCP/Col composite scaffolds with concave microgroove network were designed and prepared. The microgroove network in the composite scaffolds were supposed to guide assembly of human umbilical vascular endothelial cells (HUVECs) into well aligned tubule-like structures, thus promoting rapid angiogenesis and osteogenesis.

In Chapter 5, the conclusions of this thesis are given and the future prospects were addressed.

1.6. References

[1] Chai YC, Carlier A, Bolander J, Roberts SJ, Geris L, Schrooten J, Van Oosterwyck H, Luyten FP. Current views on calcium phosphate osteogenicity and the translation into effective bone regeneration strategies. Acta biomaterialia 2012;8:3876-87.

[2] Salgado AJ, Coutinho OP, Reis RL. Bone tissue engineering: state of the art and future trends. Macromolecular Bioscience 2004;4:743-65.

[3] Shear M, Kramer B. The Composition of Bone. III. Physico-Chemical Mechanism. Proceedings of the Society for Experimental Biology and Medicine 1928;25:283-5.

[4] Rey C, Combes C, Drouet C, Glimcher MJ. Bone mineral: update on chemical composition and structure. Osteoporosis International 2009;20:1013-21.

[5] Bilezikian JP, Raisz LG, Martin TJ. Principles of bone biology: Academic Press; 2008.

[6] Mackie E. Osteoblasts: novel roles in orchestration of skeletal architecture. The international journal of biochemistry & cell biology 2003;35:1301-5.

[7] Sodek J, Ganss B, McKee M. Osteopontin. Critical Reviews in Oral Biology & Medicine 2000;11:279-303.

[8] Favus MJ. Primer on the metabolic bone diseases and disorders of mineral metabolism: Rittenhouse Book Distributors; 2006.

[9] Davies J, Workshop BE. Bone engineering: em squared; 2000.

[10] Chen Y, Wang J, Zhu X, Tang Z, Yang X, Tan Y, Fan Y, Zhang X. Enhanced effect of β-tricalcium phosphate phase on neovascularization of porous calcium phosphate ceramics: in vitro and in vivo evidence. Acta Biomater. 2015;11:435-48.

[11] Behzadi S, Luther GA, Harris MB, Farokhzad OC, Mahmoudi M. Nanomedicine for safe healing of bone trauma: Opportunities and challenges. Biomaterials 2017;146:168-82.

[12] Kruyt MC. Tissue engineering of bone: the applicability of cell-based strategies 2004.

[13] Rose FR, Oreffo RO. Bone tissue engineering: hope vs hype. Biochemical and biophysical research communications 2002;292:1-7.

[14] Patrick CW, Mikos AG, McIntire LV. Frontiers in tissue engineering: Elsevier; 1998.

[15] Shelton WR, Papendick L, Dukes AD. Autograft versus allograft anterior cruciate ligament

reconstruction. Arthroscopy: The Journal of Arthroscopic & Related Surgery 1997;13:446-9.
[16] Dodd C, Fergusson C, Freedman L, Houghton G, Thomas D. Allograft versus autograft bone in scoliosis surgery. Bone & Joint Journal 1988;70:431-4.
[17] Ehrler DM, Vaccaro AR. The use of allograft bone in lumbar spine surgery. Clinical orthopaedics and related research 2000;371:38-45.
[18] Brosnahan R, Small LA, Bearcroft JA. Artificial bone graft implant. Google Patents; 2000.
[19] Moore WR, Graves SE, Bain GI. Synthetic bone graft substitutes. ANZ journal of surgery 2001;71:354-61.
[20] Willert H-G, Buchhorn GH, Fayyazi A, Flury R, Windler M, Köster G, Lohmann CH. Metal-on-metal bearings and hypersensitivity in patients with artificial hip joints: a clinical and histomorphological study. JBJS 2005;87:28-36.
[21] Sopyan I, Mel M, Ramesh S, Khalid K. Porous hydroxyapatite for artificial bone applications. Science and Technology of Advanced Materials 2007;8:116-23.
[22] Giannoudis PV, Dinopoulos H, Tsiridis E. Bone substitutes: an update. Injury 2005;36:S20-S7.
[23] Burg KJ, Porter S, Kellam JF. Biomaterial developments for bone tissue engineering. Biomaterials 2000;21:2347-59.
[24] Badylak SF, Freytes DO, Gilbert TW. Extracellular matrix as a biological scaffold material: structure and function. Acta biomaterialia 2009;5:1-13.
[25] Kneser U, Schaefer D, Munder B, Klemt C, Andree C, Stark G. Tissue engineering of bone. Minimally invasive therapy & allied technologies 2002;11:107-16.
[26] Hutmacher DW. Scaffolds in tissue engineering bone and cartilage. Biomaterials 2000;21:2529-43.
[27] Chen Y, Wang J, Zhu X, Tang Z, Yang X, Tan Y, Fan Y, Zhang X. Enhanced effect of β-tricalcium phosphate phase on neovascularization of porous calcium phosphate ceramics: in vitro and in vivo evidence. Acta biomaterialia 2015;11:435-48.
[28] Yilgor P, Tuzlakoglu K, Reis RL, Hasirci N, Hasirci V. Incorporation of a sequential BMP-2/BMP-7 delivery system into chitosan-based scaffolds for bone tissue engineering. Biomaterials 2009;30:3551-9.
[29] Bose S, Roy M, Bandyopadhyay A. Recent advances in bone tissue engineering scaffolds. Trends in biotechnology 2012;30:546-54.
[30] Du J, Zu Y, Li J, Du S, Xu Y, Zhang L, Jiang L, Wang Z, Chien S, Yang C. Extracellular matrix stiffness dictates Wnt expression through integrin pathway. Scientific reports 2016;6.
[31] Vo TN, Kasper FK, Mikos AG. Strategies for controlled delivery of growth factors and cells for bone regeneration. Advanced drug delivery reviews 2012;64:1292-309.
[32] Agrawal C, Ray RB. Biodegradable polymeric scaffolds for musculoskeletal tissue engineering. Journal of Biomedical Materials Research Part A 2001;55:141-50.
[33] Leong K, Cheah C, Chua C. Solid freeform fabrication of three-dimensional scaffolds for engineering replacement tissues and organs. Biomaterials 2003;24:2363-78.
[34] Yang S, Leong K-F, Du Z, Chua C-K. The design of scaffolds for use in tissue engineering. Part I. Traditional factors. Tissue engineering 2001;7:679-89.
[35] Babensee JE, Anderson JM, McIntire LV, Mikos AG. Host response to tissue engineered devices. Advanced drug delivery reviews 1998;33:111-39.
[36] Brown BN, Valentin JE, Stewart-Akers AM, McCabe GP, Badylak SF. Macrophage phenotype and remodeling outcomes in response to biologic scaffolds with and without a cellular component. Biomaterials 2009;30:1482-91.
[37] Lyons FG, Al-Munajjed AA, Kieran SM, Toner ME, Murphy CM, Duffy GP, O'Brien FJ. The healing of

bony defects by cell-free collagen-based scaffolds compared to stem cell-seeded tissue engineered constructs. Biomaterials 2010;31:9232-43.
[38] Woodard JR, Hilldore AJ, Lan SK, Park C, Morgan AW, Eurell JAC, Clark SG, Wheeler MB, Jamison RD, Johnson AJW. The mechanical properties and osteoconductivity of hydroxyapatite bone scaffolds with multi-scale porosity. Biomaterials 2007;28:45-54.
[39] Blaker JJ, Maquet V, Jérôme R, Boccaccini AR, Nazhat S. Mechanical properties of highly porous PDLLA/Bioglass® composite foams as scaffolds for bone tissue engineering. Acta biomaterialia 2005;1:643-52.
[40] Kuo CK, Ma PX. Ionically crosslinked alginate hydrogels as scaffolds for tissue engineering: part 1. Structure, gelation rate and mechanical properties. Biomaterials 2001;22:511-21.
[41] Freed LE, Vunjak-Novakovic G. Culture of organized cell communities. Advanced drug delivery reviews 1998;33:15-30.
[42] Murphy CM, Haugh MG, O'Brien FJ. The effect of mean pore size on cell attachment, proliferation and migration in collagen–glycosaminoglycan scaffolds for bone tissue engineering. Biomaterials 2010;31:461-6.
[43] Holy CE, Shoichet MS, Davies JE. Engineering three-dimensional bone tissue in vitro using biodegradable scaffolds: investigating initial cell-seeding density and culture period. Journal of biomedical materials research 2000;51:376-82.
[44] Lange R, Lüthen F, Beck U, Rychly J, Baumann A, Nebe B. Cell-extracellular matrix interaction and physico-chemical characteristics of titanium surfaces depend on the roughness of the material. Biomolecular engineering 2002;19:255-61.
[45] Diener A, Nebe B, Lüthen F, Becker P, Beck U, Neumann HG, Rychly J. Control of focal adhesion dynamics by material surface characteristics. Biomaterials 2005;26:383-92.
[46] Milleret V, Hefti T, Hall H, Vogel V, Eberli D. Influence of the fiber diameter and surface roughness of electrospun vascular grafts on blood activation. Acta biomaterialia 2012;8:4349-56.
[47] Frost H. The Biology of Fracture Healing: An Overview for Clinicians. Part II. Clinical orthopaedics and related research 1989;248:294-309.
[48] Albrektsson T. The healing of autologous bone grafts after varying degrees of surgical trauma. A microscopic and histochemical study in the rabbit. Bone & Joint Journal 1980;62:403-10.
[49] Albrektsson T. Principles of osseointegration. Dental and Maxillofacial Implantology. London: Mosby-Wolfe 1995:9-19.
[50] Johansson C, Albrektsson T, Roos A. A biomechanical and histomorphometric comparison between different types of bone implants evaluated in a rabbit model. Eur J Exp Musculoskel Research 1992;1:51-61.
[51] Scaglione S, Braccini A, Wendt D, Jaquiery C, Beltrame F, Quarto R, Martin I. Engineering of osteoinductive grafts by isolation and expansion of ovine bone marrow stromal cells directly on 3D ceramic scaffolds. Biotechnology and bioengineering 2006;93:181-7.
[52] Yuan H, Kurashina K, de Bruijn JD, Li Y, De Groot K, Zhang X. A preliminary study on osteoinduction of two kinds of calcium phosphate ceramics. Biomaterials 1999;20:1799-806.
[53] Urist MR, McLEAN FC. Osteogenetic potency and new-bone formation by induction in transplants to the anterior chamber of the eye. JBJS 1952;34:443-75.
[54] Heiple KG, Chase SW, Herndon CH. A comparative study of the healing process following different types of bone transplantation. JBJS 1963;45:1593-616.
[55] Schropp L, Kostopoulos L, Wenzel A. Bone healing following immediate versus delayed placement of titanium implants into extraction sockets: a prospective clinical study. International Journal of Oral & Maxillofacial Implants 2003;18.

[56] LeGeros RZ. Properties of osteoconductive biomaterials: calcium phosphates. Clinical orthopaedics and related research 2002;395:81-98.
[57] LeGeros RZ. Calcium phosphate-based osteoinductive materials. Chemical reviews 2008;108:4742-53.
[58] Vallet-Regi M, González-Calbet JM. Calcium phosphates as substitution of bone tissues. Progress in solid state chemistry 2004;32:1-31.
[59] Tadic D, Epple M. A thorough physicochemical characterisation of 14 calcium phosphate-based bone substitution materials in comparison to natural bone. Biomaterials 2004;25:987-94.
[60] Adams CS, Mansfield K, Perlot RL, Shapiro IM. Matrix regulation of skeletal cell apoptosis role of calcium and phosphate ions. Journal of Biological Chemistry 2001;276:20316-22.
[61] Liu X, Ma PX. Polymeric scaffolds for bone tissue engineering. 2004.
[62] Tolaimate A, Desbrieres J, Rhazi M, Alagui A. Contribution to the preparation of chitins and chitosans with controlled physico-chemical properties. Polymer 2003;44:7939-52.
[63] Park YJ, Lee YM, Park SN, Sheen SY, Chung CP, Lee SJ. Platelet derived growth factor releasing chitosan sponge for periodontal bone regeneration. Biomaterials 2000;21:153-9.
[64] Hojo M, Inokuchi S, Kidokoro M, Fukuyama N, Tanaka E, Tsuji C, Miyasaka M, Tanino R, Nakazawa H. Induction of vascular endothelial growth factor by fibrin as a dermal substrate for cultured skin substitute. Plastic and reconstructive surgery 2003;111:1638-45.
[65] Endres M, Hutmacher D, Salgado A, Kaps C, Ringe J, Reis R, Sittinger M, Brandwood A, Schantz J-T. Osteogenic induction of human bone marrow-derived mesenchymal progenitor cells in novel synthetic polymer–hydrogel matrices. Tissue engineering 2003;9:689-702.
[66] Liu L-S, Thompson AY, Heidaran MA, Poser JW, Spiro RC. An osteoconductive collagen/hyaluronate matrix for bone regeneration. Biomaterials 1999;20:1097-108.
[67] Solchaga LA, Dennis JE, Goldberg VM, Caplan AI. Hyaluronic acid-based polymers as cell carriers for tissue-engineered repair of bone and cartilage. Journal of Orthopaedic Research 1999;17:205-13.
[68] Salgado A, Gomes ME, Chou A, Coutinho O, Reis R, Hutmacher D. Preliminary study on the adhesion and proliferation of human osteoblasts on starch-based scaffolds. Materials Science and Engineering: C 2002;20:27-33.
[69] Reis R, Cunha A. 'Biological and Biomimetic Materials. Encyclopedia of Materials Science and Technology, KHJ Buschow, RW Cahn, MC Flemings, B. Ilschner, EJ Kramer, S. Mahajan, Eds., Pergamon–Elsevier Science, Amsterdam 2001:8810.
[70] Kostopoulos L, Karring T. Guided bone regeneration in mandibular defects in rats using a bioresorbable polymer. Clinical oral implants research 1994;5:66-74.
[71] Chen L, Wang M. Production and evaluation of biodegradable composites based on PHB–PHV copolymer. Biomaterials 2002;23:2631-9.
[72] Behravesh E, Yasko A, Engel P, Mikos A. Synthetic biodegradable polymers for orthopaedic applications. Clinical orthopaedics and related research 1999;367:S118-S29.
[73] Uhrich K, Ibim S, Larrier D, Langer R, Laurencin C. Chemical changes during in vivo degradation of poly (anhydride-imide) matrices. Biomaterials 1998;19:2045-50.
[74] Ibim SE, Ambrosio AM, Kwon MS, El-Amin SF, Allcock HR, Laurencin CT. Novel polyphosphazene/poly (lactide-co-glycolide) blends: miscibility and degradation studies. Biomaterials 1997;18:1565-9.
[75] Laurencin CT, El-Amin SF, Ibim SE, Willoughby DA, Attawia M, Allcock HR, Ambrosio AA. A highly porous 3-dimensional polyphosphazene polymer matrix for skeletal tissue regeneration. Journal of Biomedical Materials Research Part A 1996;30:133-8.

[76] Schantz J-T, Hutmacher DW, Chim H, Ng KW, Lim TC, Teoh SH. Induction of ectopic bone formation by using human periosteal cells in combination with a novel scaffold technology. Cell transplantation 2002;11:125-38.
[77] Kweon H, Yoo MK, Park IK, Kim TH, Lee HC, Lee H-S, Oh J-S, Akaike T, Cho C-S. A novel degradable polycaprolactone networks for tissue engineering. Biomaterials 2003;24:801-8.
[78] Saito N, Okada T, Horiuchi H, Murakami N, Takahashi J, Nawata M, Ota H, Nozaki K, Takaoka K. A biodegradable polymer as a cytokine delivery system for inducing bone formation. Nature biotechnology 2001;19:332-5.
[79] Liao CJ, Chen CF, Chen JH, Chiang SF, Lin YJ, Chang KY. Fabrication of porous biodegradable polymer scaffolds using a solvent merging/particulate leaching method. Journal of Biomedical Materials Research Part A 2002;59:676-81.
[80] Choueka J, Charvet JL, Koval KJ, Alexander H, James KS, Hooper KA, Kohn J. Canine bone response to tyrosine-derived polycarbonates and poly (L-lactic acid). Journal of Biomedical Materials Research Part A 1996;31:35-41.
[81] Ertel SI, Kohn J, Zimmerman MC, Parsons JR. Evaluation of poly (DTH carbonate), a tyrosine-derived degradable polymer, for orthopedic applications. Journal of Biomedical Materials Research Part A 1995;29:1337-48.
[82] Shung AK, Timmer MD, Jo S, Engel PS, Mikos AG. Kinetics of poly (propylene fumarate) synthesis by step polymerization of diethyl fumarate and propylene glycol using zinc chloride as a catalyst. Journal of Biomaterials Science, Polymer Edition 2002;13:95-108.
[83] Shung AK, Behravesh E, Jo S, Mikos AG. Crosslinking characteristics of and cell adhesion to an injectable poly (propylene fumarate-co-ethylene glycol) hydrogel using a water-soluble crosslinking system. Tissue engineering 2003;9:243-54.
[84] Shin H, Temenoff JS, Mikos AG. In vitro cytotoxicity of unsaturated oligo [poly (ethylene glycol) fumarate] macromers and their cross-linked hydrogels. Biomacromolecules 2003;4:552-60.
[85] Yoon JJ, Park TG. Degradation behaviors of biodegradable macroporous scaffolds prepared by gas foaming of effervescent salts. Journal of Biomedical Materials Research Part A 2001;55:401-8.
[86] Murphy WL, Dennis RG, Kileny JL, Mooney DJ. Salt fusion: an approach to improve pore interconnectivity within tissue engineering scaffolds. Tissue engineering 2002;8:43-52.
[87] Karp JM, Shoichet MS, Davies JE. Bone formation on two-dimensional poly (DL-lactide-co-glycolide)(PLGA) films and three-dimensional PLGA tissue engineering scaffolds in vitro. Journal of Biomedical Materials Research Part A 2003;64:388-96.
[88] Malafaya P, Pedro A, Peterbauer A, Gabriel C, Redl H, Reis R. Chitosan particles agglomerated scaffolds for cartilage and osteochondral tissue engineering approaches with adipose tissue derived stem cells. Journal of Materials Science: Materials in Medicine 2005;16:1077-85.
[89] Mao JS, Zhao LG, Yin YJ, De Yao K. Structure and properties of bilayer chitosan–gelatin scaffolds. Biomaterials 2003;24:1067-74.
[90] Yeong W-Y, Chua C-K, Leong K-F, Chandrasekaran M. Rapid prototyping in tissue engineering: challenges and potential. Trends in biotechnology 2004;22:643-52.
[91] Billiet T, Vandenhaute M, Schelfhout J, Van Vlierberghe S, Dubruel P. A review of trends and limitations in hydrogel-rapid prototyping for tissue engineering. Biomaterials 2012;33:6020-41.
[92] Landers R, Pfister A, Hübner U, John H, Schmelzeisen R, Mülhaupt R. Fabrication of soft tissue engineering scaffolds by means of rapid prototyping techniques. Journal of Materials Science 2002;37:3107-16.

[93] Gomes M, Malafaya P, Reis R. 'Biopolymer Methods in Tissue Engineering. Methods in Molecular Biology Series, AP Hollander, PV Hatton, Eds., The Humana Press Inc., Totowa 2003:65.
[94] Mooney DJ, Baldwin DF, Suh NP, Vacanti JP, Langer R. Novel approach to fabricate porous sponges of poly (D, L-lactic-co-glycolic acid) without the use of organic solvents. Biomaterials 1996;17:1417-22.
[95] Shea LD, Wang D, Franceschi RT, Mooney DJ. Engineered bone development from a pre-osteoblast cell line on three-dimensional scaffolds. Tissue engineering 2000;6:605-17.
[96] Kim B-S, Mooney DJ. Engineering smooth muscle tissue with a predefined structure. 1998.
[97] Lu L, Mikos AG. The importance of new processing techniques in tissue engineering. Mrs Bulletin 1996;21:28-32.
[98] Mikos AG, Thorsen AJ, Czerwonka LA, Bao Y, Langer R, Winslow DN, Vacanti JP. Preparation and characterization of poly (L-lactic acid) foams. Polymer 1994;35:1068-77.
[99] Agrawal CM, Parr JE, Lin ST. Synthetic bioabsorbable polymers for implants. American Society for Testing and Materials West Conshohocken, PA; 2000.
[100] Sachlos E, Czernuszka JT. Making tissue engineering scaffolds work. Review: the application of solid freeform fabrication technology to the production of tissue engineering scaffolds. Eur Cell Mater 2003;5:29-39; discussion -40.
[101] Yang SF, Leong KF, Du ZH, Chua CK. The design of scaffolds for use in tissue engineering. Part II. Rapid prototyping techniques. Tissue Engineering 2002;8:1-11.
[102] Doillon CJ, Whyne CF, Brandwein S, Silver FH. Collagen-Based Wound Dressings - Control of the Pore Structure and Morphology. Journal of Biomedical Materials Research 1986;20:1219-28.
[103] Sultana N, Wang M. Fabrication of HA/PHBV composite scaffolds through the emulsion freezing/freeze-drying process and characterisation of the scaffolds. Journal of Materials Science: Materials in Medicine 2008;19:2555.
[104] O'Brien FJ, Harley BA, Yannas IV, Gibson L. Influence of freezing rate on pore structure in freeze-dried collagen-GAG scaffolds. Biomaterials 2004;25:1077-86.
[105] Hollister SJ. Porous scaffold design for tissue engineering. Nature materials 2005;4:518-24.
[106] Chia HN, Wu BM. Recent advances in 3D printing of biomaterials. Journal of biological engineering 2015;9:4.
[107] Landers R, Hübner U, Schmelzeisen R, Mülhaupt R. Rapid prototyping of scaffolds derived from thermoreversible hydrogels and tailored for applications in tissue engineering. Biomaterials 2002;23:4437-47.
[108] Luo Y, Lode A, Sonntag F, Nies B, Gelinsky M. Well-ordered biphasic calcium phosphate–alginate scaffolds fabricated by multi-channel 3D plotting under mild conditions. Journal of Materials Chemistry B 2013;1:4088-98.
[109] Kalita SJ, Bose S, Hosick HL, Bandyopadhyay A. Development of controlled porosity polymer-ceramic composite scaffolds via fused deposition modeling. Materials Science and Engineering: C 2003;23:611-20.
[110] Cao T, Ho K-H, Teoh S-H. Scaffold design and in vitro study of osteochondral coculture in a three-dimensional porous polycaprolactone scaffold fabricated by fused deposition modeling. Tissue engineering 2003;9:103-12.
[111] Taboas J, Maddox R, Krebsbach P, Hollister S. Indirect solid free form fabrication of local and global porous, biomimetic and composite 3D polymer-ceramic scaffolds. Biomaterials 2003;24:181-94.
[112] Leong KF, Cheah CM, Chua CK. Solid freeform fabrication of three-dimensional scaffolds for engineering replacement tissues and organs. Biomaterials 2003;24:2363-78.

[113] Oh SH, Park SC, Kim HK, Koh YJ, Lee J-H, Lee MC, Lee JH. Degradation behavior of 3D porous polydioxanone-b-polycaprolactone scaffolds fabricated using the melt-molding particulate-leaching method. Journal of Biomaterials Science, Polymer Edition 2011;22:225-37.
[114] Gomes ME, Godinho J, Tchalamov D, Cunha A, Reis R. Design and processing of starch based scaffolds for hard tissue engineering. Journal of Applied Medical Polymers 2002;6:75-80.
[115] Wu L, Jing D, Ding J. A "room-temperature" injection molding/particulate leaching approach for fabrication of biodegradable three-dimensional porous scaffolds. Biomaterials 2006;27:185-91.
[116] Salgado A, Coutinho O, Reis R. Novel starch-based scaffolds for bone tissue engineering: cytotoxicity, cell culture, and protein expression. Tissue engineering 2004;10:465-74.
[117] Jacobs LJ, Kemmere MF, Keurentjes JT. Sustainable polymer foaming using high pressure carbon dioxide: a review on fundamentals, processes and applications. Green Chemistry 2008;10:731-8.
[118] Lee SJ, Oh SH, Liu J, Soker S, Atala A, Yoo JJ. The use of thermal treatments to enhance the mechanical properties of electrospun poly (ε-caprolactone) scaffolds. Biomaterials 2008;29:1422-30.
[119] Meijer GJ, de Bruijn JD, Koole R, van Blitterswijk CA. Cell-based bone tissue engineering. PLoS medicine 2007;4:e9.
[120] Heath CA. Cells for tissue engineering. Trends in biotechnology 2000;18:17-9.
[121] Griffith LG, Naughton G. Tissue engineering--current challenges and expanding opportunities. Science 2002;295:1009-14.
[122] Bianco P, Robey PG. Stem cells in tissue engineering. Nature 2001;414:118-21.
[123] Alison MR, Poulsom R, Forbes S, Wright NA. An introduction to stem cells. The Journal of pathology 2002;197:419-23.
[124] Preston S, Alison M, Forbes S, Direkze N, Poulsom R, Wright N. The new stem cell biology: something for everyone. Molecular Pathology 2003;56:86.
[125] Presnell SC, Petersen B, Heidaran M. Stem cells in adult tissues. Seminars in cell & developmental biology: Elsevier; 2002. p. 369-76.
[126] Reubinoff BE, Pera MF, Fong C-Y, Trounson A, Bongso A. Embryonic stem cell lines from human blastocysts: somatic differentiation in vitro. Nature biotechnology 2000;18:399-404.
[127] Itskovitz-Eldor J, Schuldiner M, Karsenti D, Eden A, Yanuka O, Amit M, Soreq H, Benvenisty N. Differentiation of human embryonic stem cells into embryoid bodies compromising the three embryonic germ layers. Molecular medicine 2000;6:88.
[128] Buttery L, Bourne S, Xynos J, Wood H, Hughes F, Hughes S, Episkopou V, Polak J. Differentiation of osteoblasts and in vitro bone formation from murine embryonic stem cells. Tissue engineering 2001;7:89-99.
[129] Wobus AM. Potential of embryonic stem cells. Molecular aspects of medicine 2001;22:149-64.
[130] Young HE, Black AC. Adult stem cells. The Anatomical Record 2004;276:75-102.
[131] Sekiya I, Larson BL, Smith JR, Pochampally R, Cui JG, Prockop DJ. Expansion of human adult stem cells from bone marrow stroma: conditions that maximize the yields of early progenitors and evaluate their quality. Stem cells 2002;20:530-41.
[132] Gimble J, Guilak F. Adipose-derived adult stem cells: isolation, characterization, and differentiation potential. Cytotherapy 2003;5:362-9.
[133] Yoshimura H, Muneta T, Nimura A, Yokoyama A, Koga H, Sekiya I. Comparison of rat mesenchymal stem cells derived from bone marrow, synovium, periosteum, adipose tissue, and muscle. Cell and tissue research 2007;327:449-62.
[134] Toma JG, Akhavan M, Fernandes KJ, Barnabé-Heider F, Sadikot A, Kaplan DR, Miller FD. Isolation of multipotent adult stem cells from the dermis of mammalian skin. Nature cell biology 2001;3:778-84.

[135] Pittenger MF, Mackay AM, Beck SC, Jaiswal RK, Douglas R, Mosca JD, Moorman MA, Simonetti DW, Craig S, Marshak DR. Multilineage potential of adult human mesenchymal stem cells. Science 1999;284:143-7.
[136] Jiang Y, Jahagirdar BN, Reinhardt RL, Schwartz RE, Keene CD, Ortiz-Gonzalez XR, Reyes M, Lenvik T, Lund T, Blackstad M. Pluripotency of mesenchymal stem cells derived from adult marrow. Nature 2002;418:41-9.
[137] Jaiswal N, Haynesworth SE, Caplan AI, Bruder SP. Osteogenic differentiation of purified, culture-expanded human mesenchymal stem cells in vitro. Journal of cellular biochemistry 1997;64:295-312.
[138] Devine SM. Mesenchymal stem cells: will they have a role in the clinic? Journal of cellular biochemistry 2002;85:73-9.
[139] Pittenger MF. When The Body Can't Heal Itself. Nature 2001;414:132-.
[140] Lee K, Silva EA, Mooney DJ. Growth factor delivery-based tissue engineering: general approaches and a review of recent developments. Journal of the Royal Society Interface 2011;8:153-70.
[141] Bessa PC, Casal M, Reis R. Bone morphogenetic proteins in tissue engineering: the road from laboratory to clinic, part II (BMP delivery). Journal of tissue engineering and regenerative medicine 2008;2:81-96.
[142] Maegawa N, Kawamura K, Hirose M, Yajima H, Takakura Y, Ohgushi H. Enhancement of osteoblastic differentiation of mesenchymal stromal cells cultured by selective combination of bone morphogenetic protein-2 (BMP-2) and fibroblast growth factor-2 (FGF-2). Journal of tissue engineering and regenerative medicine 2007;1:306-13.
[143] Lind M, Bünger C. Factors stimulating bone formation. European Spine Journal 2001;10:S102-S9.
[144] Gallea S, Lallemand F, Atfi A, Rawadi G, Ramez V, Spinella-Jaegle S, Kawai S, Faucheu C, Huet L, Baron R. Activation of mitogen-activated protein kinase cascades is involved in regulation of bone morphogenetic protein-2-induced osteoblast differentiation in pluripotent C2C12 cells. Bone 2001;28:491-8.
[145] Jadlowiec JA, Celil AB, Hollinger JO. Bone tissue engineering: recent advances and promising therapeutic agents. Expert opinion on biological therapy 2003;3:409-23.
[146] Roberts AB, Sporn MB. Transforming growth factor-β. The molecular and cellular biology of wound repair: Springer; 1988. p. 275-308.
[147] Nakajima Y, Yamagishi T, Hokari S, Nakamura H. Mechanisms involved in valvuloseptal endocardial cushion formation in early cardiogenesis: Roles of transforming growth factor (TGF)-β and bone morphogenetic protein (BMP). The Anatomical Record 2000;258:119-27.
[148] Canalis E, Agnusdei D. Insulin-like growth factors and their role in osteoporosis. Calcified tissue international 1996;58:133-4.
[149] Van der Kraan P, Buma P, Van Kuppevelt T, Van den Berg W. Interaction of chondrocytes, extracellular matrix and growth factors: relevance for articular cartilage tissue engineering. Osteoarthritis and Cartilage 2002;10:631-7.
[150] Hankemeier S, Keus M, Zeichen J, Jagodzinski M, Barkhausen T, Bosch U, Krettek C, Griensven MV. Modulation of proliferation and differentiation of human bone marrow stromal cells by fibroblast growth factor 2: potential implications for tissue engineering of tendons and ligaments. Tissue engineering 2005;11:41-9.
[151] Rasubala L, Yoshikawa H, Nagata K, Iijima T, Ohishi M. Platelet-derived growth factor and bone morphogenetic protein in the healing of mandibular fractures in rats. British Journal of Oral and Maxillofacial Surgery 2003;41:173-8.
[152] Marx RE, Carlson ER, Eichstaedt RM, Schimmele SR, Strauss JE, Georgeff KR. Platelet-rich plasma:

growth factor enhancement for bone grafts. Oral Surgery, Oral Medicine, Oral Pathology, Oral Radiology, and Endodontology 1998;85:638-46.
[153] Beard Jr EL. The American Society of Health System Pharmacists. JONA'S healthcare law, ethics and regulation 2001;3:78-9.
[154] Cheng S-L, Yang JW, Rifas L, Zhang S-F, Avioli LV. Differentiation of human bone marrow osteogenic stromal cells in vitro: induction of the osteoblast phenotype by dexamethasone. Endocrinology 1994;134:277-86.
[155] Yoon JJ, Kim JH, Park TG. Dexamethasone-releasing biodegradable polymer scaffolds fabricated by a gas-foaming/salt-leaching method. Biomaterials 2003;24:2323-9.
[156] Oshina H, Sotome S, Yoshii T, Torigoe I, Sugata Y, Maehara H, Marukawa E, Omura K, Shinomiya K. Effects of continuous dexamethasone treatment on differentiation capabilities of bone marrow-derived mesenchymal cells. Bone 2007;41:575-83.
[157] Zhang W, Feng C, Yang G, Li G, Ding X, Wang S, Dou Y, Zhang Z, Chang J, Wu C. 3D-printed scaffolds with synergistic effect of hollow-pipe structure and bioactive ions for vascularized bone regeneration. Biomaterials. 2017;135:85-95.
[158] Wang F, Zhai D, Wu C, Chang J. Multifunctional mesoporous bioactive glass/upconversion nanoparticle nanocomposites with strong red emission to monitor drug delivery and stimulate osteogenic differentiation of stem cells. Nano Res. 2016;9:1193-208.
[159] Chen Y, Wang J, Zhu X, Fan Y, Zhang X. Adsorption and release behaviors of vascular endothelial growth factor on porous hydroxyapatite ceramic under competitive conditions. J. Biomater. Tissue Eng. 2014;4:155-61.
[160] Du C, Cui F, Zhang W, Feng Q, Zhu X, De Groot K. Formation of calcium phosphate/collagen composites through mineralization of collagen matrix. J. Biomed. Mater. Res., Part A. 2000;50:518-27.
[161] Soriano I, Evora C. Formulation of calcium phosphates/poly (d, l-lactide) blends containing gentamicin for bone implantation. J. Controlled Release 2000;68:121-34.
[162] Ongpipattanakul B, Nguyen T, Zioncheck TF, Wong R, Osaka G, DeGuzman L, Lee WP, Beck LS. Development of tricalcium phosphate/amylopectin paste combined with recombinant human transforming growth factor beta 1 as a bone defect filler. J. Biomed. Mater. Res., Part A. 1997;36:295-305.
[163] Fujishiro Y, Takahashi K, Sato T. Preparation and compressive strength of α-tricalcium phosphate/gelatin gel composite cement. J. Biomed. Mater. Res. 2001;54:525-30.
[164] Kim HW, Knowles JC, Kim HE. Hydroxyapatite and gelatin composite foams processed via novel freeze-drying and crosslinking for use as temporary hard tissue scaffolds. J. Biomed. Mater. Res., Part A. 2005;72:136-45.
[165] Le Nihouannen D, Le Guehennec L, Rouillon T, Pilet P, Bilban M, Layrolle P, Daculsi G. Micro-architecture of calcium phosphate granules and fibrin glue composites for bone tissue engineering. Biomaterials. 2006;27:2716-22.
[166] Ripamonti U, Parak R, Klar RM, Dickens C, Dix-Peek T, Duarte R. The synergistic induction of bone formation by the osteogenic proteins of the TGF-β supergene family. Biomaterials. 2016;104:279-96.
[167] Wadhwa R, Lagenaur CF, Cui XT. Electrochemically controlled release of dexamethasone from conducting polymer polypyrrole coated electrode. J. Controlled Release. 2006;110:531-41.
[168] Zhang Y, Zhang M. Calcium phosphate/chitosan composite scaffolds for controlled in vitro antibiotic drug release. J. Biomed. Mater. Res. 2002;62:378-86.
[169] Ziegler J, Mayr-Wohlfart U, Kessler S, Breitig D, Günther KP. Adsorption and release properties of growth factors from biodegradable implants. J. Biomed. Mater. Res. 2002;59:422-8.

[170] Chou JW-L, Decarie D, Dumont RJ, Ensom MH. Stability of Dexamethasone in Extemporaneously Prepared Oral Suspensions. J. Can. Pharm. Hosp. 2001;54:97-103.
[171] Amjadian S, Seyedjafari E, Zeynali B, Shabani I. The synergistic effect of nano-hydroxyapatite and dexamethasone in the fibrous delivery system of gelatin and poly (l-lactide) on the osteogenesis of mesenchymal stem cells. Int. J. Pharm. 2016;507:1-11.
[172] Qiu K, Chen B, Nie W, Zhou X, Feng W, Wang W, Chen L, Mo X, Wei Y, He C. Electrophoretic deposition of dexamethasone-loaded mesoporous silica nanoparticles onto poly (L-lactic acid)/poly (ε-caprolactone) composite scaffold for bone tissue engineering. CS Appl. Mater. Interfaces 2016;8:4137-48.
[173] Frenkel SR, Di Cesare PE. Scaffolds for articular cartilage repair. Annals of biomedical engineering 2004;32:26-34.
[174] Hunziker E. Articular cartilage repair: basic science and clinical progress. A review of the current status and prospects. Osteoarthritis and cartilage 2002;10:432-63.
[175] Li L, Zhou G, Wang Y, Yang G, Ding S, Zhou S. Controlled dual delivery of BMP-2 and dexamethasone by nanoparticle-embedded electrospun nanofibers for the efficient repair of critical-sized rat calvarial defect. Biomaterials 2015;37:218-29.
[176] Urist MR, DeLange RJ, Finerman G. Bone cell differentiation and growth factors. Science 1983;220:680-6.

Chapter 2

Preparation of dexamethasone-loaded biphasic calcium phosphate nanoparticles for osteogenic differentiation of human mesenchymal stem cells

2.1 Summary

As an earliest known and readily available osteogenic inducer for stem cells, DEX plays a key role in affecting cell functions and cellular processes, especially for cell proliferation and differentiation. However, the clinical application of DEX has been limited because of its uncontrolled release. An ideal carrier is desired to control DEX release for osteogenic differentiation of stem cells and bone tissue engineering. Biphasic calcium phosphate nanoparticles (BCP NPs) should be a potential carrier for DEX due to their osteoconductive property and good biocompatibility as a bone graft biomaterial. In this part, DEX-loaded BCP NPs were prepared by two methods: (1) immersion of BCP NPs in a DEX solution (defined as DEX/BCP NPs), (2) DEX incorporation during BCP NPs formation in a calcifying solution (defined as DEX@BCP NPs). The DEX@BCP NPs showed higher DEX loading amount and more sustainable DEX release than did the DEX/BCP NPs. The DEX@BCP NPs were used for culture of hMSCs and showed a promotive effect on proliferation of hMSCs. Furthermore, the DEX@BCP NPs significantly increased the alkaline phosphatase (ALP) activity, calcium deposition and gene expressions of osteogenic markers of hMSCs when compared to BCP NPs without DEX loading. The results demonstrated BCP NPs are a good carrier for DEX loading and the DEX@BCP NPs should have useful guidance for bone tissue engineering.

2.2 Introduction

Bone defect has become one of the big menaces in human daily life. Although bone is one of the few regenerative tissues in human body, its regenerative ability is limited [1]. Some bone defects undergo incomplete fracture healing (nonunion fractures) and sometimes the defect size is beyond the body's healing capacity (critical size defects) [2, 3]. Therefore, further intervention is required to treat these fractures and defects. At present, autologous and allogenic bone grafts are the two main choices to replace the damaged bone. However, both of them have many problems such as limited autologous donor tissues, donor site

morbidity and immunological rejection of allogenic grafts [4]. Instead, a number of artificially synthesized biomaterials such as ceramics, alloys and polymers have been developed for the repair of bone defects [5-7]. Although these biomaterials are osteoconductive, they generally do not have osteoinductive capacity [8, 9]. On the other hand, osteoinductive cues such as bone growth factors are able to induce bone formation, even in nonskeletal sites (e.g., muscle) [10]. Hence, combination of an osteoconductive biomaterial with osteoinductive cues is supposed to overcome the limitations of conventional bone graft biomaterials. Such hybrid biomaterials can have both osteoconductive and osteoinductive capacities and accelerate bone formation and regeneration when implanted.

Protein growth factors are most commonly used as osteoinductive cues. However, there are some shortages of protein growth factors such as the limited sources, high price, short half-life and easily lost activity [11, 12]. One way to solve those problems is using stable and inexpensive low-molecular-weight molecules to substitute the role of protein growth factors. One of such low molecular weight molecules used for bone regeneration is dexamethasone (DEX). DEX is a kind of glucocorticoid with high potency and long-acting property [13]. As one of the earliest known and readily available osteogenic inducers for mesenchymal stem cells (MSCs), DEX plays a key role in controlling expression of osteogenic marker genes [14]. MSCs cultured with continuous DEX treatment exhibit higher expression level of osteogenic markers and a higher positive rate of osteogenic colony formation than those without DEX treatment [15]. To date, several DEX delivery methods are available, ranging from systemic injection [16], eluting coating [17, 18], and loading within biodegradable polymer carriers [19, 20]. Nevertheless, systemic injection has the obvious disadvantage of exposing the whole body to high dosage of the drug, while the release of DEX from eluting coatings can neither last as long as the required period for biomedical application nor release appropriate dose in response to the dynamic change of the local biochemical environment.

Compared with biodegradable polymer carriers, calcium phosphate nanoparticles (CaP NPs) have been showing enormous potential as carriers of osteoinductive factors because CaP NPs are the inorganic component of natural bone. CaP NPs are biocompatible and biodegradable [21, 22], which are essential properties for drug carriers. Furthermore, synthesis of CaP NPs is a straightforward precipitation process. Incorporation of drug molecules only requires molecules of interest be present during the particle formation [23-25]. Hence, CaP NPs have been widely used as carriers for drugs [26, 27], proteins [28, 29], DNA and RNA [30, 31]. Nevertheless, to our knowledge, no literature has reported the application of CaP as the carrier of DEX. Therefore, in this study DEX was incorporated in biphasic calcium phosphate nanoparticles (BCP NPs) by immersion method and precipitation method to prepare DEX-loaded BCP NPs. The release profile of DEX and their effects on the osteogenic differentiation of human bone marrow-derived MSCs (hMSCs) were investigated.

2.3 Materials and methods

2.3.1 Materials

Calcium nitrate tetrahydrate ($Ca(NO_3)_2 \cdot 4H_2O$, 99.9%), ammonium phosphate dibasic ($(NH_4)_2HPO_4$, ≥ 98.0%), dexamethasone ($C_{22}H_{29}FO_5$, ≥97%), ammonium hydroxide solution (NH_4OH, 28.0~30.0%), Dulbecco's Modified Eagle's Medium (DMEM), penicillin, streptomycin, β-glycerophosphate, alizarin Red S, 2-amino-2-methyl-1,3-propanediol, naphthol AS-MX phosphate, fast blue RR salt, trypsin/EDTA were purchased from Sigma-Aldrich (St. Louis, MO, USA). Fetal bovine serum (FBS) was purchased from Gibco Lab. (Grand Island, NY, USA). Hydrochloric acid and 4% paraformaldehyde were purchased from Wako

Pure Chemical Industries, Ltd. (Tokyo, Japan). WST-1 reagent was obtained from Roche Molecular Biochemicals (Mannheim, Germany). Cellstain Live-Dead Double Staining kit was purchased from Dojindo Lab. (Kumamoto, Japan). Pierce® BCA Protein Assay Kit was purchased from Thermo Fisher Scientific Inc. (Rockford, USA). Sensolyte® pNPP Alkaline Phosphatase Assay Kit was purchased from AnaSpec Inc. (California, USA). RNeasy Mini Kit was purchased from Qiagen (Hilden, Germany). All the chemical reagents were used as received without further purification. The water used in all the experiments was ultrapure water with a resistivity of 18.2 MΩ.cm purified by a Q-POD Milli-Q water purification system (Millipore Corp., Billerica, MA, USA).

2.3.2 Synthesis of BCP NPs and DEX-loaded BCP NPs

Biphasic calcium phosphate (HA/TCP = 60/40, theoretical value) nanoparticles (BCP NPs) were synthesized according to a previously reported method with some modifications [32]. 50.0 mL of 0.5 M calcium nitrate tetrahydrate solution was added dropwise to 33.4 mL of 0.5 M ammonium phosphate dibasic solution at a speed of 150 mL/h by a syringe pump (KD Scientific Inc., USA). The reaction was conducted in a 55 °C water bath under magnetic stirring (700 rpm). The pH value in the reaction solution was real-time monitored by an F-23 pH/ION meter (HORIBA Ltd., Japan). Ammonium hydroxide solution was added dropwise to the reaction solution during the whole reaction procedure to keep the pH value to be 9.5. After that, the reaction was maintained for another 30 minutes in the 55 °C water bath at the same stirring speed. Subsequently, the slurry was kept at room temperature for 36 hours for an aging process to form the stable BCP NPs.

Based on the BCP NPs preparation procedure, two methods were used to load DEX in the BCP NPs. For the first method, the BCP NPs were prepared and then immersed in an ethanol solution of DEX with different concentrations. The ethanol solution of DEX was prepared by dissolving different amount of DEX (0.5, 1.0, 1.5, 2.0, 2.5, 3.0, 3.5, 4.0, 4.5 and 5.0 mg) in 2 mL ethanol. The mixture solution was further stirred by a magnetic stirrer (700 rpm) at room temperature for 50 minutes to prepare the DEX-loaded BCP NPs (defined as DEX/BCP NPs). For the second method, DEX was incorporated during the formation of the BCP NPs. At first, different amount of DEX (0.5, 1.0, 1.5, 2.0, 2.5, 3.0, 3.5, 4.0, 4.5 and 5.0 mg) was dissolved in 2 mL ethanol. The 2-mL ethanol solution of DEX was added to 48.0 mL of 0.52 M calcium nitrate tetrahydrate aqueous solution. Subsequently, the mixture solution of DEX and calcium nitrate tetrahydrate was added dropwise to 33.4 mL of 0.5 M ammonium phosphate dibasic solution in a 55 °C water bath under magnetic stirring (700 rpm). Ammonium hydroxide solution was added dropwise to the reaction solution during the whole reaction procedure to keep the pH value to be 9.5. The reaction was maintained for another 30 minutes in the 55 °C water bath at the same stirring speed. Finally, the reaction was kept at room temperature for 36 hours for aging to get the slurry of DEX-loaded BCP NPs (defined as DEX@BCP NPs). The BCP NPs, DEX/BCP NPs and DEX@BCP NPs prepared above were collected by centrifuging the respective slurries at 8000 rpm for 5 min and washed with Milli-Q water for more than five times until the pH value of the supernatant liquid returned to 7. The NPs were re-dispersed in Milli-Q water and stored at 4 °C for further use.

The morphology of the prepared NPs was observed with a JEOL 2100F transmission electron microscope (TEM, JEOL, Tokyo, Japan) with an operating voltage of 200 kV. The TEM samples were prepared by dropping 8 μL of the NPs solution onto a carbon-covered copper grid, following by drying in air. Hydrodynamic size and zeta potential measurements were performed on a DelsaTM Nano C Particle Analyzer (Beckman Coulter, Fullerton, CA, USA). The X-ray diffraction (XRD) patterns of the NPs were characterized using a Rigaku Rint-2000 Ultima III X-ray diffractometer (Rigaku, Tokyo, Japan).

2.3.3 Measurement of DEX loading amount and *in vitro* release profile

To measure the DEX loading amount, 10 mg DEX/BCP NPs or DEX@BCP NPs prepared with different initial feeding amount of DEX were dissolved in 0.3 mL 1 M HCl. And then 1.7 mL PBS (pH 7.4) was added to dilute the samples. The DEX concentration in the samples was determined by using a UV-vis spectrophotometer (Jasco Corp., Tokyo, Japan) at 242 nm with a calibration curve of free DEX. The loading amount was calculated from the concentration, solution volume and amount of DEX/BCP NPs or DEX@BCP NPs. The loading efficiency of DEX was calculated by dividing the loading amount with the initial feeding amount of DEX. *In vitro* release of DEX from the DEX/BCP NPs or DEX@BCP NPs was carried out in PBS solution (pH 7.4). The DEX/BCP NPs or DEX@BCP NPs (20 mg) were suspended in 1 mL of PBS. The suspension solution of DEX/BCP NPs or DEX@BCP NPs was transferred to dialysis bags (cut-off molecular weight: 1000 Da) and the bags were placed in centrifuge tubes containing 4 mL PBS. The tubes were shaken at a speed of 60 rpm at 37 °C. At time points of 0.25, 0.5, 0.75, 1, 1.25, 1.5, 1.75, 2, 2.5, 3, 5, 7, 9, 11, 13, 15, 17, 19 and 21 days, the amount of DEX released in the PBS was monitored via a UV-vis spectrophotometer at 242 nm. Percentage of DEX released from the DEX/BCP NPs or DEX@BCP NPs was calculated by dividing the total amount of released DEX with the loading amount of DEX. At each time point, three samples of DEX/BCP NPs or DEX@BCP NPs were used for the measurements to calculate the means and standard deviations.

2.3.4 Cell culture and cell proliferation assay

Human bone marrow-derived mesenchymal stem cells (hMSCs, passage 2) were purchased from LONZA (Walkersville MD, USA). The cells were cultured in 175 cm2 tissue culture flasks (BD Falcon, USA) with normal cell culture medium at 37 °C and 5% CO2 and passaged after reaching confluence. The passage 4 hMSCs were seeded in 24-well cell culture plates at a density of 0.5 × 104 cells/cm2 and were cultured at 37 °C and 5% CO2. The cell culture medium was DMEM supplemented with 10% FBS, 100 U/mL penicillin and 100 μg/mL streptomycin. After culture for 6 h, the medium was changed. The hMSCs cultured in 24-well cell culture plate with 1 mL of fresh cell culture medium without NPs supplement in each well was designated as a negative control (NC). The hMSCs cultured in 24-well cell culture plate with 1 mL fresh cell culture medium supplemented with 10 mM β-glycerophosphate and 100 nM dexamethasone but without NPs in each well were designated as a positive control (PC). The hMSCs cultured in 24-well cell culture plate with 1 mL fresh cell culture medium supplemented with 10 mM β-glycerophosphate and NPs (BCP NPs or DEX@BCP NPs) at different concentrations (25, 100, 250 and 500 μg/mL) in each well were designated as experimental groups. For all the groups, the medium was changed every 3 days.

The viability of hMSCs of different groups after culture for 1, 3 and 7 days was analysed by a WST-1 assay. The cells were washed with PBS and 1 mL of WST-1 solution (100 μL of WST-1 stock solution diluted with 900 μL of complete medium) was added into each well. The cells were further cultured for another 3 h. Afterwards, the solution was transferred to 96-well plates (200 μL per well). The absorbance of each well was measured at 440 nm using a plate reader (Benchmark Plus, Bio-Rad, Hercules, CA, USA). Every four samples of each group were used for the measurement to calculate means and standard deviations. In addition, live/dead staining of hMSCs was conducted with a cell stain live/dead double staining kit to confirm the live and dead cells in all groups. The hMSCs cultured for 3 days were washed twice with warm PBS and incubated in serum-free DMEM medium containing calcein-AM and propidium iodide (PI) for 15 min. An inverted fluorescence microscope (Olympus, Japan) was used to capture the live/dead images.

2.3.5 Alkaline phosphatase (ALP) staining and ALP activity assay

ALP expression of the hMSCs in different groups after culture for 14 days was visualized by ALP staining. The cells were washed twice with PBS and subsequently fixed with 4% paraformaldehyde at room temperature for 10 min. The fixed cells were further washed twice with PBS and incubated with 0.1% naphthol AS-MX phosphate and 0.1% fast blue RR salt in 56 mM 2-amino-2-methyl-1,3-propanediol working solution (pH = 9.9) at room temperature for 10 min. After the working solution was discarded and and the plates were washed with PBS, the cells were observed using an optical microscope.

ALP activity assay was carried out by using the Sensolyte® pNPP alkaline phosphatase assay kit (Anaspec, USA) according to the manufacturer's instructions. After being cultured for 14 days, the cells in each well were washed twice with PBS, lysed with 0.2% Triton-X 100, scraped off the plates and collected into a microcentrifugation tube. After incubation at 4 °C for 10 min under agitation, the lysate was centrifuged at 2500× g for 10 min to collect the supernatant. The supernatant was incubated with p-nitrophenyl phosphate (pNPP) substrate solution and the color change was measured with a plate reader at a wavelength of 405 nm. A calibration curve was drawn by using ALP standard solution to determine the concentration of ALP in each well. The relative ALP amount was normalized by total protein amount analysed by a Pierce® BCA Protein Assay Kit. Every three wells of each sample were used for the measurements to calculate the means and standard deviations.

2.3.6 Alizarin Red S (ARS) staining and calcium deposition assay

After 21 days of culture, calcium deposition of the hMSCs in all groups was measured by ARS staining. The cells were washed twice with PBS, fixed with 4% paraformaldehyde at room temperature for 10 min and incubated with 0.1% Alizarin Red S solution at room temperature for 30 min. The stained cells were washed twice with PBS and observed using an optical microscope. For a quantitative calcium deposition assay, the stained cells were dried in air overnight and then eluted with 5% perchloric acid at room temperature for 20 min. The solution in each well was transferred into a 96-well plate and the absorbance was recorded with a plate reader at 405 nm. The results were normalized by total protein amount. Every three wells of each sample were used for the measurements.

2.3.7 Quantitative real-time polymerase chain reaction (PCR)

To analyse gene expression of the osteogenic markers of the hMSCs in different groups after culture for 21 days, the cells were washed twice with PBS and collected for RNA extraction with the RNAeasy Mini kit (Qiagen, Netherlands) according to the manufacturer's instructions. A first stand cDNA synthesis kit was used to convert the obtained RNA to cDNA. Real-time PCR was performed on a 7500 Real-Time PCR system (Applied Biosystems, USA) according to previously reported protocol [33]. The expression level of GAPDH, a housekeeping gene, was used as an endogenous control. The relative expression level of each target gene was calculated by using $2^{-\Delta\Delta Ct}$ formula and gene expression in negative control was used as a reference. The primers and probes used for real time PCR are listed in Table 1.1.

2.3.8 Statistical analysis

All data are presented as mean ± standard deviation (SD) with experiments repeated in triplicate (n = 3).

Statistical analysis was performed using One-way ANOVA to evaluate the significance of the experimental data. A difference was considered significant when the p-value was less than 0.05. The data indicated with (*) refers to $p < 0.05$ compared with the negative control; (△) refers to $p < 0.05$ compared with the positive control; (#) refers to $p < 0.05$ compared with BCP NPs.

Table 1.1. The primers and probes for real-time PCR.

mRNA	Oligonucleotide
18 S rRNA	Hs99999901_s1
GAPDH	Hs99999905_m1
ALP	Forward 5'-GACCCTTGACCCCCACAAT-3' Reverse 5'-GCTCGTACTGCATGTCCCCT-3' Probe 5'-TGGACTACCTATTGGGTCTCTTCGAGCCA-3'
Runx2	Hs00231692_m1
IBSP	Forward 5'-TGCCTTGAGCCTGCTTCC-3' Reverse 5'-GCAAAATTAAAGCAGTCTTCATTTTG-3' Probe 5'-CTCCAGGACTGCCAGAGGAAGCAATCA-3'
BMP-2	Hs00154192_m1

2.4 Results

2.4.1 Synthesis and characterization of DEX-loaded BCP NPs

The BCP NPs were prepared from calcium nitrate tetrahydrate solution and ammonium phosphate dibasic solution by liquid precipitation. DEX was introduced in the BCP NPs to prepare DEX-loaded BCP NPs (DEX/BCP NPs and DEX@BCP NPs). The DEX/BCP NPs were prepared by immersing BCP NPs in a DEX solution and DEX@BCP NPs were prepared by introducing DEX during the formation of BCP NPs. The BCP NPs and DEX@BCP NPs prepared with a DEX feeding amount of 4.5 mg were used for characterization. The BCP NPs and DEX@BCP NPs could be easily dispersed in water to form stable colloid suspension solution (Fig. 2.1a). The XRD spectra of the BCP NPs and DEX@BCP NPs showed that the diffraction peaks of HA and β-TCP phases were identified (Fig. 2.1b). Major peaks at $2\theta = 25.9^o$, 31.8^o, 46.7^o and 49.5^o indicated hydroxyapatite (HA) lattice planes of (0 0 2), (2 1 1), (2 2 2) and (2 1 3), respectively. Peaks at $2\theta = 28.0^o$, 33.6^o and 53.2^o indicated β-tricalcium phosphate (β-TCP) lattice planes of (2 1 4), (1 1 12) and (2 0 20), respectively. The XRD spectrum of DEX@BCP NPs was similar to that of DEX@BCP NPs except that the XRD spectrum of DEX@BCP NPs had some slightly higher level of noise, which should be due to the DEX incorporation. No detectable alterations in the broadness of the typical peaks related to HA and β-TCP lattice plane were observed after the DEX loading. The results showed that both BCP NPs and DEX@BCP NPs were composed of HA and β-TCP, indicating the biphasic components of calcium phosphate in the NPs. Incorporation of DEX did not affect the biphasic characteristics of BCP NPs.

Dynamic light scattering (DLS) was used to measure the average hydrodynamic size of the BCP NPs and DEX@BCP NPs dispersed in water (Fig. 2.1c). The hydrodynamic size of the BCP NPs and DEX@BCP NPs was 895.0 ± 211.2 nm and 605.6 ± 191.0 nm, respectively. Furthermore, zeta potential was measured to confirm the surface charge of the prepared NPs (Fig. 2.1d). The zeta potential of the BCP NPs was -27.9 ± 1.9 mV, while that of the DEX@BCP NPs was -22.6 ± 1.0 mV. Incorporation of DEX into the BCP NPs

decreased the zeta potential of the NPs.

The BCP NPs and DEX@BCP NPs were observed by TEM to show the crystal morphology of BCP NPs before and after DEX loading. The BCP NPs had short rod-like morphology and agglomerated into needle-like crystals (Fig. 2.2a-b). The DEX@BCP NPs had similar size and morphology to those of the BCP NPs (Fig. 2.2c-d). The rod-like BCP NPs and DEX@BCP NPs had a size of 25-70 nm in length and 4-20 nm in width. The results indicated that loading of DEX did not affect the size and morphology of BCP NPs. The larger hydrodynamic sizes of the BCP NPs and DEX@BCP NPs than those measured from their TEM images should be due to agglomeration of the NPs in water.

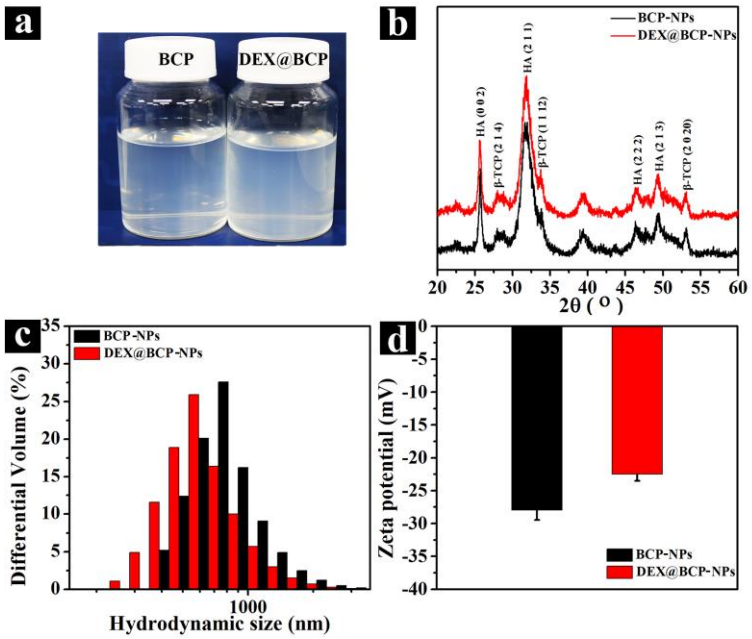

Fig. 2.1. Gross appearance photographs of aqueous solution of the BCP NPs and DEX@BCP NPs (a), X-ray diffraction (XRD) pattern (b), hydrodynamic size (c) and zeta potential (d) of the BCP NPs and DEX@BCP NPs.

2.4.2 DEX loading and release profile of DEX-loaded BCP NPs

The amount of DEX loaded in the DEX/BCP NPs and DEX@BCP NPs prepared with different initial feeding amount of DEX (0.5, 1.0, 1.5, 2.0, 2.5, 3.0, 3.5, 4.0, 4.5 and 5.0 mg) was determined by using a UV-vis spectrophotometer (Fig. 2.3). For the DEX/BCP NPs prepared by method 1, the loading amount increased from 45.1 ± 11.0 ng/mg DEX/BCP NPs (DEX feeding amount: 0.5 mg) to 192.0 ± 11.3 ng/mg DEX/BCP NPs (DEX feeding amount: 4.0 mg) (Fig. 2.3a). When the feeding amount of DEX was 4.5 and 5.0 mg, the loading amount was 186.8 ± 15.6 and 189.8 ± 17.3 ng/mg DEX/BCP NPs, respectively, which indicated the DEX loading amount reached saturation. With the increase of DEX feeding amount, the loading efficiency of DEX decreased from 22.9 ± 3.5 % to 9.6 ± 0.9 % (Fig. 2.3b).

For the DEX@BCP NPs prepared by method 2, the DEX loading amount increased from 158.8 ± 14.3 to 593.8 ± 19.8 ng/mg DEX@BCP NPs with the increasing of initial feeding amount of DEX from 0.5 to 4.5 mg (Fig. 2.3a). When the initial feeding amount of DEX was 5.0 mg, the loading amount was 590.0 ± 19.2 ng/mg, which was almost the same as the loading amount when the initial feeding amount of DEX was 4.5 mg. The results indicated the loading amount reached saturation when the feeding amount of DEX was

higher than 4.5 mg. Increase of the initial feeding amount of DEX resulted in decreasing of loading efficiency from 80.7 ± 1.7 % to 30.0 ± 1.0 % (Fig. 2.3b).

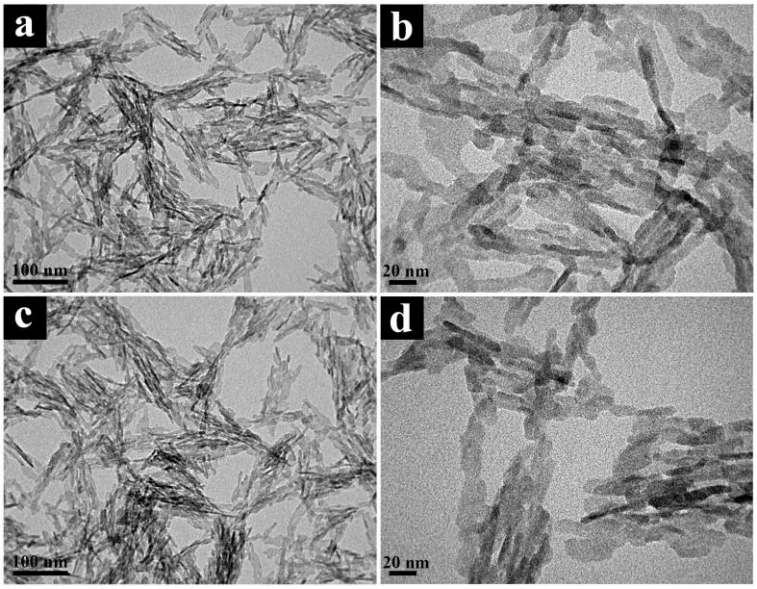

Fig. 2.2. TEM images of the BCP NPs (a and b) and DEX@BCP NPs (c and d) at low (a, c) and high (b, d) magnifications. Scale bar: (a) and (c), 100 nm; (b) and (d), 20 nm.

Based on the results of loading amount and loading efficiency, the DEX/BCP NPs and DEX@BCP NPs prepared with a feeding amount of 4.5 mg DEX were used for further release profile assay. The DEX/BCP NPs and DEX@BCP NPs showed different DEX release profiles (Fig. 2.3c and d). There was a rapid release of DEX during the first 3 d for both DEX/BCP NPs and DEX@BCP NPs. The accumulated DEX release percentage for the DEX/BCP NPs reached 82.6 ± 3.4% at day 3 and slightly increased in the following days. However, the accumulated DEX release percentage from the DEX@BCP NPs only reached 40.5 ± 3.9% at day 3 and a further sustained and controlled DEX release was observed over the 21-day period (Fig. 2.3d). The total amount of DEX released from the DEX/BCP NPs after 21 days was 176.2 ± 5.3 ng/mg DEX/BCP NPs, while that released from the DEX@BCP NPs after 21 d was 505.5 ± 19.1 ng/mg DEX@BCP NPs (Fig. 2.3c). The percentage of released DEX for DEX/BCP NPs and DEX@BCP NPs after 21 days was 94.3 ± 2.8 % and 85.1 ± 3.2 %, respectively (Fig. 2.3d).

The loading amount and release profile results indicated that the DEX@BCP NPs prepared with a feeding amount of 4.5 mg DEX reached the highest loading amount of DEX and had a sustained release of DEX for a prolonged period. High loading of DEX and sustained release of DEX are important properties of carriers for drugs and growth factors. Therefore, from all the DEX-loading BCP NPs (DEX/BCP NPs and DEX@BCP NPs), only the DEX@BCP NPs prepared with a feeding amount of 4.5 mg DEX were used for other experiments including the previous characterization and the following cell culture. The BCP NPs without DEX incorporation was used as a counterpart.

2.4.3 Cell culture and cell proliferation assay

The viability and proliferation of hMSCs cultured with BCP NPs and DEX@BCP NPs prepared with a feeding amount of 4.5 mg DEX for 1, 3 and 7 days were assessed by using live/dead staining and WST-1

assay (Fig. 2.4). The hMSCs after incubation with the BCP NPs and DEX@BCP NPs at a concentration of 25, 100, 250 and 500 μg/mL (denoted as BCP-25, BCP-100, BCP-250, BCP-500, DEX@BCP-25, DEX@BCP-100, DEX@BCP-250 and DEX@BCP-500, respectively) for 3 d were visualized by a live/dead staining (Fig. 2.4a). The cells showed well spreading morphology. No dead cells (red color) were observed in any of the groups. All the cells cultured with BCP NPs and DEX@BCP NPs and the control groups showed high viability. The results indicated the BCP NPs and DEX@BCP NPs at the studied concentrations did not affect cell viability.

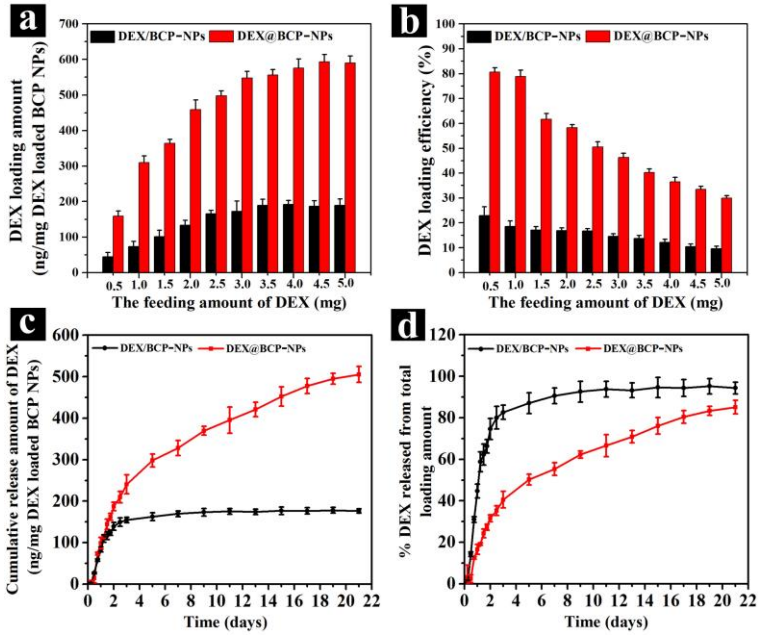

Fig. 2.3. Relation of DEX loading amount (a) and DEX loading efficiency (b) of the DEX/BCP NPs and DEX@BCP NPs with different initial feeding amount of DEX. Cumulative amount (c) and percentage (d) of released DEX from the DEX/BCP NPs and DEX@BCP NPs prepared with a feeding amount of 4.5 mg DEX. Data represent means ± SD, N=3.

WST-1 assay results showed that the cell viability of hMSCs after being cultured with the BCP NPs and DEX@BCP NPs for 1 day had no significant difference as compared to the negative and positive controls (Fig. 2.4b). The cells cultured with the BCP NPs and DEX@BCP NPs and control groups proliferated with increase of culture time. After culture for 3 days, the DEX@BCP NPs did not show evident influence on cell viability even at a high concentration of 500 μg/mL. After culture for 7 days, proliferation of hMSCs cultured with the BCP NPs was slightly higher than that of the negative control. Proliferation of hMSCs cultured with the DEX@BCP-25, DEX@BCP-100 and DEX@BCP-250 was slightly higher than that of the positive control, while the proliferation of hMSCs cultured with the DEX@BCP-500 was slightly lower than that of the positive control.

2.4.4 ALP staining and ALP activity assay

ALP is generally considered as an early stage marker of osteogenic differentiation [34]. The ALP staining and ALP activity assay were performed to investigate the osteogenic differentiation activity of hMSCs after 14 days of culture (Fig. 2.5). ALP staining demonstrated that slightly more intense staining was

observed in the cells cultured with the BCP-100, BCP-250 and BCP-500 NPs than that of the negative control group (Fig. 2.5a). Each concentration of DEX@BCP NPs showed higher degree of ALP staining than that of the BCP NPs. Meanwhile, when compared to the positive control, the cells cultured with the DEX@BCP NPs displayed a concentration-dependent increase of ALP staining level. ALP activity assay showed the cells cultured with the BCP-250, BCP-500, DEX@BCP-25, DEX@BCP-100, DEX@BCP-250 and DEX@BCP-500 had significantly higher ALP amount than did the negative control. For each concentration, DEX@BCP NPs showed significantly higher ALP amount than did the cells cultured with the BCP NPs. The ALP amount in the cells cultured with the DEX@BCP-250 and DEX@BCP-500 was higher than that of the positive control. The results indicated that ALP activity in hMSCs was promoted by the DEX@BCP NPs in a concentration-dependent manner.

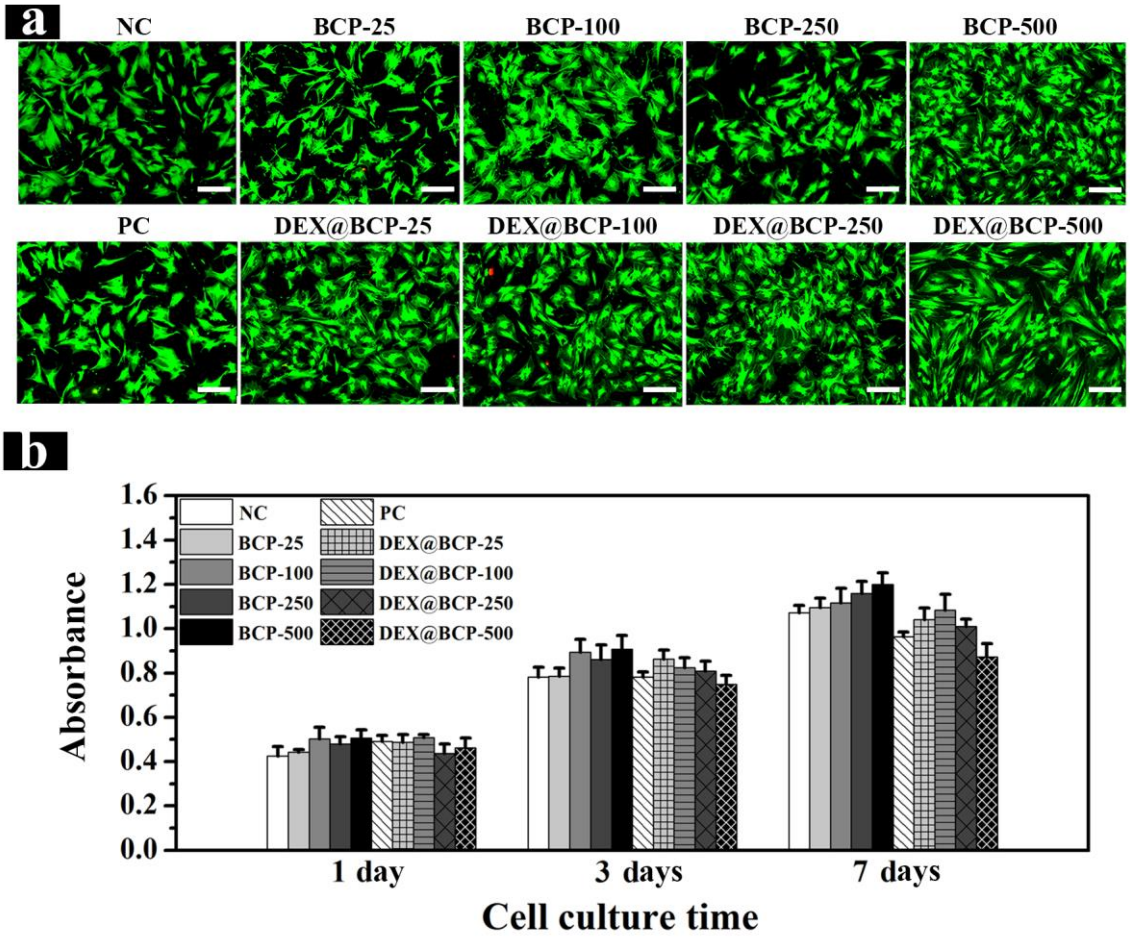

Fig. 2.4. Live/dead staining of hMSCs after culture with the BCP NPs and DEX@BCP NPs for 3 days (a) and proliferation of hMSCs after culture with the BCP NPs and DEX@BCP NPs for 1, 3 and 7 days (b). The DEX@BCP NPs prepared with a feeding amount of 4.5 mg DEX were used. The NPs concentrations were 25, 100, 250 and 500 μg/mL. NC and PC are negative and positive controls, respectively. Scale bar: 100 μm. Data represent means ± SD, N=3.

2.4.5 ARS staining and calcium deposition assay

To confirm bone matrix maturation and mineralization, calcium deposition was evaluated after hMSCs

were cultured with each concentration of the BCP NPs and DEX@BCP NPs for 21 days (Fig. 2.6). All of the experimental groups except BCP-25 group were positively stained. The ARS staining became thicker and denser with the increase of the BCP NPs and DEX@BCP NPs concentration. At the same concentration, the cells cultured with the DEX@BCP NPs were more strongly stained than the cells cultured with the BCP NPs. A quantitative analysis of ARS staining was performed by eluting ARS from the stained cells (Fig. 2.6b). Compared to cells cultured with the BCP NPs, the cells cultured with the DEX@BCP NPs displayed a significant increase in the calcium deposition. There was no significant difference between the cells cultured with the DEX@BCP-25 and the positive control. However, calcium deposition of the cells cultured with the DEX@BCP-100, DEX@BCP-250 and DEX@BCP-500 was significantly higher than that of the positive group, which showed an increasing trend in a concentration-dependent manner.

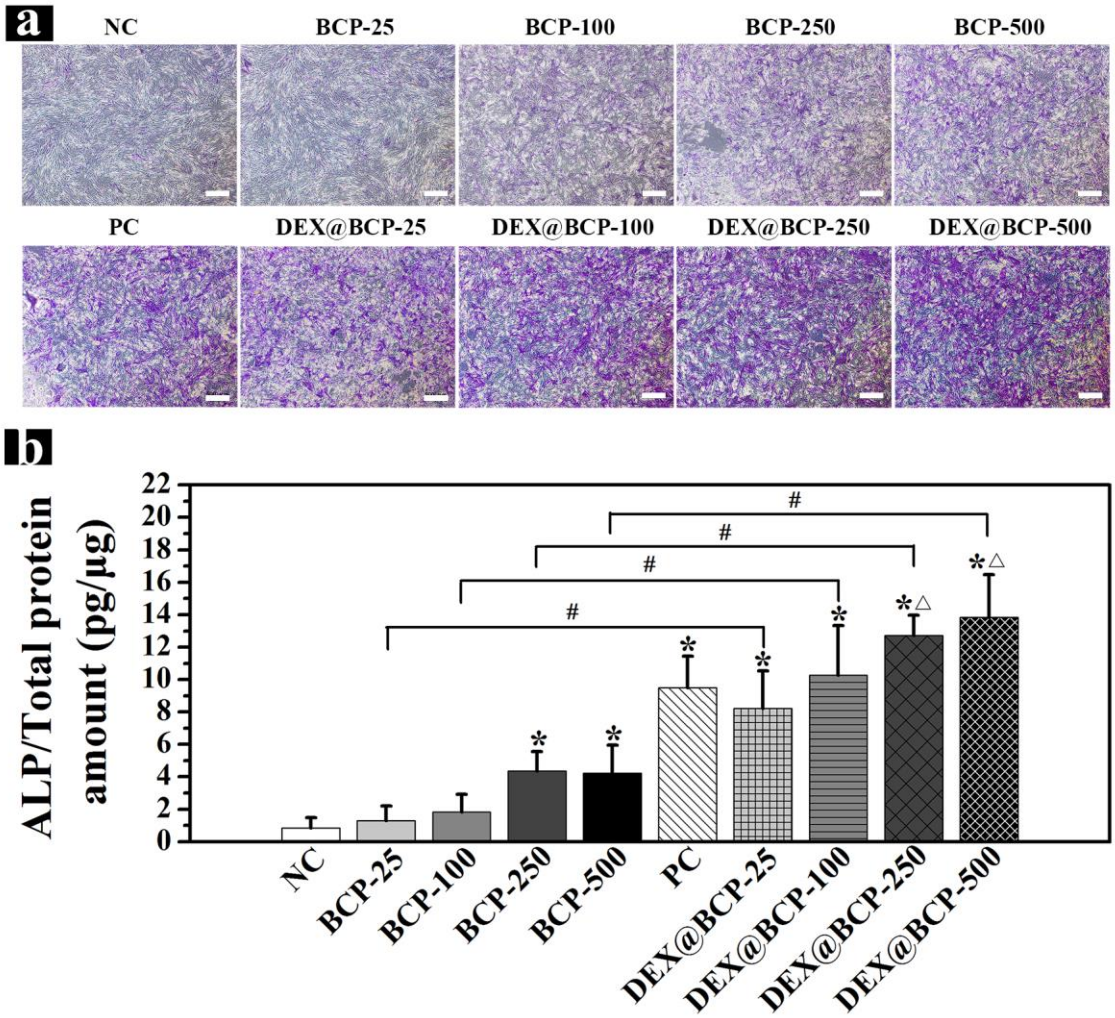

Fig. 2.5. ALP staining (a) and ALP activity assay (b) of hMSCs after culture with the BCP NPs and DEX@BCP NPs at a concentration of 25, 100, 250 and 500 μg/mL for 14 days. The DEX@BCP NPs prepared with a feeding amount of 4.5 mg DEX were used. Scale bar: 500 μm. Data represent means ± SD, N=3. (*) refers to $p < 0.05$ compared with negative control; (△) refers to $p < 0.05$ compared with positive control; (#) refers to $p < 0.05$ compared with BCP NPs.

2.4.6 Gene expression analysis

The expression of osteogenic marker genes such as ALP, runt-related transcription factor 2 (Runx2), bone sialoprotein 2 (IBSP) and bone morphogenetic protein-2 (BMP-2) in hMSCs were analysed by quantitative real-time PCR after 21 days of culture (Fig. 2.7). The results showed that both BCP NPs and DEX@BCP NPs up-regulated the gene expression of ALP, Runx2, IBSP and BMP-2 when compared to the negative control. The expression of these genes in the cells cultured with the DEX@BCP NPs was significantly higher than that of the cells cultured with the BCP NPs at the same concentrations. When compared to the positive control, ALP and IBSP genes were significantly up-regulated by the DEX@BCP-250 and DEX@BCP-500 (Fig. 2.7a and 2.7c). Runx2 gene was significantly up-regulated by the DEX@BCP-100, DEX@BCP-250 and DEX@BCP-500 (Fig. 2.7b). BMP-2 gene was significantly up-regulated by the DEX@BCP-250 (Fig. 2.7d). The results suggested that the DEX@BCP NPs stimulated gene expression of the osteogenic markers in hMSCs in a concentration-dependent manner. DEX@BCP NPs at a higher concentration resulted in higher expressions of osteogenic marker genes. The gene expression results were in good agreement with the ALP activity and calcium deposition assay results.

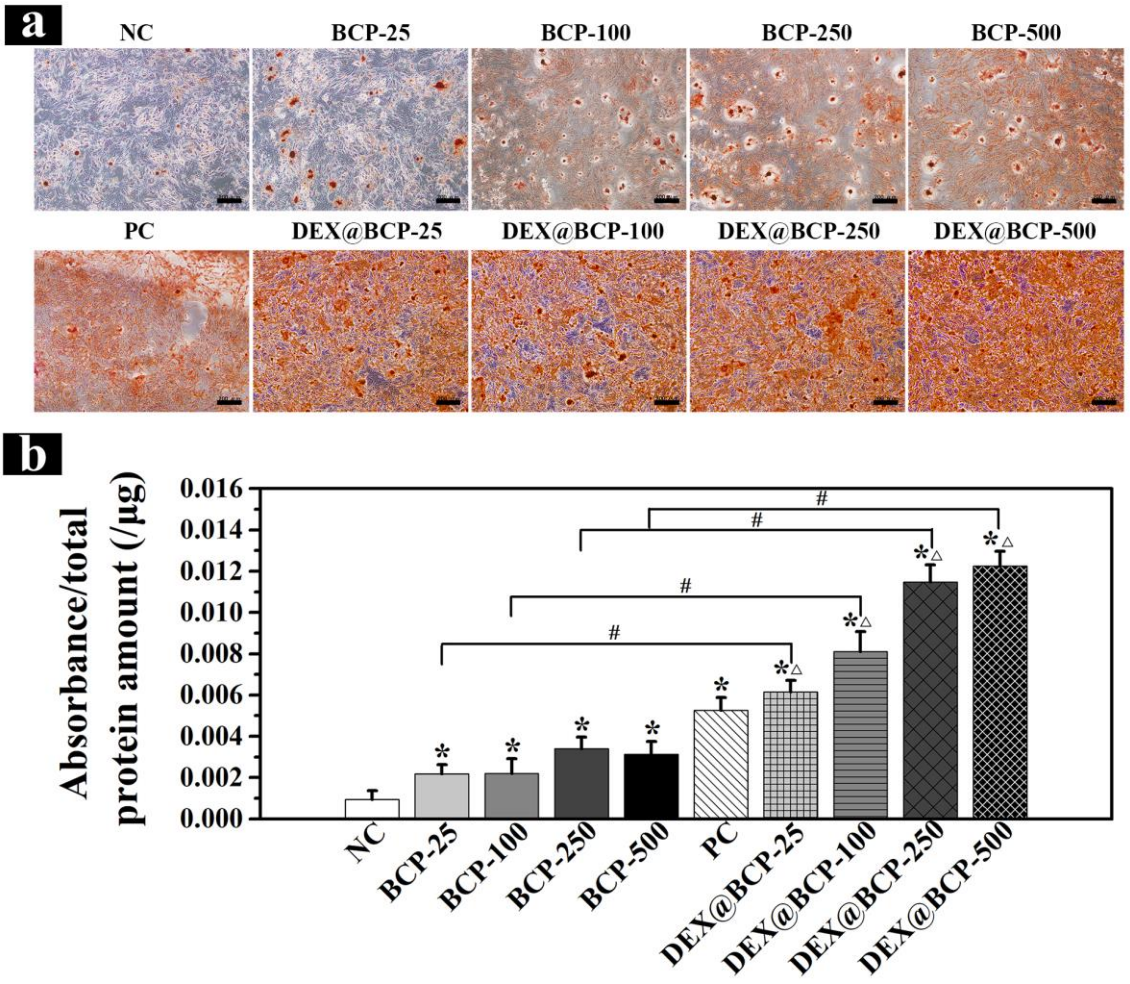

Fig. 2.6. ARS staining (a) and calcium deposition assay (b) of hMSCs after culture with the BCP NPs and DEX@BCP NPs at a concentration of 25, 100, 250 and 500 μg/mL for 21 days. The DEX@BCP NPs prepared with a feeding amount of 4.5 mg DEX were used. Scale bar: 200 μm. Data represent means ± SD, N=3. (*) refers to $p < 0.05$ compared with negative control; (△) refers to $p < 0.05$ compared with positive control; (#) refers to $p < 0.05$ compared with BCP NPs.

2.5 Discussion

DEX is an osteogenic inducer for stem cells which is widely used in bone tissue engineering [35, 36]. It plays a key role in controlling regulation of genes and cellular processes essential for cellular growth and differentiation [37]. Combination of DEX with a biomaterial carrier should maximize the therapeutic effect of DEX. On the other hand, the main inorganic component of natural bone, CaP NPs, has been frequently used as a carrier for drugs, proteins, DNA and RNA for the skeletal or other systems [9, 38, 39]. Because formation of CaP NPs is a straightforward precipitation reaction, incorporation of other molecules or drugs only requires the molecules or drugs of interest be present during the CaP formation process [23, 25, 40]. CaP has different phases including hydroxyapatite (HA), tricalcium phosphate (TCP), octacalcium phosphate (OCP), dicalcium phosphate dehydrate (DCPD) and so on [41, 42]. Among them, HA and β-TCP are two important CaP biomaterials used in bone repair. HA has high strength but poor degradability, while β-TCP has good degradability but low strength. Combination of HA and β-TCP to prepare biphasic calcium phosphate (BCP) has been proposed and shown great clinical potential [22, 43-45]. In present study, BCP NPs were prepared as DEX carrier because of their osteoconductive properties and desirable characteristics as a bone graft biomaterial. The DEX-loaded BCP NPs were prepared by immersion BCP NPs into DEX aqueous solution (DEX/BCP NPs) or DEX incorporation during BCP NPs precipitation (DEX@BCP NPs). The biphasic characteristic of the BCP NPs and DEX@BCP NPs was demonstrated by the XRD analysis (Fig. 2.1b).

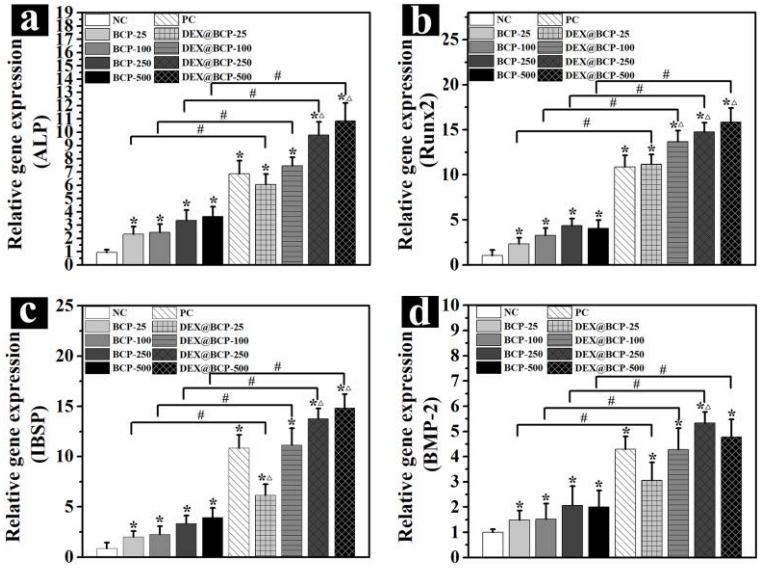

Fig. 2.7. Expression of ALP (a), Runx2 (b), IBSP (c) and BMP-2 (d) of hMSCs after culture with the BCP NPs and DEX@BCP NPs at a concentration of 25, 100, 250 and 500 μg/mL for 21 d. Data represent means ± SD, N=3. (*) refers to $p < 0.05$ compared with negative control; (△) refers to $p < 0.05$ compared with positive control; (#) refers to $p < 0.05$ compared with BCP NPs.

The prepared BCP NPs and DEX@BCP NPs had short rod-like shape and agglomerated in water as shown in Fig. 2.2. The agglomeration of CaP NPs should be due to the electrostatic interaction of calcium and phosphate ions on the surface of CaP NPs [46, 47]. Incorporation of DEX during BCP precipitation resulted in similar crystal morphology while a slightly smaller hydrodynamic size and lower zeta potential

(Fig. 2.1c). The decrease of hydrodynamic size and zeta potential of the DEX@BCP NPs should be due to the shielding effect of DEX. In the preparation of DEX@BCP NPs, OH groups in DEX might electrostatically interact with the calcium ions and then resulted in encapsulation of DEX in the DEX@BCP NPs. DEX molecules might partially affect the electrostatic interaction between calcium and phosphate ions of the DEX@BCP NPs, thus reducing the agglomeration of DEX@BCP NPs. Some bone matrix proteins, bovine serum albumin and amylase have been also reported to retard CaP crystal growth when present during precipitation of CaP [48-50].

The DEX@BCP NPs showed higher loading amount and loading efficiency than the DEX/BCP NPs (Fig. 2.1a and b). DEX could be adsorbed only on the surface of the BCP NPs when the DEX/BCP NPs were prepared. In contrast, DEX could be not only adsorbed on the surface of BCP NPs but also encapsulated in the BCP NPs during the liquid precipitation when the DEX@BCP NPs were prepared. The double effects of surface adsorption and encapsulation should increase the loading amount and efficiency of DEX in the DEX@BCP NPs.

The DEX/BCP NPs and DEX@BCP NPs showed different DEX release profiles (Fig. 2.3c and d). The DEX/BCP NPs and DEX@BCP NPs both revealed rapid DEX release during the first 3 days. 82.6 ± 3.4% of the loaded DEX in the DEX/BCP NPs and 40.5 ± 3.9% of the loaded DEX in the DEX@BCP NPs was released during the first 3 days. The rapid release of DEX in the first 3 days should be due to the adsorbed DEX. Therefore, most of the loaded DEX was released from the adsorption type loading model (DEX/BCP NPs). Because DEX was both adsorbed and encapsulated in the DEX@BCP NPs, the DEX@BCP NPs showed a sustained and controlled release of DEX. Many studies have used CaP particles as drug carriers just by coating the drugs onto the surface of CaP particles [51-53]. However, a rapid initial burst release of drugs is accompanied with these drug-loaded CaP particles and the drugs release cannot last as long as needed [54-57]. The DEX@BCP NPs should meet the prolonged period release requirement because the DEX release could last more than 21 days.

The DEX@BCP NPs at different concentrations (25, 100, 250 and 500 μg/mL) maintained high cell viability and promoted proliferation of hMSCs. The control BCP NPs also showed a promotive effect on proliferation of hMSCs, which should be due to the locally released Ca 2+ and PO43- [58], After 7 days culture, the proliferation of hMSCs cultured with the DEX@BCP NPs was lower than that cultured with the BCP NPs. This should be due to the osteogenic differentiation of hMSCs cultured with the DEX@BCP NPs. It has been reported that proliferation of the hMSCs was retarded when DEX was used to stimulate the differentiation of hMSCs [59, 60].

The ALP activity assay, Ca deposition and gene expression results indicated that the DEX@BCP NPs promoted osteogenic differentiation of hMSCs. The promotive capacity of the DEX@BCP NPs should be the synergistic effects of the BCP NPs and DEX. Numerous studies have reported that various types of CaPs including BCP can not only induce the ectopic bone formation *in vivo*, but also promote the osteogenic differentiation of MSCs *in vitro*, due to the increased local concentrations of calcium and phosphate ions [43, 61, 62]. In this study, DEX was released from the DEX@BCP NPs in a sustainable manner and the released DEX could effectively maintain the concentration to stimulate the osteogenic differentiation of hMSCs. At day 3, the amount of released DEX was 240.5 ± 23.4 ng/mg DEX@BCP NPs that was 40.5 ± 3.9 % of the total loaded amount. Based on the released data, the released DEX concentration in the culture medium was calculated to be about 24 ng/mL for the DEX@BCP-100 group, 60 ng/mL for the DEX@BCP-250 group and 120 ng/mL for the DEX@BCP-500 group. DEX concentration in positive control group was 39.6 ng/mL. Given that the maximal stimulation effect of DEX on osteoblast differentiation is 10−8 to 10−6 M (3.96 ng/mL to 396 ng/mL) [63-65], all the three groups (DEX@BCP-100, DEX@BCP-250, and DEX@BCP-500) presented the proper concentration for triggering osteogenic differentiation of hMSCs. The increase of DEX@BCP NPs concentrations resulted in the increasing amount of the released DEX, as well as the local

concentration of calcium and phosphate ions. The DEX@BCP NPs combined the advantages of both BCP NPs and DEX. They should be useful for osteogenic differentiation of stem cells and bone tissue engineering.

2.6 Conclusions

Biphasic calcium phosphate nanoparticles (BCP NPs) were prepared as the DEX carrier. DEX was incorporated in the BCP NPs by immersion of BCP NPs in a DEX solution or addition of DEX in the reaction solution during BCP NPs formation. The DEX@BCP NPs prepared by the second method showed a higher DEX loading amount and loading efficiency than did the DEX/BCP NPs prepared by the first method. Incorporation of DEX did not change the biphasic characteristics of BCP NPs. The DEX@BCP NPs had a more sustainable and longer release of DEX than did the DEX/BCP NPs. The DEX@BCP NPs maintained high cell viability and promoted proliferation of hMSCs. The hMSCs cultured with the DEX@BCP NPs showed high ALP activity, positive calcium deposition and up-regulated expression of osteogenic marker genes. The DEX@BCP NPs could release DEX in a sustained way and enhance osteogenic differentiation of hMSCs. The results should provide useful information for the preparation of DEX-loaded systems for bone tissue engineering.

2.7 References

[1] Bringhurst FR, Demay MB, Krane SM, Kronenberg HM. Bone and mineral metabolism in health and disease. Harrisons principles of internal medicine 2005;16:2238.
[2] Bringhurst F, Demay M, Krane S, Kronenberg H. Bone and mineral metabolism in health and disease. Harrisons principles of internal medicine 2005;16:2238.
[3] Alam MI, Asahina I, Ohmamiuda K, Takahashi K, Yokota S, Enomoto S. Evaluation of ceramics composed of different hydroxyapatite to tricalcium phosphate ratios as carriers for rhBMP-2. Biomaterials 2001;22:1643-51.
[4] Calori G, Mazza E, Colombo M, Ripamonti C. The use of bone-graft substitutes in large bone defects: any specific needs? Injury 2011;42:S56-S63.
[5] Xu M, Li H, Zhai D, Chang J, Chen S, Wu C. Hierarchically porous nagelschmidtite bioceramic–silk scaffolds for bone tissue engineering. J. Mater. Chem. B 2015;3:3799-809.
[6] Huang S-C, Wu B-C, Ding S-J. Stem cell differentiation-induced calcium silicate cement with bacteriostatic activity. J. Mater. Chem. B 2015;3:570-80.
[7] Higuchi A, Ling Q-D, Hsu S-T, Umezawa A. Biomimetic cell culture proteins as extracellular matrices for stem cell differentiation. Chem. Rev. 2012;112:4507-40.
[8] Zou Z, Liu X, Chen L, Lin K, Chang J. Dental enamel-like hydroxyapatite transformed directly from monetite. J. Mater. Chem. 2012;22:22637-41.
[9] Zhu H, Zhai D, Lin C, Zhang Y, Huan Z, Chang J, Wu C. 3D plotting of highly uniform Sr 5 (PO 4) 2 SiO 4 bioceramic scaffolds for bone tissue engineering. J. Mater. Chem. B 2016;4:6200-12.
[10] Mohan S, Baylink DJ. Bone growth factors. Clin. Orthop. Relat. Res. 1991;263:30-48.
[11] Urist MR, DeLange RJ, Finerman G. Bone cell differentiation and growth factors. Science 1983;220:680-6.
[12] Marx RE, Carlson ER, Eichstaedt RM, Schimmele SR, Strauss JE, Georgeff KR. Platelet-rich plasma:

growth factor enhancement for bone grafts. Oral Surgery, Oral Medicine, Oral Pathology, Oral Radiology, and Endodontology 1998;85:638-46.
[13] Beard Jr EL. The American Society of Health System Pharmacists. JONA'S healthcare law, ethics and regulation 2001;3:78-9.
[14] Cheng S-L, Yang JW, Rifas L, Zhang S-F, Avioli LV. Differentiation of human bone marrow osteogenic stromal cells in vitro: induction of the osteoblast phenotype by dexamethasone. Endocrinology. 1994;134:277-86.
[15] Oshina H, Sotome S, Yoshii T, Torigoe I, Sugata Y, Maehara H, Marukawa E, Omura K, Shinomiya K. Effects of continuous dexamethasone treatment on differentiation capabilities of bone marrow-derived mesenchymal cells. Bone 2007;41:575-83.
[16] Kiefer R, Kreutzberg GW. Effects of dexamethasone on microglial activation in vivo: selective downregulation of major histocompatibility complex class II expression in regenerating facial nucleus. J. Neuroimmunol. 1991;34:99-108.
[17] Zhou X, Feng W, Qiu K, Chen L, Wang W, Nie W, Mo X, He C. BMP-2 derived peptide and dexamethasone incorporated mesoporous silica nanoparticles for enhanced osteogenic differentiation of bone mesenchymal stem cells. ACS Appl. Mater. Interfaces 2015;7:15777-89.
[18] Gan Q, Zhu J, Yuan Y, Liu H, Qian J, Li Y, Liu C. A dual-delivery system of pH-responsive chitosan-functionalized mesoporous silica nanoparticles bearing BMP-2 and dexamethasone for enhanced bone regeneration. J. Mater. Chem. B 2015;3:2056-66.
[19] Wadhwa R, Lagenaur CF, Cui XT. Electrochemically controlled release of dexamethasone from conducting polymer polypyrrole coated electrode. J. Controlled Release 2006;110:531-41.
[20] Nanda HS, Nakamoto T, Chen S, Cai R, Kawazoe N, Chen G. Collagen microgel-assisted dexamethasone release from PLLA-collagen hybrid scaffolds of controlled pore structure for osteogenic differentiation of mesenchymal stem cells. J. Biomater. Sci., Polym. Ed. 2014;25:1374-86.
[21] Chen Y, Wang J, Zhu X, Fan Y, Zhang X. Adsorption and release behaviors of vascular endothelial growth factor on porous hydroxyapatite ceramic under competitive conditions. J. Biomater. Tissue Eng. 2014;4:155-61.
[22] Chen Y, Wang J, Zhu X, Tang Z, Yang X, Tan Y, Fan Y, Zhang X. Enhanced effect of β-tricalcium phosphate phase on neovascularization of porous calcium phosphate ceramics: in vitro and in vivo evidence. Acta Biomater. 2015;11:435-48.
[23] Sokolova V, Rotan O, Klesing J, Nalbant P, Buer J, Knuschke T, Westendorf AM, Epple M. Calcium phosphate nanoparticles as versatile carrier for small and large molecules across cell membranes. J. Nanopart. Res. 2012;14:910.
[24] Temchura VV, Kozlova D, Sokolova V, Überla K, Epple M. Targeting and activation of antigen-specific B-cells by calcium phosphate nanoparticles loaded with protein antigen. Biomaterials 2014;35:6098-105.
[25] Haedicke K, Kozlova D, Gräfe S, Teichgräber U, Epple M, Hilger I. Multifunctional calcium phosphate nanoparticles for combining near-infrared fluorescence imaging and photodynamic therapy. Acta Biomater. 2015;14:197-207.
[26] SHAO F-W, CAI Y-R, YAO J-M. Porous Hydroxyapatite Nanoparticles as a Carrier of Ascorbic Acid [J]. Chem. Res. Chin. Univ. 2010;6:010.
[27] Li S, Wang K, Chang K-CA, Zong M, Wang J, Cao Y, Bai Y, Wei T, Zhang Z. Preparation and evaluation of nano-hydroxyapatite/poly (styrene-divinylbenzene) porous microsphere for aspirin carrier. Sci. China: Chem. 2012;55:1134-9.
[28] Hadjicharalambous C, Kozlova D, Sokolova V, Epple M, Chatzinikolaidou M. Calcium phosphate

nanoparticles carrying BMP-7 plasmid DNA induce an osteogenic response in MC3T3-E1 pre-osteoblasts. J. Biomed. Mater. Res., Part A 2015;103:3834-42.
[29] Matsumoto T, Okazaki M, Inoue M, Yamaguchi S, Kusunose T, Toyonaga T, Hamada Y, Takahashi J. Hydroxyapatite particles as a controlled release carrier of protein. Biomaterials 2004;25:3807-12.
[30] Wu H-C, Lin F-H. Evaluation of magnetic-hydroxyapatite nanoparticles for gene delivery carrier. Biomedical Engineering: Applications, Basis and Communications 2010;22:33-9.
[31] Sokolova V, Epple M. Inorganic nanoparticles as carriers of nucleic acids into cells. Angew. Chem., Int. Ed. 2008;47:1382-95.
[32] Ji J, Ran J, Gou L, Wang F, Cheng S, Fu X. Synthesis of HA/β-TCP biphasic bioceramic powders by a modified co-precipitation method. J. Funct. Mater. 2003;34:597-9.
[33] Cai R, Nakamoto T, Kawazoe N, Chen G. Influence of stepwise chondrogenesis-mimicking 3D extracellular matrix on chondrogenic differentiation of mesenchymal stem cells. Biomaterials 2015;52:199-207.
[34] Li J, Chen Y, Yang Y, Kawazoe N, Chen G. Sub-10 nm gold nanoparticles promote adipogenesis and inhibit osteogenesis of mesenchymal stem cells. J. Mater. Chem. B 2017;5:1353-62.
[35] Kim H, Kim HW, Suh H. Sustained release of ascorbate-2-phosphate and dexamethasone from porous PLGA scaffolds for bone tissue engineering using mesenchymal stem cells. Biomaterials 2003;24:4671-9.
[36] Su Y, Su Q, Liu W, Lim M, Venugopal JR, Mo X, Ramakrishna S, Al-Deyab SS, El-Newehy M. Controlled release of bone morphogenetic protein 2 and dexamethasone loaded in core–shell PLLACL–collagen fibers for use in bone tissue engineering. Acta Biomater. 2012;8:763-71.
[37] Jaiswal N, Haynesworth SE, Caplan AI, Bruder SP. Osteogenic differentiation of purified, culture-expanded human mesenchymal stem cells in vitro. J. Cell. Biochem. 1997;64:295-312.
[38] Zhang Y, Zhai D, Xu M, Yao Q, Chang J, Wu C. 3D-printed bioceramic scaffolds with a Fe 3 O 4/graphene oxide nanocomposite interface for hyperthermia therapy of bone tumor cells. J. Mater. Chem. B 2016;4:2874-86.
[39] Sun T-W, Zhu Y-J, Qi C, Chen F, Jiang Y-Y, Zhang Y-G, Wu J, Wu C. Templated solvothermal synthesis of magnesium silicate hollow nanospheres with ultrahigh specific surface area and their application in high-performance protein adsorption and drug delivery. J. Mater. Chem. B 2016;4:3257-68.
[40] Temchura VV, Kozlova D, Sokolova V, Uberla K, Epple M. Targeting and activation of antigen-specific B-cells by calcium phosphate nanoparticles loaded with protein antigen. Biomaterials 2014;35:6098-105.
[41] Adams MP, Carol Urban PhD R. Pharmacology: Connections to nursing practice: Prentice Hall; 2015.
[42] Tian T, Han Y, Ma B, Wu C, Chang J. Novel Co-akermanite (Ca 2 CoSi 2 O 7) bioceramics with the activity to stimulate osteogenesis and angiogenesis. J. Mater. Chem. B 2015;3:6773-82.
[43] Wang J, Chen Y, Zhu X, Yuan T, Tan Y, Fan Y, Zhang X. Effect of phase composition on protein adsorption and osteoinduction of porous calcium phosphate ceramics in mice. J. Biomed. Mater. Res., Part A 2014;102:4234-43.
[44] Yuan H, Van Blitterswijk CA, De Groot K, De Bruijn JD. Cross-species comparison of ectopic bone formation in biphasic calcium phosphate (BCP) and hydroxyapatite (HA) scaffolds. Tissue Eng. 2006;12:1607-15.
[45] Chen Z, Yuen J, Crawford R, Chang J, Wu C, Xiao Y. The effect of osteoimmunomodulation on the osteogenic effects of cobalt incorporated β-tricalcium phosphate. Biomaterials 2015;61:126-38.
[46] Saeri MR, Afshar A, Ghorbani M, Ehsani N, Sorrell CC. The wet precipitation process of hydroxyapatite. Mater. Lett. 2003;57:4064-9.
[47] Mobasherpour I, Heshajin MS, Kazemzadeh A, Zakeri M. Synthesis of nanocrystalline hydroxyapatite

by using precipitation method. J. Alloys Compd. 2007;430:330-3.
[48] Štulajterová R, Medvecký Ľ. Effect of calcium ions on transformation brushite to hydroxyapatite in aqueous solutions. Colloids Surf., A 2008;316:104-9.
[49] Leonor I, Alves C, Azevedo HS, Reis R. Effects of protein incorporation on calcium phosphate coating. Mater. Sci. Eng. C 2009;29:913-8.
[50] Rohanizadeh R, Padrines M, Bouler J, Couchourel D, Fortun Y, Daculsi G. Apatite precipitation after incubation of biphasic calcium-phosphate ceramic in various solutions: Influence of seed species and proteins. J. Biomed. Mater. Res. 1998;42:530-9.
[51] Schmidt HT, Gray BL, Wingert PA, Ostafin AE. Assembly of aqueous-cored calcium phosphate nanoparticles for drug delivery. Chem. Mater. 2004;16:4942-7.
[52] Bose S, Tarafder S. Calcium phosphate ceramic systems in growth factor and drug delivery for bone tissue engineering: a review. Acta Biomater. 2012;8:1401-21.
[53] Le Guéhennec L, Soueidan A, Layrolle P, Amouriq Y. Surface treatments of titanium dental implants for rapid osseointegration. Dent. Mater. 2007;23:844-54.
[54] Rickard D, Sullivan T, Shenker B, Leboy Pa, Kazhdan I. Induction of rapid osteoblast differentiation in rat bone marrow stromal cell cultures by dexamethasone and BMP-2. Dev. Biol. 1994;161:218-28.
[55] Beresford J, Joyner C, Devlin C, Triffitt J. The effects of dexamethasone and 1, 25-dihydroxyvitamin D3 on osteogenic differentiation of human marrow stromal cells in vitro. Arch. Oral Biol. 1994;39:941-7.
[56] Kano S, Yamazaki A, Otsuka R, Ohgaki M, Akao M, Aoki H. Application of hydroxyapatite-sol as drug carrier. Bio-Med. Mater. Eng. 1994;4:283-90.
[57] Song HY, Islam S, Lee BT. A novel method to fabricate unidirectional porous hydroxyapatite body using ethanol bubbles in a viscous slurry. J. Am. Ceram. Soc. 2008;91:3125-7.
[58] Tang Z, Wang Z, Qing F, Ni Y, Fan Y, Tan Y, Zhang X. Bone morphogenetic protein Smads signaling in mesenchymal stem cells affected by osteoinductive calcium phosphate ceramics. J. Biomed. Mater. Res., Part A 2015;103:1001-10.
[59] Walsh S, Jordan G, Jefferiss C, Stewart K, Beresford J. High concentrations of dexamethasone suppress the proliferation but not the differentiation or further maturation of human osteoblast precursors in vitro: relevance to glucocorticoid-induced osteoporosis. Rheumatology 2001;40:74-83.
[60] D'ippolito G, Schiller PC, Ricordi C, Roos BA, Howard GA. Age-related osteogenic potential of mesenchymal stromal stem cells from human vertebral bone marrow. J. Bone Miner. Res. 1999;14:1115-22.
[61] Hench LL. Bioceramics: from concept to clinic. J. Am. Ceram. Soc. 1991;74:1487-510.
[62] Zhang L, Hanagata N, Maeda M, Minowa T, Ikoma T, Fan H, Zhang X. Porous hydroxyapatite and biphasic calcium phosphate ceramics promote ectopic osteoblast differentiation from mesenchymal stem cells. Sci. Technol. Adv. Mater. 2009;10:025003.
[63] Peister A, Mellad JA, Larson BL, Hall BM, Gibson LF, Prockop DJ. Adult stem cells from bone marrow (MSCs) isolated from different strains of inbred mice vary in surface epitopes, rates of proliferation, and differentiation potential. Blood 2004;103:1662-8.
[64] DiGirolamo CM, Stokes D, Colter D, Phinney DG, Class R, Prockop DJ. Propagation and senescence of human marrow stromal cells in culture: a simple colony-forming assay identifies samples with the greatest potential to propagate and differentiate. Br. J. Haematol. 1999;107:275-81.
[65] Richards CD, Langdon C, Deschamps P, Pennica D, Shaughnessy SG. Stimulation of osteoclast differentiation in vitro by mouse oncostatin M, leukaemia inhibitory factor, cardiotrophin-1 and interleukin 6: synergy with dexamethasone. Cytokine 2000;12:613-21.

Chapter 3

Preparation of dexamethasone-loaded biphasic calcium phosphate nanoparticles/collagen porous composite scaffolds for bone tissue engineering

3.1 Summary

As an attractive strategy, bone tissue engineering (bone TE) has been widely investigated to repair bone defects. However, the rapid and effective bone regeneration of large non-healing defects is still a great challenge. Multifunctional scaffolds having osteoinductivity and osteoconductivity are desirable to fasten functional bone tissue regeneration. In this part, composite scaffolds of collagen and biphasic calcium phosphate nanoparticles (BCP NPs) with a controlled and sustained release nature of DEX and controlled pore structures were prepared for bone tissue engineering. DEX was introduced in BCP NPs during preparation of BCP NPs and then the DEX-loaded NPs were hybridized with collagen scaffolds, which pore structures were controlled by using pre-prepared ice particulates as a porogen material. The composite scaffolds had well controlled and interconnected pore structures, high mechanical strength and sustained release of DEX. The composite scaffolds showed good biocompatibility and promoted osteogenic differentiation of hMSCs when used for three-dimensional culture of hMSCs. Subcutaneous implantation of the DEX@BCP/Col composite scaffolds at the dorsa of athymic nude mice demonstrated that the composite scaffolds facilitated ectopic bone tissue regeneration. The results indicated the DEX@BCP/Col composite scaffolds had high potential for bone tissue engineering.

3.2 Introduction

Nowadays, autografts and allografts are the most common solutions for repair of large-sized bone defects. Nevertheless, they have some drawbacks such as the limited sources, extra invasive surgery and immunological rejection [1]. Therefore, more and more attention has been drawn to bone tissue engineering (bone TE). Bone TE is a strategy combining biotechnology and biomaterials to induce new bone regeneration, which is a complex and dynamic process that starts with cell migration and adhesion followed by cell proliferation, differentiation, matrix formation along with remodeling of bone [2]. Scaffolds have been used for bone TE to control cell functions and keep regeneration spaces. Besides good biocompatibility

and biodegradability, scaffolds used for bone TE should have excellent osteoconductivity, osteoinductivity, interconnected porous structure and high mechanical property [3-5]. Osteoconductivity can ensure migration, adhesion and survival of osteogenic cells. Osteoinductivity can induce osteogenic differentiation of stem cells [6].

Many efforts have been made to prepare scaffolds for bone TE. To mimic the extracellular matrix composition of bone, a variety of strategies have been considered, including usage of the components present in natural bone [7], controlling of pore structure and interconnectivity [8], construction of multiple scale architectures [9] and incorporation of growth factors [10]. For example, calcium phosphate (CaP) has been hybridized with polymers in the forms of tablets [11], blends [12], pastes [13] or cements [14]. However, these CaP/polymer composite scaffolds do not have appropriate pore structures for cell accommodation and migration. In particular, their pore interconnectivity is poor [15-17].

To render scaffolds with good osteoinductivity, growth factors have been incorporated in the scaffolds. Nevertheless, the most commonly used growth factors such as bone morphogenetic proteins (BMPs) and transforming growth factor beta (TGF-β) are proteins and can easily lose their bioactivity during the preparation procedures [18]. To minimize denaturation and maintain their bioactivity, growth factors are generally introduced in scaffolds by physical adsorption. The release of physically adsorbed proteins always exhibits an initial burst and cannot last for a long period [19-24]. On the other hand, dexamethasone (DEX), as a low molecular weight osteoinductive factor, has drawn much attention for incorporation in scaffolds for bone TE because of its high stability even in tough chemical environment [25]. DEX and hydroxyapatite nanoparticles have been hybridized with gelatin and poly(L-lactide) to construct hydroxyapatite/DEX/PLLA/gelatin composite scaffold by electrospinning technique [26]. DEX-loaded mesoporous silica nanoparticles have been deposited onto poly(L-lactic acid)/poly(ε–caprolactone) nanofibrous scaffold by electrophoretic deposition [27]. A dual delivery system of BMP-2 and DEX has been designed by co-electrospinning the blending solution that is composed of BMP-2-encapsulated bovine serum albumin nanoparticles, DEX and poly(ε-caprolactone)-co-poly(ethylene glycol) (PCE) copolymer [28]. These composite scaffolds have shown the synergistic effects of the released osteogenic factors. However, the problems of initial burst release and a short release period of DEX need to be solved. Furthermore, simultaneous release of both DEX and calcium and phosphorus ions is desirable for synergistic promotion of new bone regeneration.

In this study, composite scaffolds of collagen and DEX-loaded biphasic CaP nanoparticles (BCP NPs) were prepared for a sustainable release of DEX together with the calcium and phosphorous ions. DEX was incorporated in the BCP NPs during their preparation to allow the DEX being physically locked in the crystals of BCP NPs for a sustainable and simultaneous release profile of DEX, calcium and phosphorous ions. The microporous structure of the composite scaffolds was controlled by using pre-prepared ice particulates as a porogen material. The composite scaffolds were used for three-dimensional culture of human bone marrow-derived mesenchymal stem cells (hMSCs). Their effects on proliferation and osteogenic differentiation of hMSCs were compared with collagen scaffold and BCP NPs/collagen composite scaffold. Subcutaneous implantation of the composite scaffolds at the dorsa of athymic nude mice was used to demonstrate their promotive effects on ectopic bone tissue regeneration.

3.3 Materials and methods

3.3.1 Preparation of BCP NPs and DEX@BCP NPs

Biphasic calcium phosphate nanoparticles (BCP NPs) were prepared by adding dropwise 75.0 mL of 0.5 M calcium nitrate tetrahydrate ($Ca(NO_3)_2 \cdot 4H_2O$, Sigma-Aldrich, USA) solution to 50 mL of 0.5 M ammonium phosphate dibasic ($(NH_4)_2HPO_4$, Sigma-Aldrich, USA)) solution by a syringe pump (KD Scientific Inc., USA) [29]. After reacting at 55 °C and a pH of 9.5 for 30 minutes under stirring (700 rpm), the slurry was aged for 36 hours at room temperature to form stable BCP NPs. DEX-loaded BCP NPs (denoted as DEX@BCP NPs) were prepared by adding dropwise the mixture solution of DEX and $Ca(NO_3)_2 \cdot 4H_2O$ (75.0 mL) to 50 mL of 0.5 M $(NH_4)_2HPO_4$ solution. The mixture solution of DEX and $Ca(NO_3)_2 \cdot 4H_2O$ was prepared by adding 3 mL of 0.75, 1.50 and 2.25 mg/mL of DEX in ethanol to 72.0 mL of 0.52 M $Ca(NO_3)_2 \cdot 4H_2O$ solution. The reaction was continued in a 55 °C water bath for 30 minutes under stirring and then aged for 36 hours at room temperature to obtain stable DEX@BCP NPs. The DEX@BCP NPs prepared at the three different DEX feeding concentrations were denoted as DEX1@BCP NPs, DEX2@BCP NPs and DEX3@BCP NPs, respectively. The prepared DEX@BCP NPs were dispersed in 20 mL ethanol and shaken at 200 rpm and room temperature for 20 minutes followed with centrifugation at 8000 rpm. The washing with ethanol was repeated for 3 times to remove the DEX adsorbed on the surface of the DEX@BCP NPs.

3.3.2 Preparation of DEX@BCP NPs/collagen composite scaffolds

A 2.5% (w/v) solution of collagen was prepared by dissolving porcine type I collagen (Nitta Gelatin, Japan) in a 10% (v/v) ethanol aqueous solution. Ice particulates were prepared by spaying pure water in liquid nitrogen and ice particulates with the diameters between 425 and 500 μm were obtained by sieving the ice particulates through two sieves having a respective mesh size of 425 and 500 μm [30]. The BCP NPs, DEX1@BCP NPs, DEX2@BCP NPs and DEX3@BCP NPs were individually dispersed in a 10% (v/v) ethanol aqueous solution to prepare their respective dispersion solution. The collagen solution, NPs dispersion solution and ice particulates were kept in a -5 °C low temperature chamber (Espec, Osaka, Japan) for 2 hours to balance their temperature to -5 °C.

To optimize the mass ratio of NPs and collagen in the composite scaffolds, a series of porous BCP/collagen (BCP/Col) composite scaffolds with a different mass ratio of BCP NPs/collagen were prepared. At first, 3 mL of the pre-cooled BCP NPs suspension solution at a concentration of 187, 140, 112 and 93 mg/mL was added dropwise to 11 mL of the pre-cooled collagen solution (2.5% (w/v)) at -5 °C and mixed well. The final concentration of collagen in the collagen/BCP NPs suspension solution was 2.0% (w/v). The mass ratio of the BCP NPs/collagen was 2: 1, 1.5: 1, 1.2: 1 and 1: 1 (w/w), respectively. Subsequently, the temperature-balanced ice particulates were added to the collagen/BCP NPs suspension solution at a ratio of 50: 50 (w/v) at -5 °C. The components were mixed carefully to allow the ice particulates being homogeneously distributed in the collagen/BCP NPs suspension solution without air bubble generation and then poured into silicone frames which were placed on PFA film-wrapped copper plates. The entire constructs were placed at -12 °C for 12 hours to slowly freeze the mixture solution and then frozen at -80 °C for 6 hours. Finally, the frozen constructs were freeze-dried for 2 days in a Wizard 2.0 freeze dryer (VirTis, Gardiner, NY). The freeze-dried constructs were cross-linked with 50 mM 1-ethyl-3-(3-dimethylaminopropyl) carbodiimide (EDC, Peptide Institute, Inc.) and 20 mM N-hydroxysuccimide (NHS, Wako Pure Chemical Industries, Ltd.) in an 80% (v/v) ethanol aqueous solution at room temperature under gentle shaking (~ 20 rpm) for 8 hours. After cross-linking, the BCP/Col composite scaffolds were washed 3 times with Milli-Q water and immersed in a 0.1 M glycine aqueous solution to block unreacted NHS residues. The BCP/Col composite scaffolds were washed with water for 6 times and freeze-dried for usage of the following experiments.

After preparation of the serial BCP/Col composite scaffolds, the pore structure and mechanical property were measured to determine the optimal mass ratio of BCP NPs/collagen in the scaffold. The optimized mass ratio of BCP NPs/collagen was 1: 1 and used for fabrication of the DEX@BCP NPs/collagen (DEX@BCP/Col) composite scaffolds. The preparation procedure of DEX1@BCP NPs/collagen (DEX1@BCP/Col), DEX2@BCP NPs/collagen (DEX2@BCP/Col) and DEX3@BCP NPs/collagen (DEX3@BCP/Col) composite scaffolds was the same as that of BCP/Col composite scaffolds described above by changing the BCP NPs to DEX1@BCP NPs, DEX2@BCP NPs and DEX3@BCP NPs, respectively. Control collagen (Col) scaffold was prepared by the same procedure as that of the BCP/Col composite scaffolds by using 2.0% (w/v) collagen solution without addition of any NPs.

3.3.3 Characterization of NPs and scaffolds

A JEOL 2100F transmission electron microscope (TEM, JEOL, Japan) was used to visualize the morphology of the NPs. An aqueous solution containing 10 μL of NPs was dropped on a carbon-coated copper grid to prepare the samples for TEM. The elemental mapping of the NPs was obtained on a field-emission electron microscope (JEM-2100F, JEOL, Japan). The pore structures of the Col, BCP/Col, DEX1@BCP/Col, DEX2@BCP/Col and DEX3@BCP/Col scaffolds were observed with a scanning electron microscope (SEM, S-4800, Hitachi, Japan). The cross-sections of the scaffolds were coated with platinum by a sputter coater (E-1030, Hitachi, Japan) before observation. The pore size was analyzed by measuring the diameters of pores (≥40 pores per image) from four SEM images of each type of scaffolds with an ImageJ software (ImageJ2, NIH, USA). The mechanical property of the scaffolds was measured by a static compression mechanical test machine (TA. XTPlus, Texture Technologies Corp., USA). The scaffolds were punched into cylindrical discs (Φ6 mm × H3 mm). The cylindrical discs were hydrated by degassing the discs in phosphate buffered saline (PBS) and soaked in PBS for 2 hours before testing. Each sample was compressed at a rate of 0.1 mm/s to generate stress-strain curves. The Young's modulus was calculated from the initial linear region of the stress-strain curves. 3 samples were tested for each type of the scaffolds. The porosity of the scaffolds was calculated according to Archimedes' principle by the following formula: porosity = $V_{pore}/V = ((W_2 - W_1)/\rho/V) \times 100\%$, where V_{pore} is the volume of the pore, V is the total volume of the scaffold, W_1 is the dry weight of the scaffold, W_2 is the weight of the scaffold with water and ρ is the density of water [30]. 3 samples of each scaffold were used for the measurement to calculate the mean and standard deviation.

3.3.4 DEX release from DEX@BCP/Col composite scaffolds

The DEX release experiment of the DEX1@BCP/Col, DEX2@BCP/Col and DEX3@BCP/Col composite scaffolds was performed in a PBS solution (pH 7.4). The scaffolds were punched into cylindrical discs (Φ6 mm × H3 mm). Every 2 discs were immersed in 2 mL of PBS and gently shaken (60 rpm) at 37 °C. The released amount of DEX was measured at 242 nm by a UV-vis spectrophotometer after incubation for 0.5, 1, 2, 4, 7, 10, 13, 16, 19, 22, 25, 28, 31 and 35 days. To measure the total loading amount of DEX in the DEX@BCP/Col composite scaffolds, every 2 discs of the scaffolds were dissolved in 2 mL of a 6 M hydrochloric acid (HCl, Wako, Japan) solution for 3 hours. And then the mixture solution was centrifuged at 8000 rpm for 10 minutes. The supernatant was taken out to measure the amount of DEX. The percentage of the DEX released from each type of the DEX@BCP/Col composite scaffolds was determined by dividing the release amount by the total loading amount of DEX. Each experiment was carried out in triplicate.

3.3.5 *In vitro* cell culture

The Col, BCP/Col and DEX@BCP/Col scaffolds were punched into cylindrical samples (Φ6 mm × H3 mm) and sterilized with ethylene oxide gas for 5 hours. The sterilized samples were conditioned in Dulbecco's Modified Eagle Medium (DMEM, Sigma-Aldrich, USA) at 37 °C for 4 hours. Human mesenchymal stem cells (hMSCs, passage 2) were purchased (Lonza, USA) and sub-cultured in MSCBM medium (Lonza, Swiss). The sub-cultured hMSCs at passage 4 were harvested by treatment with a trypsin/EDTA solution after reaching confluence. The harvested hMSCs were re-suspended in DMEM to prepare a cell suspension solution of 2×10^6 cells/mL for cell seeding. 85 μL of the cell suspension solution was dropped on the top side of the scaffold discs. After being cultured for 3 hours, the scaffold discs were turned upside down and another 85 μL of the cell suspension solution was dropped on another side of the scaffold discs. The total cell number seeded to each scaffold was 3.4×10^5. The cells/scaffold constructs were divided into seven groups: Col scaffold (Col), Col scaffold with additional free DEX in medium (Col+DEX), BCP/Col scaffold (BCP/Col), BCP/Col scaffold with additional free DEX in medium (BCP/Col+DEX), DEX@BCP/Col scaffolds with three different DEX loading amount (DEX1@BCP/Col, DEX2@BCP/Col and DEX3@BCP/Col). The Col, BCP/Col, DEX1@BCP/Col, DEX2@BCP/Col and DEX3@BCP/Col groups were cultured in DMEM supplemented with 10 mM β-glycerophosphate (2 mL medium per scaffold). The Col+DEX and BCP/Col+DEX groups were cultured in DMEM supplemented with 100 nM DEX and 10 mM β-glycerophosphate (2 mL medium per scaffold). The Col and BCP/Col were used as negative controls, while the Col+DEX and BCP/Col+DEX were used as positive controls. All groups were cultured under an atmosphere of 5% CO_2 at 37 °C with a shaking speed of 60 rpm. Medium was changed every 3 days with the addition of fresh 100 nM DEX or 10 mM β-glycerophosphate.

3.3.6 Analysis of cell attachment, distribution, viability and proliferation

Cell attachment and distribution were analyzed by SEM observation and cell nucleus staining. For SEM observation, the samples were washed with PBS for 3 times and fixed with 2.5% glutaraldehyde at room temperature for 1 hour after being cultured for 1 day. After being washed with PBS and water each for 3 times, the fixed samples were freeze-dried and their cross-sections were observed by SEM. For nucleus staining, the samples cultured for 1 day were washed with PBS for 3 times and fixed in 10% neutral buffered formalin for 24 hours. The fixed samples were dehydrated, embedded in paraffin and sectioned to get the vertical cross sections at a thickness of 7 μm. The cross-sections were de-paraffinized and the cell nuclei were stained with 2 μg/ml 4',6-diamidino-2-phenylindole dihydrochloride (DAPI, Dojindo, Japan). The stained cross-sections were observed with a fluorescence microscope (Olympus, Japan).

Live/dead staining was performed to evaluate cell viability by using calcein-AM and propidium iodide staining reagents (Cellstain Double Staining Kit, Dojindo, Japan). After being cultured for 7 days, the samples were washed twice with warm PBS and incubated in serum-free DMEM medium containing calcein-AM and propidium iodide for 15 minutes. The stained samples were observed with an inverted fluorescence microscope (Olympus, Japan) to capture the live/dead cell images.

Cell proliferation was investigated by measuring DNA amount in each sample after 1, 7, 14 and 28 days of culture. The samples were washed 3 times with water, freeze-dried for 48 hours and digested with a papain solution (400 μg/mL) containing 5 mM EDTA and 5 mM L-cysteine in 0.1 M phosphate buffer at a pH of 6.0. An aliquot of the papain digests was used for quantification of DNA content with Hoechst 33258 dye (Sigma-Aldrich, USA) by a fluorescence spectrometer (FP8500, JASCO, Japan). At each time point, every 4 samples of each type of cells/scaffold constructs were used for the measurement.

3.3.7 ALP staining and ALP activity assay

Alkaline phosphatase (ALP) staining and ALP activity assay were conducted after the cells/scaffold constructs were cultured for 14 days. The samples were washed with PBS for 3 times and then fixed with 4% paraformaldehyde for 10 minutes at room temperature. The fixed samples were washed with PBS for 2 times and incubated in a 56 mM 2-amino-2-methyl-1,3-propanediol aqueous solution (pH = 9.9) containing 0.1% fast blue RR salt and 0.1% naphthol AS-MX phosphate for 10 minutes at room temperature. After being washed with PBS for 3 times, the stained samples were sectioned by a blade to prepare vertical cross-sections. The cross-sections were observed with an optical microscope.

A Sensolyte® *p*NPP alkaline phosphatase assay kit (Anaspec, USA) was used to analyze the ALP activity according to manufacturer's instruction. The samples cultured for 14 days were washed with PBS for 3 times, immersed into liquid nitrogen and then crushed into powder by an electric crusher. The powder was collected into a micro-centrifugation tube and 0.2% Triton X-100 was added to lyse the cells. After stirring for 10 minutes at 4 °C, the lysate was centrifuged for 10 minutes at 2500× *g* for collection of the supernatant. And then the supernatant was incubated with a *p*-nitrophenyl phosphate (*p*NPP) substrate solution followed by colorimetric detection at 405 nm. By using an ALP standard solution, a calibration curve was obtained. The DNA content in each sample after 14 days of culture was used to normalize the ALP amount. Each experiment was carried out in triplicate.

3.3.8 PCR assay of *in vitro* samples

The expression of osteogenesis-related genes encoding *ALP*, runt-related transcription factor-2 (RUNX2), bone sialoprotein 2 (*IBSP*) and bone morphogenetic protein-2 (*BMP-2*) in the cells/scaffold constructs was analyzed by real-time PCR (RT-PCR). After 28 days of *in vitro* culture, the samples were washed with PBS for 3 times and frozen in liquid nitrogen. The frozen samples were crushed into powder and dissolved in Sepasol solution (Nacalai Tesque, Japan) to isolate RNA from the cells. For conversion of the RNA to cDNA, a first stand cDNA synthesis kit (Applied Biosystems, USA) was used. A 7500 Real-Time PCR system (Applied Biosystems, USA) was used to perform the RT-PCR [31]. Expression of GAPDH (a housekeeping gene) was used as an endogenous control. The relative gene expression was calculated by using the $2^{-\Delta\Delta Ct}$ method. The gene expression of cells in the Col group was used as a reference. Each experiment was carried out in triplicate. The primers and probes are listed in Table 1.

3.3.9 *In vivo* implantation

All the animal experiment procedures were approved by the Animal Experiments Committee of the National Institute for Materials Science and the experiment was conducted according to the committee guidelines. For *in vivo* implantation, the cells/scaffold constructs were prepared under the same condition as those used for *in vitro* cell culture. After 1 week of *in vitro* culture, the samples were subcutaneously implanted in the back of the 6 weeks old athymic nude mice. Every mouse was implanted with 4 cells/scaffold constructs. After implantation for 6 and 12 weeks, the mice were sacrificed to retrieve the implants. The gross appearance of the harvested implants after 12 weeks of implantation was observed with an OLYMPUS DP22 light microscope (Olympus, Japan). The facade and lateral areas of the implants were measured by an OLYMPUS CellSens Standard software (Olympus, Japan). The initial facade and lateral areas of the hydrated cells/scaffold constructs before implantation were also measured. Each experiment was

carried out in triplicate.

3.3.10 Histological and immunohistochemical evaluations of *in vivo* implants

The harvested implants were washed with PBS for 3 times and fixed in 10% neutral-buffered formalin solution at room temperature for 48 hours. The samples were then decalcified in decalcifying solution B (Wako Pure Chemical Industries, Ltd., Japan) for 48 hours, dehydrated in serial dilutions of ethanol and embedded in paraffin. The samples were sectioned to get the vertical cross-sections of a thickness of 7 μm. The cross-sections were stained with hematoxylin and eosin (H&E, MUTO Pure Chemicals CO., Ltd., Japan). The stained cross-sections were observed under a light microscope.

The cross-sections were also immunohistochemically stained for collagen type I (Col I) and osteocalcin (OCN). The deparaffinized cross-sections were incubated with proteinase K for antigen retrieval for 10 minutes, peroxidase blocking solution for 5 minutes and 10% goat serum solution for 30 minutes. And then the cross-sections were incubated with the primary antibodies of rabbit monoclonal anti-human collagen I (working concentration, 1: 1500; Abcam, UK) and rabbit polyclonal anti-human osteocalcin (5 μg/mL working concentration; Abcam, UK) for 2 hours followed by incubation with the peroxidase-labeled polymer-conjugated secondary antibody (DakoCytomation EnVision+; Dako, Denmark) for 1 hour. The cross-sections were finally incubated with 3,3'-diaminobenzidine (DAB; Liquid DAB+ Substrate Chromogen System, Dako) for 10 minutes to develop color. Nuclei were counterstained with hematoxylin. All procedures were performed at room temperature.

3.3.11 PCR assay of *in vivo* implants

After 12 weeks of implantation, the harvested implants were cleaned of any surrounding soft tissue and washed with PBS for 3 times. All the experiment procedures to analyze the expression of osteogenesis-related genes were the same as those used for *in vitro* cell culture samples. Every 3 samples were used for the analysis.

3.3.12 Statistical analysis

All data were reported as the mean ± standard deviation (SD). One-way ANOVA statistical analysis was performed to evaluate the significance of the experimental data followed by a Tukey's post hoc test for pairwise comparison. All statistical analyses were executed using Kyplot 2.0 beta 15. When the p-value was less than 0.05, the difference was considered significant. The data were indicated with * for $p < 0.05$, ** for $p < 0.01$ and *** for $p < 0.001$.

3.4 Results

3.4.1 Characteristics of NPs and BCP/Col composite scaffolds

The BCP NPs were prepared by reacting a $Ca(NO_3)_2 \cdot 4H_2O$ aqueous solution with a $(NH_4)_2HPO_4$ aqueous solution. The DEX@BCP NPs were prepared by adding DEX in the $Ca(NO_3)_2 \cdot 4H_2O$ aqueous solution during formation of the BCP NPs. The DEX@BCP NPs prepared with 2.25, 4.5 and 6.75 mg of

DEX were referred as DEX1@BCP NPs, DEX2@BCP NPs and DEX3@BCP NPs, respectively. TEM observation showed the BCP NPs were short rod-like and most of them were agglomerated into needle-like crystals (Fig. 3.1a). Incorporation of the DEX didn't change the size and morphology of the BCP NPs (Fig. 3.1b-d). The elemental mapping (Fig. 3.2) showed that Ca and P were detected both in the BCP NPs and in the DEX3@BCP NPs, while element F derived from DEX was only detected in the DEX3@BCP NPs. Elemental mapping of the DEX3@BCP NPs showed that element F was uniformly distributed across the entire DEX3@BCP NPs, indicating existence of DEX within the DEX3@BCP NPs. As shown in our previous study, both BCP NPs and DEX@BCP NPs were negatively charged and incorporation of DEX decreased the zeta potential of the BCP NP. The BCP NPs and DEX@BCP NPs had larger hydrodynamic size than their size measured from TEM images, indicating their agglomeration in aqueous solution [29]. The BCP NPs were hybridized with collagen to prepare the BCP/Col composite scaffolds by using pre-prepared ice particulates as a porogen material to control the porous structures. Different mass ratio of BCP NPs and collagen was used to optimize the preparation condition. SEM observation showed that the pore structures of the BCP/Col composite scaffolds prepared with different mass ratio of BCP NPs/collagen had obvious difference. Although all the BCP/Col composite scaffolds had many spherical large pores, most of the large pores in the BCP/Col composite scaffold prepared with the mass ratio of BCP NPs/collagen of 2: 1 were not well interconnected (Fig. 3.3a, f). When the mass ratio of BCP NPs/collagen decreased, the spherical large pores became more interconnected by more small pores. The small pores were formed at the wall of the spherical large pores and their number increased with the decrease of the mass ratio of BCP NPs/collagen. SEM observation at a high magnification showed that the BCP NPs could be observed at the surfaces of the spherical large pores in the BCP/Col composite scaffolds. The surface roughness of the spherical large pores decreased with the decrease of mass ratio of BCP NPs/collagen. When the mass ratio of BCP NPs/collagen was 1: 1, the BCP/Col composite scaffold had similar porous structure to that of the control Col scaffold (Fig. 3.3d, e, i, j).

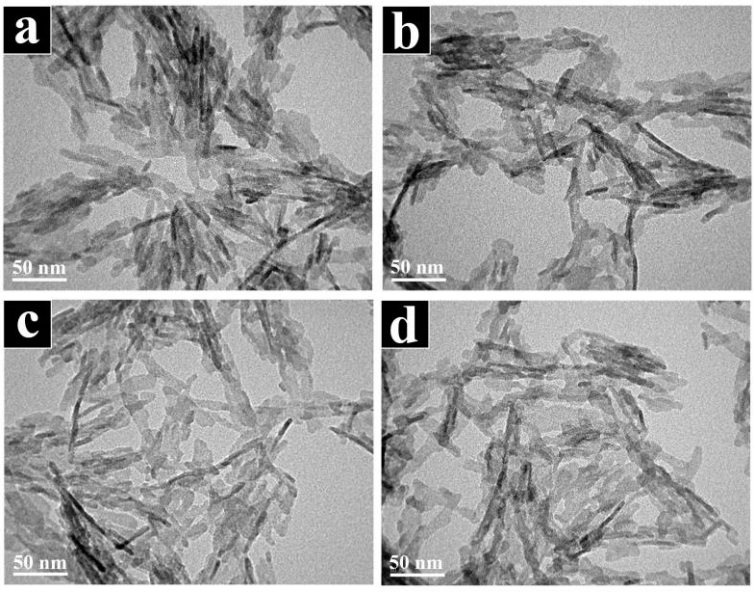

Fig. 3.1. TEM images of the prepared BCP NPs (a), DEX1@BCP NPs (b), DEX2@BCP NPs (c) and DEX3@BCP NPs (d).

Analysis of the pore size (Fig. 3.3k) showed that there was no significant difference of the size of

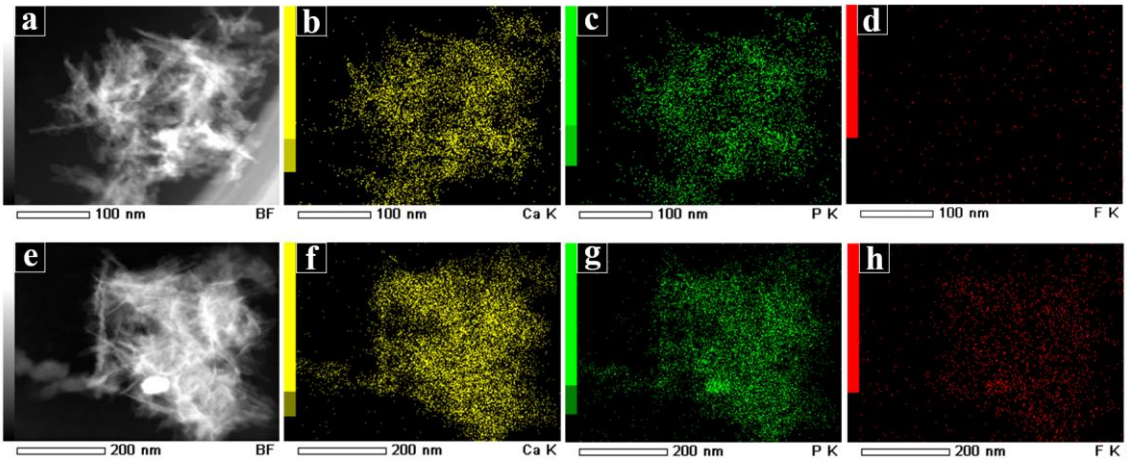

Fig. 3.2. Dark-field TEM images (a, e) and elemental mapping images of the BCP NPs (b-d) and DEX3@BCP NPs (f-h). Elementary analysis of calcium (b, f), phosphorus (c, g) and fluorine (d and h) were carried out. The intensity of the signals for the element of Ca, P, and F are shown in yellow, green and red colors, respectively.

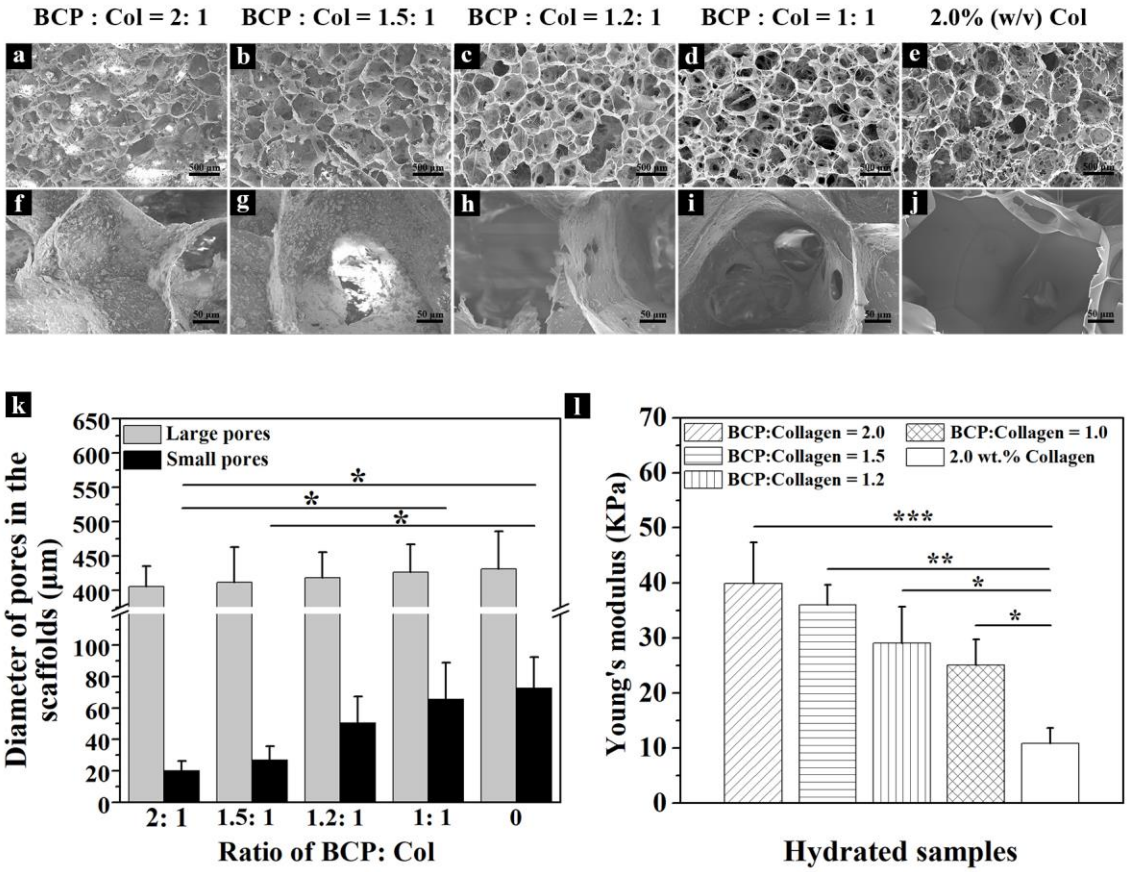

Fig. 3.3. SEM images (a-j) of the cross-sections of the Col scaffold and BCP/Col composite scaffolds prepared with a different mass ratio of BCP NPs/collagen (BCP: Col) at low (a-e) and high (f-j) magnifications. Scale bar: (a-e), 500 μm; (f-j), 50 μm. Diameter of the large pores and the small pores in the Col scaffold and the BCP/Col composite scaffolds prepared with a different mass ratio of BCP NPs/collagen (k). Young's modulus of the hydrated scaffolds of the Col and BCP/Col prepared with a different mass ratio of BCP NPs/collagen (l). Data represent mean ± SD, N = 3. Significant difference: *, $p < 0.05$; **, $p < 0.01$; ***, $p < 0.001$.

spherical larges pores in the control Col scaffold and all the 4 types of BCP/Col composite scaffolds prepared at different ratio of BCP NPs/collagen. The size of the spherical large pores was in a range of 405~450 μm, which was predominantly determined by the pre-prepared ice particulates used as the porogen material. On the other hand, the size of small pores interconnecting the spherical large pores was dependent on the mass ratio of BCP NPs/collagen. The size of small pores increased from 20.0 ± 6.2 μm to 65.3 ± 23.5 μm when the mass ratio of BCP NPs/collagen decreased from 2: 1 to 1: 1. The size of small pores in the BCP/Col composite scaffold prepared at BCP: Col mass ratio of 1: 1 had no significant difference from that in the control Col scaffold (72.7 ± 19.8 μm).

A mechanical compression test was used to measure the Young's modulus of the scaffolds. The Young's modulus of all the BCP/Col composite scaffolds was significantly higher than that of the control Col scaffold (Fig. 3.3l). Hybridization with BCP NPs reinforced the scaffolds. The mass ratio of BCP NPs/collagen had evident effect on the Young's modulus. The Young's modulus of the BCP/Col composite scaffolds decreased with the decrease of mass ratio of BCP NPs/collagen. Noticeably, even with the lowest mass ratio of BCP NPs/collagen, the Young's modulus of the BCP/Col composite scaffold was 2.5-fold higher than that of the Col scaffold. These results indicated that the BCP had opposite effects on the pore structure and mechanical property of the composite scaffolds. Both interconnected pore structure and high mechanical property are important properties of porous scaffolds. The BCP/Col composite scaffold prepared at the BCP NPs/collagen mass ratio of 1: 1 had the best interconnected pore structure and still very high mechanical property when being compared with other BCP/Col composite scaffolds and the control Col scaffold. Therefore, the BCP NPs/collagen mass ratio of 1: 1 was chosen as the optimal condition for the preparation of BCP/Col scaffolds. This mass ratio was also used for preparation of the DEX1@BCP/Col, DEX2@BCP/Col and DEX3@BCP/Col composite scaffolds for the following experiments.

3.4.2 Characteristics of DEX@BCP/Col composite scaffolds

The BCP/Col, DEX1@BCP/Col, DEX2@BCP/Col and DEX3@BCP/Col composite scaffolds that were used for cell culture were prepared by the above described method with the NPs/collagen mass ratio of 1: 1. Their pore structures and mechanical properties were compared with those of control Col scaffold (Fig. 3.4). All the scaffolds had well interconnected large pores with the same size. The spherical large pores were distributed homogeneously throughout the scaffolds and their size was almost equal to the size of the pre-prepared ice particulates used as porogen material (Fig. 3.4k). The size of the small pores was also the same for all the scaffolds. The spherical large pores should be derived from the pre-prepared ice particulates, while the small pores should be derived from the new ice crystals formed during the pre-freezing process. The small pores provided good interconnections among the spherical large pores. The average size of small pores was around 70 μm (Fig. 3.4k), making the scaffolds well interconnected and the porosity of all the scaffolds was higher than 97.8 % (Table 3.1). The high porosity and good interconnectivity should be beneficial for cell migration and spatial distribution. The surface of spherical large pores in the composite scaffolds was much rougher than that of the control Col scaffold (Fig. 3.4f). The BCP NPs and DEX@BCP NPs were homogeneously embedded into the collagen matrices on the pore walls and therefore increased the pore surface roughness of the composite scaffolds (Fig. 3.4g-j).

The Young's modulus of BCP/Col, DEX1@BCP/Col, DEX2@BCP/Col and DEX3@BCP/Col scaffolds was measured and compared with that of the Col scaffold (Fig. 3.4l). The BCP/Col, DEX1@BCP/Col, DEX2@BCP/Col and DEX3@BCP/Col composite scaffolds showed similar Young's modulus, which was significantly higher than that of the control Col scaffold. Incorporation of DEX in the BCP NPs did not affect the porous structures and mechanical properties of the composite scaffolds.

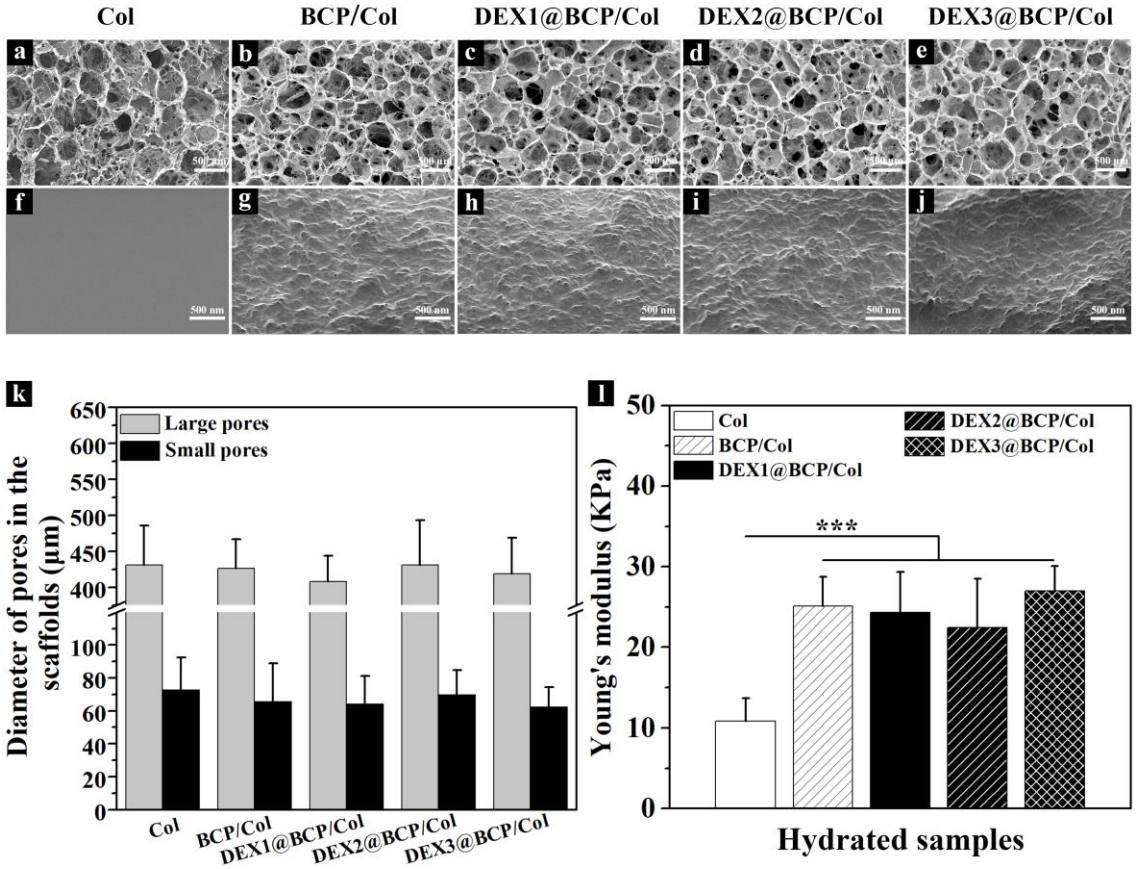

Fig. 3.4. SEM images (a-j) of cross-sections of the Col scaffold and BCP/Col composite scaffolds prepared with a different mass ratio of BCP NPs/collagen (BCP: Col) at low (a-e) and high (f-j) magnifications. Scale bar: (a-e), 500 μm; (f-j), 50 μm. Diameter of the large pores and the small pores in the Col scaffold and the BCP/Col composite scaffolds prepared with a different mass ratio of BCP NPs/collagen (k). Young's modulus of the hydrated scaffolds of the Col and BCP/Col prepared with a different mass ratio of BCP NPs/collagen (l). Data represent mean ± SD, N = 3. Significant difference: *, $p < 0.05$; **, $p < 0.01$; ***, $p < 0.001$.

Table 3.1. Porosity of Col, BCP/Col, DEX1@BCP/Col, DEX2@BCP/Col and DEX3@BCP/Col scaffolds.

Sample	Col	BCP/Col	DEX1@BCP/Col	DEX2@BCP/Col	DEX3@BCP/Col
Porosity (%)	98.6 ± 0.3	98.1 ± 0.6	97.8 ± 0.5	98.0 ± 0.7	98.3 ± 0.2

3.4.3 DEX release from DEX@BCP/Col composite scaffolds

The loading amount of DEX in the DEX1@BCP/Col, DEX2@BCP/Col and DEX3@BCP/Col was 387.9 ± 46.8, 705.5 ± 62.3 and 856.2 ± 70.4 ng/scaffold, respectively. The loading amount and cumulative release amount of DEX from the DEX@BCP/Col scaffolds increased with increasing of the DEX feeding amount in the DEX@BCP NPs (Fig. 3.5a). The release of DEX was observed over a 35-day period. After incubation for 35 days, the cumulative release amount of DEX from the DEX1@BCP/Col, DEX2@BCP/Col and DEX3@BCP/Col was 339.9 ± 35.8, 553.5 ± 38.3 and 712.5 ± 57.1 ng/scaffold, respectively. Based on the DEX loading amount, the percentage of released DEX was calculated (Fig. 3.5b). After 35 days, the DEX

release percentage from the DEX1@BCP/Col, DEX2@BCP/Col and DEX3@BCP/Col was 87.6 ± 9.2 %, 78.4 ± 5.2 % and 83.2 ± 6.7 %, respectively.

3.4.4 Cell adhesion, distribution, viability and proliferation during *in vitro* culture

The biocompatibility of Col, BCP/Col and DEX@BCP/Col composite scaffolds was evaluated by examination of adhesion, distribution, viability and proliferation of hMSCs in the scaffolds. For all the Col, BCP/Col and DEX@BCP/Col composite scaffolds, hMSCs could be seeded homogeneously throughout the whole scaffolds (Fig. 3.6). SEM observation showed that hMSCs well adhered on the walls of the spherical large pores in all the scaffolds (Fig. 3.7a). When compared to the control Col scaffold, hMSCs seeded in the BCP/Col and DEX@BCP/Col scaffolds showed more filopodia and more widely spread. Live/dead staining was performed to evaluate cell viability after 7 days culture. Most of the hMSCs were alive (green fluorescence) and few dead cells (red fluorescence) were observed in all the scaffolds. The results indicated high viability of hMSCs when being cultured in the scaffolds (Fig. 3.7b). DNA quantification showed that hMSCs proliferated in the porous scaffolds in a time-dependent manner (Fig. 3.7c). After being cultured for 4 weeks, the cell number in the BCP/Col was significantly higher than that of other groups. The cell number in the DEX1@BCP/Col and DEX2@BCP/Col was significantly higher than that of Col+DEX. These results indicated BCP NPs showed obvious stimulation to the proliferation of hMSCs, while DEX showed a little inhibition to the proliferation of hMSCs.

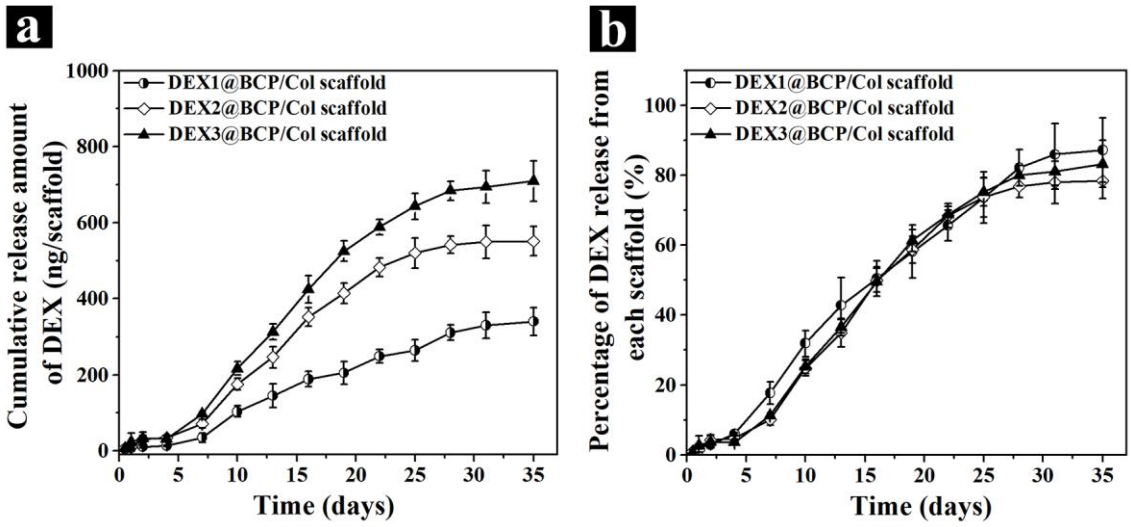

Fig. 3.5. Cumulative amount (a) and percentage (b) of the released DEX from the DEX1@BCP/Col, DEX2@BCP/Col and DEX3@BCP/Col composite scaffolds. Data represent means ± SD, N=3.

3.4.5 ALP staining and ALP activity assay

ALP staining (Fig. 3.8a) demonstrated that a slightly more intense staining was observed in the cells cultured in the BCP/Col scaffold when compared to the Col group, while the staining intensity in all the DEX-contained groups was obviously stronger than that of the groups without DEX. The staining intensity of the BCP/Col+DEX was stronger than those of the Col+DEX and DEX1@BCP/Col, while similar to those of the DEX2@BCP/Col and DEX3@BCP/Col. The results of ALP activity assay corresponded well with that of the ALP staining (Fig. 3.8b). The ALP activity in all the culture conditions increased in an order of Col < BCP/Col< DEX1@BCP/Col < Col+DEX ≈ DEX2@BCP/Col < BCP/Col+DEX < DEX3@BCP/Col. The

results of ALP staining and ALP activity assay demonstrated that the BCP NPs showed some stimulation on osteogenic differentiation of hMSCs. The DEX@BCP/Col composite scaffolds with a higher loading amount of DEX resulted in more significant stimulation on the osteogenic differentiation of hMSCs.

3.4.6 Expression of osteogenesis-related genes of *in vitro* samples

The expression of osteogenic marker genes in hMSCs was analyzed by RT-PCR after 28 days culture in the scaffolds (Fig. 3.9). The expression of ALP, RUNX2, IBSP and BMP-2 genes was up-regulated by the BCP/Col and DEX@BCP/Col scaffolds when compared to the Col scaffold. ALP and RUNX2 genes showed similar expression patterns, being up-regulated in an increasing order of Col< BCP/Col < Col+DEX < DEX1@BCP/Col < BCP/Col+DEX < DEX2@BCP/Col< DEX3@BCP/Col (Fig. 3.9a, 3.9c). IBSP gene expression was up-regulated in an order of Col< Col+DEX < BCP/Col < BCP/Col+DEX < DEX1@BCP/Col < DEX2@BCP/Col< DEX3@BCP/Col (Fig. 3.9b). BMP-2 gene expression increased in an order of Col< BCP/Col < Col+DEX < DEX1@BCP/Col < DEX2@BCP/Col < BCP/Col+DEX < DEX3@BCP/Col (Fig. 3.9d). The results suggested that both BCP NPs and DEX showed some stimulation to the expression of osteogenic genes. The DEX@BCP/Col scaffolds stimulated osteogenic gene expression of hMSCs in a DEX amount-dependent manner. The composite scaffolds containing higher amount of DEX (DEX2@BCP/Col and DEX3@BCP/Col) had better stimulatory effects on osteogenic gene expression.

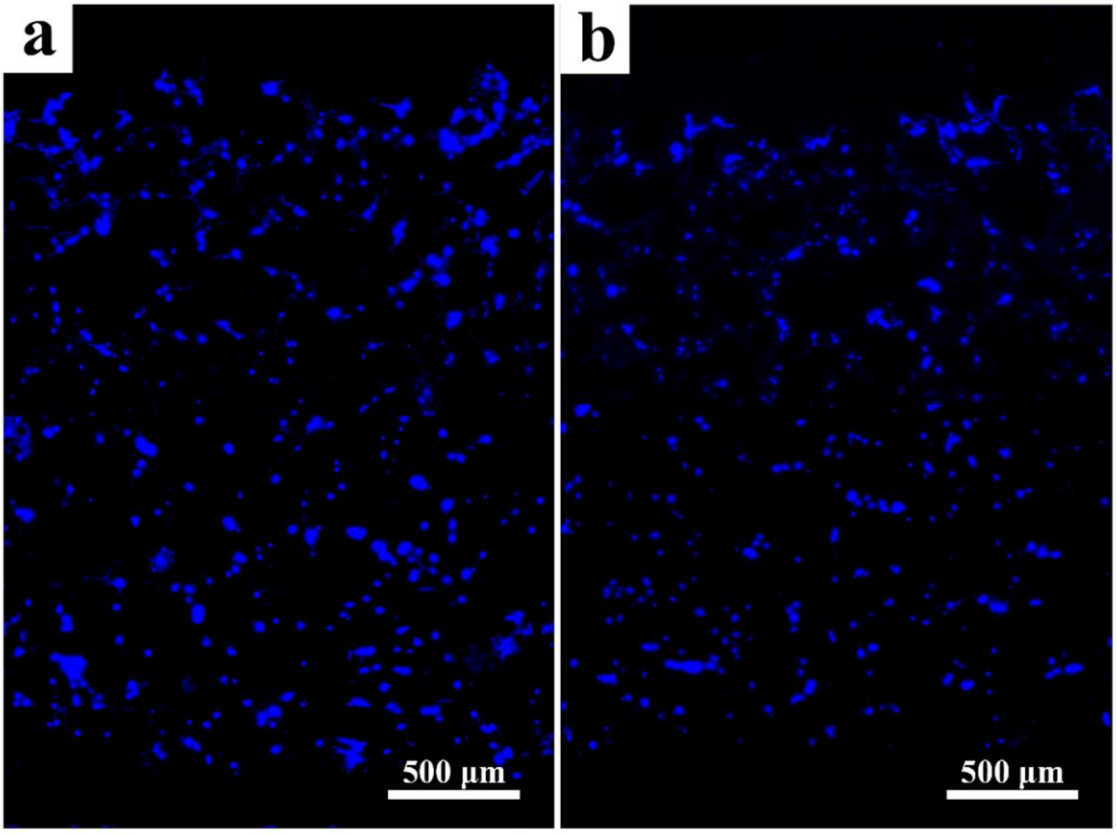

Fig. 3.6. Cell distributions in the Col scaffold (a) and DEX1@BCP/Col composite scaffold (b) after 1 day of culture. Cell nuclei were stained by DAPI and observed under a fluorescence microscope. The blue fluorescence indicates cell nuclei labelled by DAPI.

3.4.7 Gross appearance and histological analysis of *in vivo* implants

The cells/scaffold constructs were implanted into the dorsa of nude mice for 6 and 12 weeks. Gross appearance of the implants after 12 weeks implantation is shown in Fig. 3.10a. The Col and Col+DEX implants were flesh-colored with evident deformation of their shapes. The implants of the composite scaffolds were reddish, which should be due to regeneration of capillary blood vessels in the scaffolds. Measurement of the facade and lateral areas showed that the size of the Col and Col+DEX implants significantly decreased when compared to their initial size. However, the size of the composite scaffold implants had no obvious change (Fig. 3.10b, c).

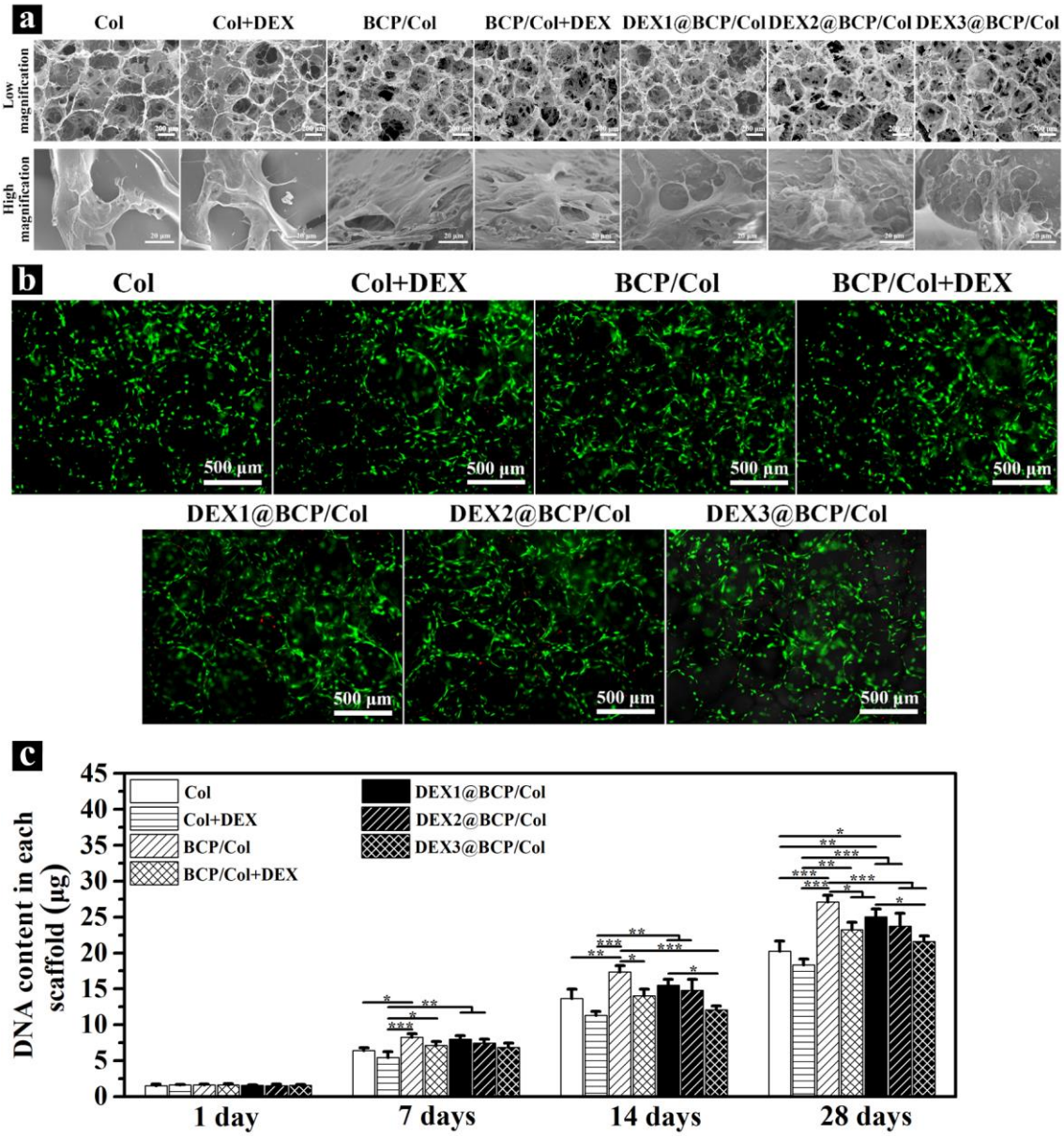

Fig. 3.7. SEM images of the cross-sections of the Col, BCP/Col and DEX@BCP/Col scaffolds after 1-day *in vitro* culture (a). Live/dead staining of the hMSCs in the scaffolds after 7 days *in vitro* culture (b). Quantification of DNA content in the scaffolds after 1, 7, 14 and 28 days *in vitro* culture (c). Data represent mean ± SD, N = 4. Significant difference: *, $p < 0.05$; **, $p < 0.01$; ***, $p < 0.001$.

H&E staining showed clear cell infiltration, uniform cell distribution and homogenous deposition of ECM throughout all the implants (Fig. 3.10d, e). After 6 weeks, new bone formation was observed in the BCP/Col, BCP/Col+DEX, DEX1@BCP/Col, DEX2@BCP/Col and DEX3@BCP/Col implants while not evident in the Col implant. The signs for new bone formation in the DEX1@BCP/Col, DEX2@BCP/Col and DEX3@BCP/Col implants were more evident than those in the BCP/Col and BCP/Col+DEX implants. Furthermore, new blood vessels that were characterized by the presence of lining endothelial cells and red blood cells were observed in the BCP/Col, BCP/Col+DEX, DEX1@BCP/Col, DEX2@BCP/Col and DEX3@BCP/Col implants (Fig. 3.11). After 12 weeks implantation, the new bone formation became more obvious than the 6 weeks implants, in particular for the BCP/Col+DEX, DEX1@BCP/Col, DEX2@BCP/Col and DEX3@BCP/Col implants. The area of the newly formed bone in the DEX3@BCP/Col was much higher than those in the DEX1@BCP/Col and DEX2@BCP/Col implants. Plenty of new blood vessels were formed in the BCP/Col, BCP/Col+DEX and DEX@BCP/Col implants.

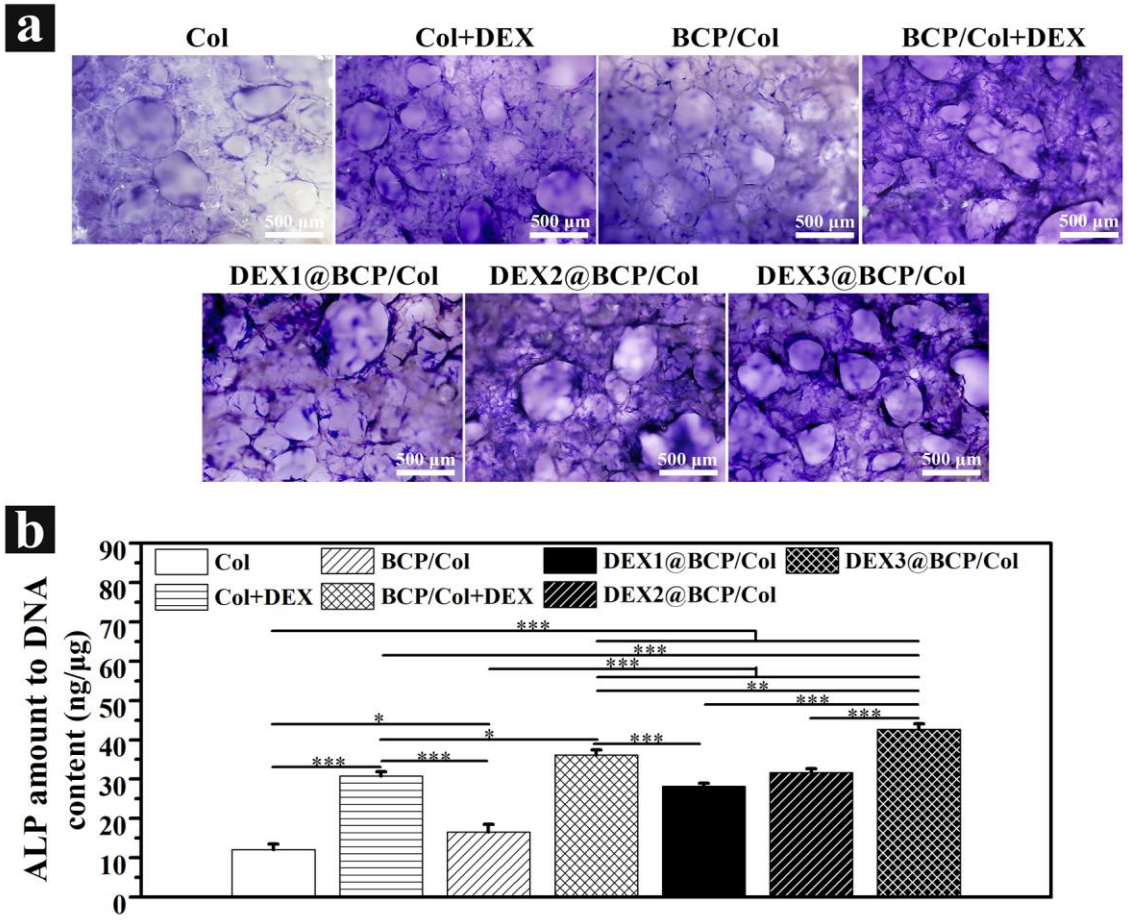

Fig. 3.8. ALP staining (a) and ALP activity assay (b) of the hMSCs in the Col, BCP/Col and DEX@BCP/Col scaffolds after 14 days *in vitro* culture. Data represent mean ± SD, N = 3. Significant difference: *, $p < 0.05$; **, $p < 0.01$; ***, $p < 0.001$. ALP staining (a) and ALP activity assay (b) of the hMSCs in the Col, BCP/Col and DEX@BCP/Col scaffolds after 14 days *in vitro* culture. Data represent mean ± SD, N = 3. Significant difference: *, $p < 0.05$; **, $p < 0.01$; ***, $p < 0.001$.

3.4.8 Immunohistochemical staining of osteogenesis-related proteins

To detect the presence of osteogenesis-related proteins, immunohistochemical staining of human Col I and OCN was carried out for the 6 and 12 weeks implants (Fig. 3.12). The Col I and OCN proteins were detected in all the implants except the Col implant. Expression of Col I and OCN in the BCP/Col+DEX, DEX1@BCP/Col, DEX2@BCP/Col and DEX3@BCP/Col implants was much higher than that in the Col+DEX and BCP/Col implants after both 6 and 12 weeks implantation. The expression of Col I and OCN in the DEX1@BCP/Col, DEX2@BCP/Col and DEX3@BCP/Col implants was the highest. The results indicated the osteogenesis degree in the DEX1@BCP/Col, DEX2@BCP/Col and DEX3@BCP/Col was much higher than that of the other groups.

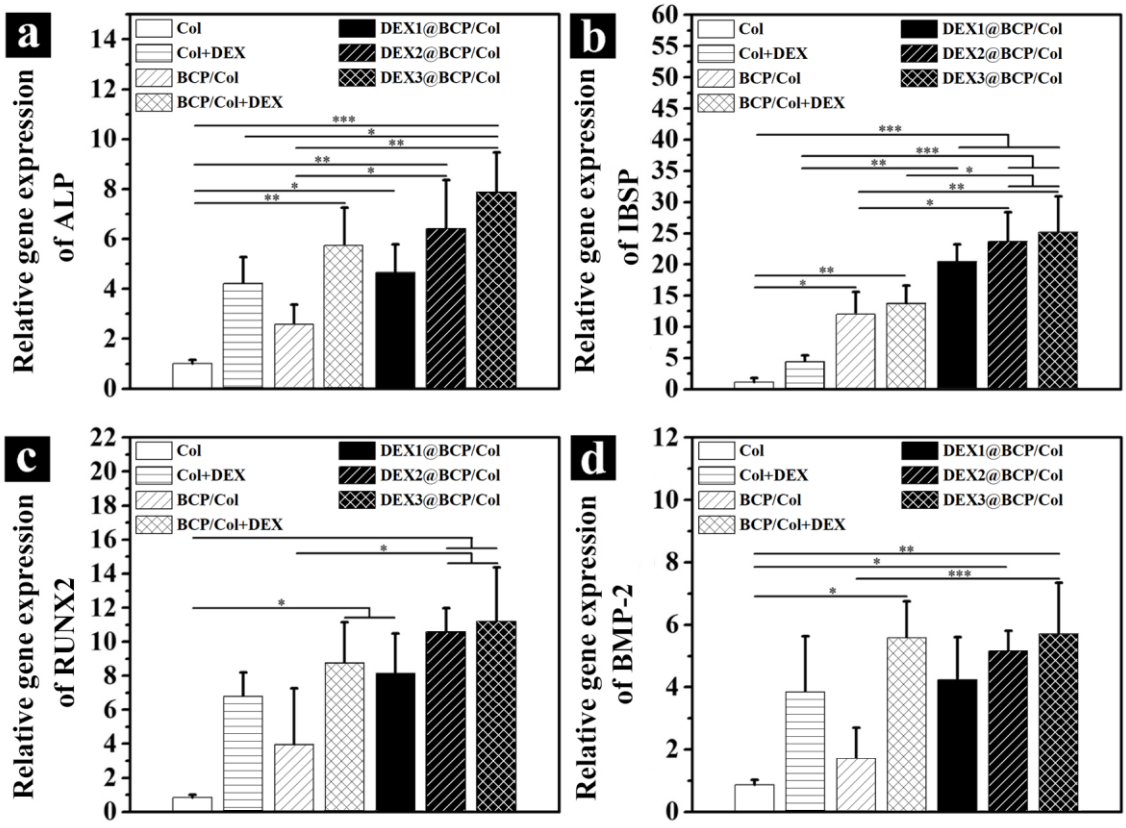

Fig. 3.9. Gene expression of ALP (a), IBSP (b), RUNX2 (c) and BMP-2 (d) of the hMSCs in the Col, BCP/Col and DEX@BCP/Col scaffolds after 28 days *in vitro* culture. Data represent mean ± SD, N = 3. Significant difference: *, $p < 0.05$; **, $p < 0.01$; ***, $p < 0.001$.

3.4.9 Expression of osteogenesis-related genes of *in vivo* implants

The expression of osteogenic marker genes after *in vivo* implantation for 12 weeks was analyzed by RT-PCR (Fig. 3.13). The results showed that the expression of ALP, RUNX2, IBSP and BMP-2 genes was up-regulated by the BCP/Col, DEX1@BCP/Col, DEX2@BCP/Col and DEX3@BCP/Col implants compared to the Col implant. When compared to the Col+DEX implant, ALP gene was slightly up-regulated in the BCP/Col, BCP/Col+DEX, DEX1@BCP/Col and DEX2@BCP/Col implants, while significantly up-regulated in the DEX3@BCP/Col implant (Fig. 3.13a); IBSP was significantly up-regulated in the BCP/Col+DEX, DEX1@BCP/Col, DEX2@BCP/Col and DEX3@BCP/Col implants (Fig. 3.13b); RUNX2 and BMP-2 were slightly up-regulated in the BCP/Col and BCP/Col+DEX implants, while significantly

up-regulated in the DEX1@BCP/Col, DEX2@BCP/Col and DEX3@BCP/Col implants (Fig. 3.13c, d). The PCR results indicated the DEX1@BCP/Col, DEX2@BCP/Col and DEX3@BCP/Col implants showed the highest expression level of osteogenesis-related genes, which increased with the increase of DEX loading amount.

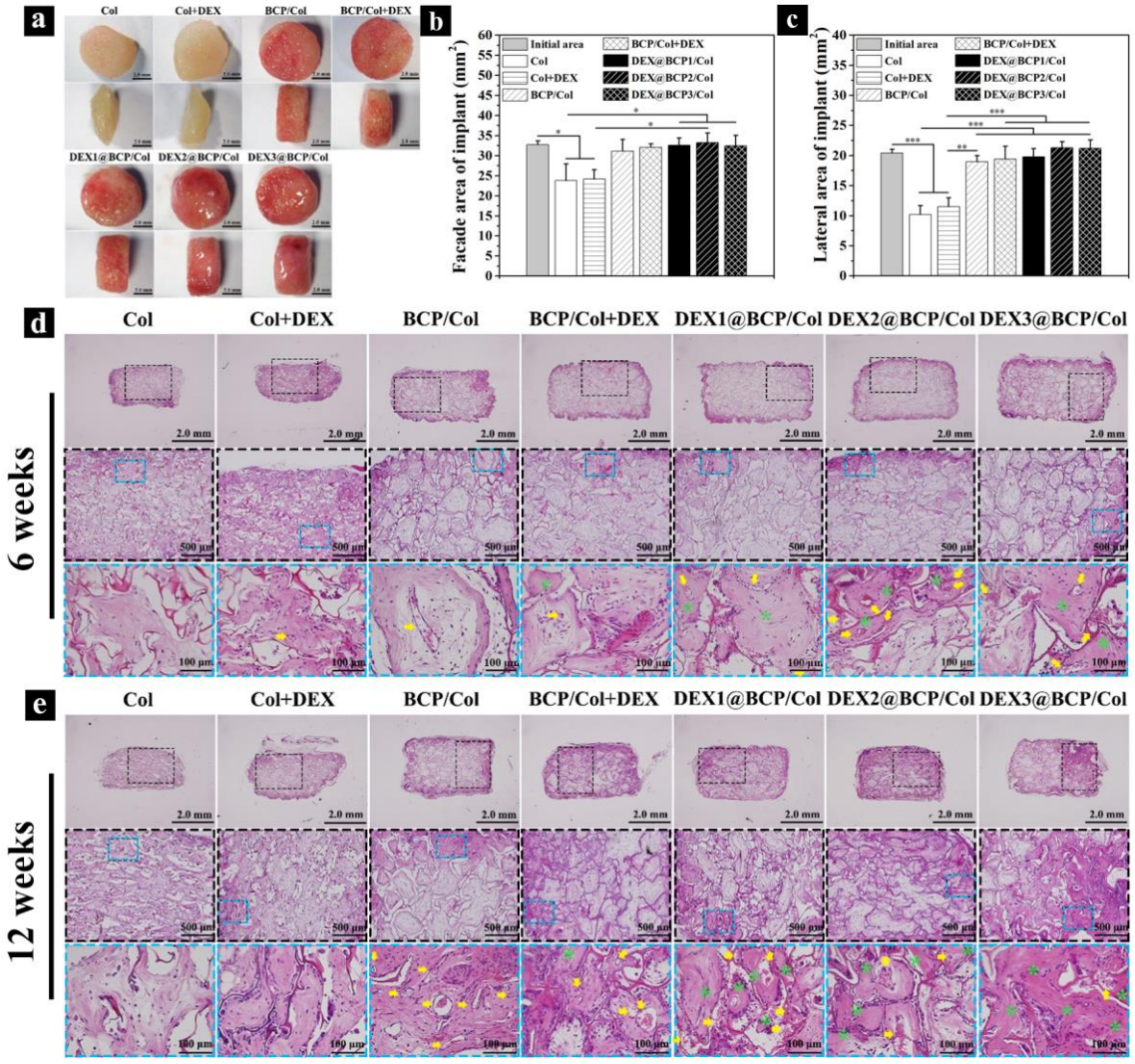

Fig. 3.10. Gross appearance (a), facade area (b) and lateral area (c) of the cells/scaffold constructs of the Col, BCP/Col and DEX@BCP/Col scaffolds after 12 weeks implantation. Scale bar: 2.0 mm. Data represent mean ± SD, N = 3. Significant difference: *, $p < 0.05$; **, $p < 0.01$; ***, $p < 0.001$. Photomicrographs of the H&E staining of the decalcified sections of the implants after *in vivo* implantation for 6 weeks (d) and 12 weeks (e). Yellow arrows indicate the new blood vessels. Green stars indicate the new bone formation.

3.5 Discussion

Mimicking the osteogenic matrices of bone is an important strategy to prepare biomimetic scaffolds for bone TE. Composition of natural bone is about 35% organic (primarily collagen type I) and about 65% inorganic (nanocrystalline calcium phosphate, CaP) [32]. Both collagen and CaP have been used to prepare the bone TE scaffolds. Although collagen scaffolds have shown good biological performance, they have the problem of insufficient mechanical stability [33]. On the other hand, CaP scaffolds have good mechanical

property while lacking appropriate degradability and pore structure [34]. Combination of collagen and CaP may be a useful strategy for preparation of porous scaffolds with a better performance for bone TE. In this study, biphasic calcium phosphate nanoparticles (BCP NPs) were hybridized with collagen to prepare BCP/Col composite scaffolds. Ice particulates, which are nontoxic and easily removed through freeze-drying, were used as the porogen material to control the pore structures such as pore size and interconnectivity [35]. In natural bone, the mass ratio of inorganic to organic compositions is about 2: 1. The BCP/Col composite scaffold prepared with the BCP NPs/collagen mass ratio of 2: 1 exhibited the highest mechanical property. However, most of the spherical large pores formed in the 2: 1 BCP/Col composite scaffold were isolated pores without interconnection (Fig. 3.3). Pore interconnectivity is extremely important for bone TE scaffolds to facilitate cell seeding, migration and distribution throughout the scaffolds [36]. When ice particulates were used as the porogen material, the spherical large pores formed in scaffold should be the negative replicas of the ice particulates, while the interconnective small pores should be the replicas of the ice crystals formed in situ to connect the large ice particulates during the pre-freezing process [37]. The BCP NPs in the BCP NPs/Col/ice particulates mixture might influence the formation of new ice crystals. In particular, too many BCP NPs at the BCP NPs/collagen mass ratio of 2: 1 might inhibit the formation of the ice crystals connecting the porogen ice particulates. When the mass ratio of BCP NPs/collagen was decreased to 1: 1, the BCP/Col composite scaffold had the same pore structure as that of the control Col scaffold and its mechanical property was still very high (Fig. 3.3). Therefore, the BCP NPs/collagen mass ratio of 1: 1 was chosen as the optimal ratio to prepare the BCP/Col and DEX@BCP/Col composite scaffolds for other experiments.

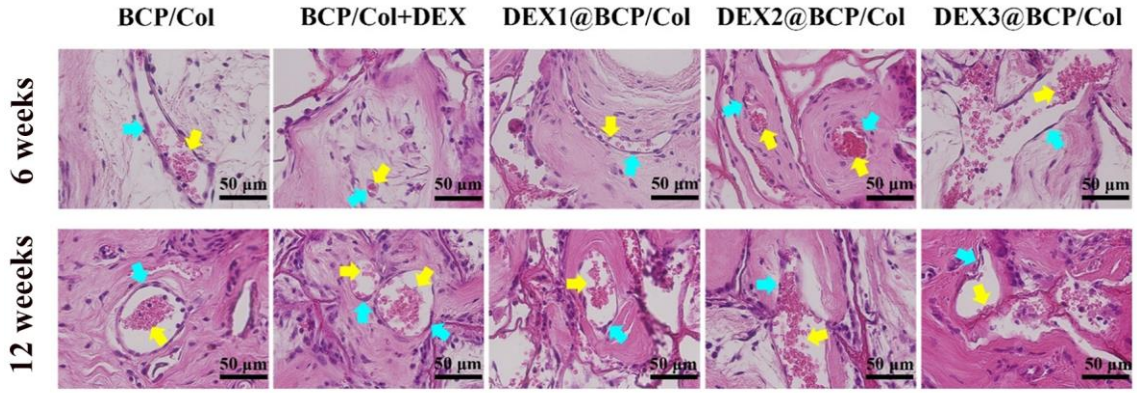

Fig. 3.11. Presence of the newly formed blood vessels in the cells/scaffold constructs after implantation for 6 and 12 weeks. The yellow arrows indicate the red blood cells in the blood vessels. The blue arrows indicate the endothelial cells lining the blood vessels.

Bone tissue has a hierarchical structure ranging from macroscale to nanoscale [38]. Many studies have attempted to mimic architecture of natural bone [39, 40]. In this study, the nano-sized DEX@BCP NPs were distributed homogenously on the walls of the DEX@BCP/Col composite scaffolds, providing nanocomposite surfaces for cell adhesion (Fig. 3.4). Due to the well-controlled pore structures with nanoscale features, hMSCs could migrate and adhere in the DEX@BCP/Col composite scaffolds and showed homogenous distribution throughout the scaffolds (Fig. 3.6, Fig. 3.7a). The cells had high viability and proliferated in the scaffolds (Fig. 3.7b, c). BCP NPs showed some stimulatory effects on proliferation of hMSCs, which was in accordance with previous studies [7, 41]. These results indicated good biocompatibility of the DEX@BCP/Col composite scaffolds.

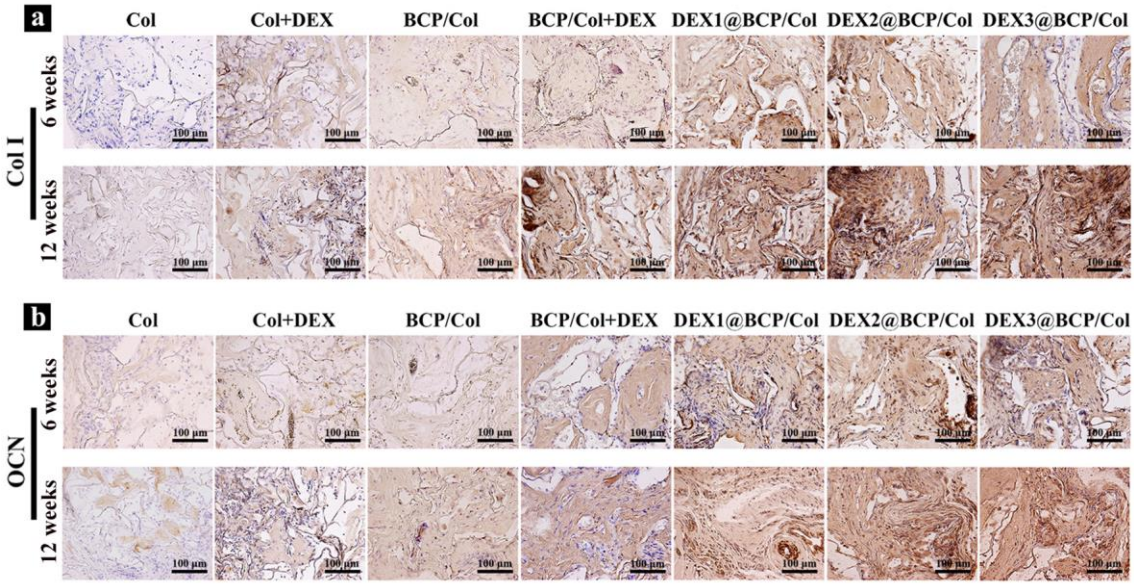

Fig. 3.12. Immunohistochemical staining of Col I (a) and OCN (b) in the decalcified sections of the cells/scaffold constructs of the Col, BCP/Col and DEX@BCP/Col scaffolds after 6 weeks and 12 weeks implantation. The sections were counterstained with hematoxylin. The brown signals show the presence of Col I and OCN in the cells/scaffold constructs. The blue signals show the cell nuclei.

Osteoinductive cues are important for bone TE [42]. As a useful osteoinductive factor, DEX was incorporated into the BCP NPs and further hybridized with collagen to prepare the DEX@BCP/Col composite scaffolds. DEX was loaded in the BCP NPs during the nucleation and growth of the crystals of the BCP NPs. The low molecular weight molecule DEX should be physically locked in BCP NPs. When the DEX-loaded BCP NPs were degraded, DEX was released [29]. The DEX@BCP/Col scaffolds showed a controlled and sustained release profile of DEX which could last for 35 days (Fig. 3.5). The released amount of DEX could be regulated by varying the initial DEX loading amount in the DEX@BCP NPs. From the 7^{th} to 31^{th} day of cell culture, the average release amount of DEX from the DEX1@BCP/Col, DEX2@BCP/Col and DEX3@BCP/Col scaffolds during every three days was 36.9 ± 17.4, 62.7 ± 29.5 and 74.7 ± 36.0 ng/scaffold, respectively (Fig. 3.5a). 3 days was the medium change time of the positive control that was cultured in medium containing 100 nM (39.6 ng/mL) free DEX. The released amount of DEX from the DEX@BCP/Col scaffolds during cell culture could match the amount of free DEX supplemented in the positive control samples.

Rapid bone regeneration requires effective osteogenic differentiation of stem cells within the scaffolds [43]. ALP activity and gene expression of ALP, RUNX2, IBSP and BMP-2 demonstrated that hMSCs cultured in the DEX@BCP/Col composite scaffolds showed obvious osteogenic differentiation. The DEX@BCP/Col composite scaffolds with different initial loading amount of DEX stimulated the osteogenic differentiation in a DEX amount-dependent manner (Fig. 3.8 and 3.9). The *in vivo* implantation further confirmed the enhanced osteogenic differentiation of hMSCs in the DEX@BCP/Col scaffolds. From the histological results, ectopic new bone formation in the DEX@BCP/Col composite scaffolds was observed (green stars in Fig. 3.10d, 3.10e). IHC staining for Col I and OCN, as well as gene expression of ALP, RUNX2, IBSP and BMP-2 further proved the osteogenic differentiation of hMSCs and new bone regeneration in the DEX@BCP/Col composite scaffolds in the *in vivo* environment (Fig. 3.12 and 3.13). All the *in vitro* and *in vivo* analyses confirmed the DEX@BCP/Col scaffolds stimulated osteogenic differentiation of hMSCs.

Another interesting result in this study is the regeneration of capillary blood vessels in the BCP/Col and

DEX@BCP/Col composite scaffolds after *in vivo* implantation (Fig. 3.10d, e, Fig. 3.11). Bone healing is highly dependent on adequate angiogenesis [44]. Some previous studies have reported that CaP can stimulate the angiogenesis of scaffolds due to the enhanced adsorption of angiogenesis-related growth factors and constant release of Ca^{2+} which facilitate angiogenesis [45]. The embedded BCP NPs in the DEX@BCP/Col composite scaffolds showed similar stimulatory effect on angiogenesis. This should be another advantage of the DEX@BCP/Col composite scaffolds.

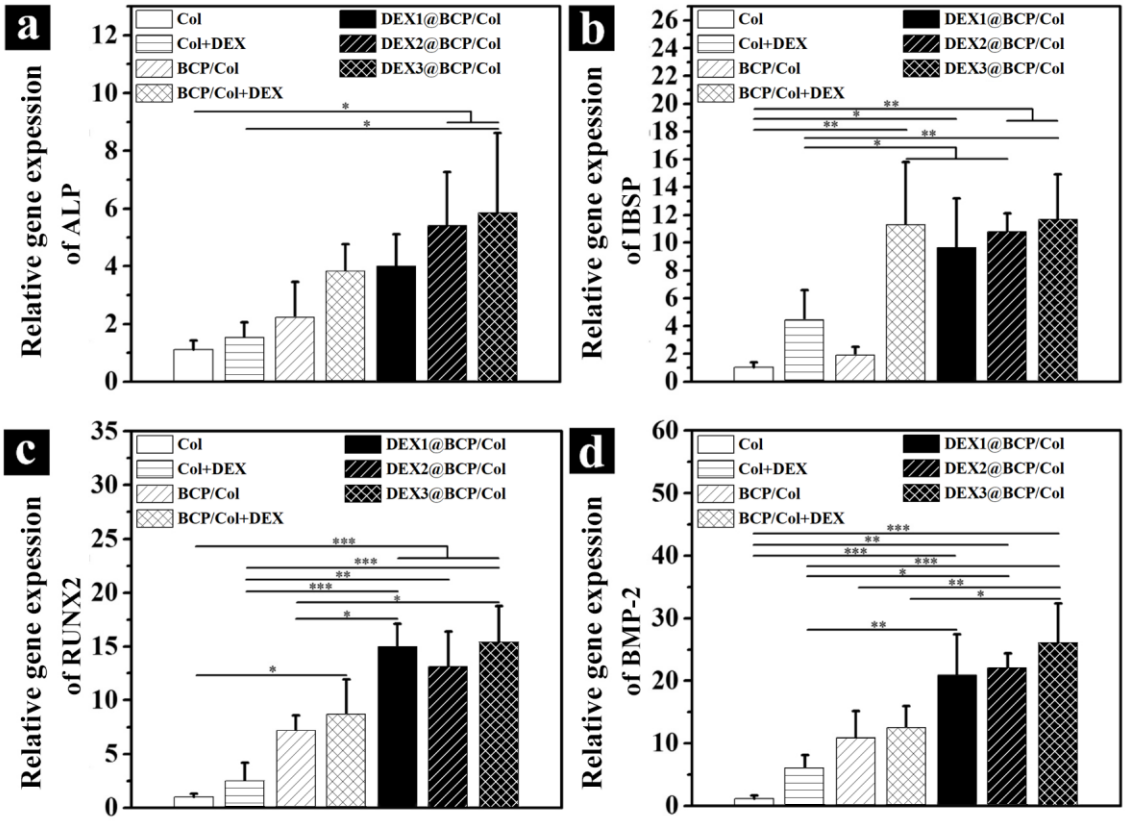

Fig. 3.13. Gene expression of ALP (a), IBSP (b), RUNX2 (c) and BMP-2 (d) of the hMSCs in the Col, BCP/Col and DEX@BCP/Col scaffolds after 12 weeks implantation. Data represent mean ± SD, N = 3. Significant difference: *, $p < 0.05$; **, $p < 0.01$; ***, $p < 0.001$.

Based on the results, a mechanism of promotive effect of the DEX@BCP/Col composite scaffolds on osteogenic differentiation of hMSCs was proposed. Firstly, the well-controlled microporous structures of the DEX@BCP/Col composite scaffolds allowed cell migration and homogeneous cell distribution. The nano-structured pore surfaces promoted cell adhesion. Secondly, the good mechanical property of the DEX@BCP/Col composite scaffolds supported cell proliferation and ECM production. Thirdly, degradation of the DEX@BCP/Col composite scaffolds could sustainably release DEX, Ca^{2+} and PO_4^{3-} ions in an appropriate amount. The released DEX, Ca^{2+} and PO_4^{3-} ions could function synergistically to up-regulate the expression of osteogenic genes and proteins, resulting in the osteogenic differentiation of hMSCs. Angiogenesis was also promoted by the constant release of Ca^{2+} ions to facilitate the metabolic activities. All these factors worked together to promote osteogenic differentiation of hMSCs for new bone regeneration.

In summary, combination of porous Col scaffold and DEX@BCP NPs exerted synergistic effects on the osteogenesis and angiogenesis. Considering the advantages of porous collagen scaffold and the superior performance of the DEX@BCP NPs on the osteogenic differentiation of hMSCs, combination of these

factors may provide an effective strategy for bone TE. On the other hand, although the Young's modulus of the DEX@BCP/Col composite scaffolds was 2.5-fold higher than the porous collagen scaffold and much higher than some other literature-reported NPs/polymer composite scaffolds [46-48], it was still much lower than that of natural bone. For practical applications, the DEX@BCP/Col composite scaffolds can be used as substitution for non-weight-bearing bones such as the skull cranial bones, or as substitution for weight-bearing bones which can be physically fixed at initial stage of the bone reconstruction to avoid load-bearing. Rapid generation of new bone tissue in the composite scaffolds can be expected due to their excellent osteoconductivity and osteoinductivity, during which the mechanical property of the implants can dramatically increase until the whole scaffolds are replaced by newly formed bone tissue.

3.6 Conclusions

DEX-loaded BCP NPs/Col composite scaffolds with precisely controlled pore structures and a sustained release of DEX were prepared. The DEX@BCP NPs were distributed homogeneously on the walls of the scaffolds, enhancing the mechanical property and roughness of the scaffolds. The sustained and prolonged release of DEX from the scaffolds could last for 35 days. The DEX@BCP/Col scaffolds with different DEX loading amount had good biocompatibility and stimulated osteogenic differentiation of hMSCs and new bone tissue regeneration during *in vitro* culture and *in vivo* implantation. The DEX@BCP/Col composite scaffold with the highest DEX loading amount showed the most promising potential for bone tissue engineering. The DEX@BCP/Col composite scaffolds should provide some useful guidance for bone tissue engineering.

3.7 References

[1] Giannoudis PV, Dinopoulos H, Tsiridis E. Bone substitutes: an update. Injury. 2005;36:S20-S7.
[2] Salgado AJ, Coutinho OP, Reis RL. Bone tissue engineering: state of the art and future trends. Macromol. Biosci. 2004;4:743-65.
[3] Xu M, Li H, Zhai D, Chang J, Chen S, Wu C. Hierarchically porous nagelschmidtite bioceramic–silk scaffolds for bone tissue engineering. J. Mater. Chem. B 2015;3:3799-809.
[4] Fang X, Xie J, Zhong L, Li J, Rong D, Li X, Ouyang J. Biomimetic gelatin methacrylamide hydrogel scaffolds for bone tissue engineering. J. Mater. Chem. B. 2016;4:1070-80.
[5] Kim IG, Hwang MP, Du P, Ko J, Ha C-w, Do SH, Park K. Bioactive cell-derived matrices combined with polymer mesh scaffold for osteogenesis and bone healing. Biomaterials. 2015;50:75-86.
[6] Xia L, Zhang N, Wang X, Zhou Y, Mao L, Liu J, Jiang X, Zhang Z, Chang J, Lin K. The synergetic effect of nano-structures and silicon-substitution on the properties of hydroxyapatite scaffolds for bone regeneration. J. Mater. Chem. B. 2016;4:3313-23.
[7] Chen Y, Wang J, Zhu X, Tang Z, Yang X, Tan Y, Fan Y, Zhang X. Enhanced effect of β-tricalcium phosphate phase on neovascularization of porous calcium phosphate ceramics: in vitro and in vivo evidence. Acta Biomater. 2015;11:435-48.
[8] Zhang W, Feng C, Yang G, Li G, Ding X, Wang S, Dou Y, Zhang Z, Chang J, Wu C. 3D-printed scaffolds with synergistic effect of hollow-pipe structure and bioactive ions for vascularized bone regeneration. Biomaterials. 2017;135:85-95.
[9] Wang F, Zhai D, Wu C, Chang J. Multifunctional mesoporous bioactive glass/upconversion nanoparticle nanocomposites with strong red emission to monitor drug delivery and stimulate osteogenic differentiation of stem cells. Nano Res. 2016;9:1193-208.

[10] Chen Y, Wang J, Zhu X, Fan Y, Zhang X. Adsorption and release behaviors of vascular endothelial growth factor on porous hydroxyapatite ceramic under competitive conditions. J. Biomater. Tissue Eng. 2014;4:155-61.
[11] Du C, Cui F, Zhang W, Feng Q, Zhu X, De Groot K. Formation of calcium phosphate/collagen composites through mineralization of collagen matrix. J. Biomed. Mater. Res., Part A. 2000;50:518-27.
[12] Soriano I, Evora C. Formulation of calcium phosphates/poly (d, l-lactide) blends containing gentamicin for bone implantation. J. Controlled Release 2000;68:121-34.
[13] Ongpipattanakul B, Nguyen T, Zioncheck TF, Wong R, Osaka G, DeGuzman L, Lee WP, Beck LS. Development of tricalcium phosphate/amylopectin paste combined with recombinant human transforming growth factor beta 1 as a bone defect filler. J. Biomed. Mater. Res., Part A. 1997;36:295-305.
[14] Fujishiro Y, Takahashi K, Sato T. Preparation and compressive strength of α-tricalcium phosphate/gelatin gel composite cement. J. Biomed. Mater. Res. 2001;54:525-30.
[15] Kim HW, Knowles JC, Kim HE. Hydroxyapatite and gelatin composite foams processed via novel freeze-drying and crosslinking for use as temporary hard tissue scaffolds. J. Biomed. Mater. Res., Part A. 2005;72:136-45.
[16] Le Nihouannen D, Le Guehennec L, Rouillon T, Pilet P, Bilban M, Layrolle P, Daculsi G. Micro-architecture of calcium phosphate granules and fibrin glue composites for bone tissue engineering. Biomaterials. 2006;27:2716-22.
[17] Lee YM, Park YJ, Lee SJ, Ku Y, Han SB, Klokkevold PR, Choi SM, Chung CP. Tissue engineered bone formation using chitosan/tricalcium phosphate sponges. J. Periodontol. 2000;71:410-7.
[18] Ripamonti U, Parak R, Klar RM, Dickens C, Dix-Peek T, Duarte R. The synergistic induction of bone formation by the osteogenic proteins of the TGF-β supergene family. Biomaterials. 2016;104:279-96.
[19] Wadhwa R, Lagenaur CF, Cui XT. Electrochemically controlled release of dexamethasone from conducting polymer polypyrrole coated electrode. J. Controlled Release. 2006;110:531-41.
[20] Zhang Y, Zhang M. Calcium phosphate/chitosan composite scaffolds for controlled in vitro antibiotic drug release. J. Biomed. Mater. Res. 2002;62:378-86.
[21] Itoh S, Kikuchi M, Takakuda K, Koyama Y, Matsumoto HN, Ichinose S, Tanaka J, Kawauchi T, Shinomiya K. The biocompatibility and osteoconductive activity of a novel hydroxyapatite/collagen composite biomaterial, and its function as a carrier of rhBMP-2. J. Biomed. Mater. Res. 2001;54:445-53.
[22] Yamamoto M, Ikada Y, Tabata Y. Controlled release of growth factors based on biodegradation of gelatin hydrogel. J. Biomater. Sci., Polym. Ed. 2001;12:77-88.
[23] Lee Y-M, Park Y-J, Lee S-J, Ku Y, Han S-B, Klokkevold PR, Chung C-P. The bone regenerative effect of platelet-derived growth factor-BB delivered with a chitosan/tricalcium phosphate sponge carrier. J. Periodontol. 2000;71:418-24.
[24] Ziegler J, Mayr-Wohlfart U, Kessler S, Breitig D, Günther KP. Adsorption and release properties of growth factors from biodegradable implants. J. Biomed. Mater. Res. 2002;59:422-8.
[25] Chou JW-L, Decarie D, Dumont RJ, Ensom MH. Stability of Dexamethasone in Extemporaneously Prepared Oral Suspensions. J. Can. Pharm. Hosp. 2001;54:97-103.
[26] Amjadian S, Seyedjafari E, Zeynali B, Shabani I. The synergistic effect of nano-hydroxyapatite and dexamethasone in the fibrous delivery system of gelatin and poly (l-lactide) on the osteogenesis of mesenchymal stem cells. Int. J. Pharm. 2016;507:1-11.
[27] Qiu K, Chen B, Nie W, Zhou X, Feng W, Wang W, Chen L, Mo X, Wei Y, He C. Electrophoretic deposition of dexamethasone-loaded mesoporous silica nanoparticles onto poly (L-lactic acid)/poly (ε-caprolactone) composite scaffold for bone tissue engineering. CS Appl. Mater. Interfaces 2016;8:4137-48.

[28] Li L, Zhou G, Wang Y, Yang G, Ding S, Zhou S. Controlled dual delivery of BMP-2 and dexamethasone by nanoparticle-embedded electrospun nanofibers for the efficient repair of critical-sized rat calvarial defect. Biomaterials 2015;37:218-29.
[29] Chen Y, Li J, Kawazoe N, Chen G. Preparation of dexamethasone-loaded calcium phosphate nanoparticles for osteogenic differentiation of human mesenchymal stem cells. J. Mater. Chem. B 2017;5:6801-10.
[30] Zhang Q, Lu H, Kawazoe N, Chen G. Pore size effect of collagen scaffolds on cartilage regeneration. Acta Biomater. 2014;10:2005-13.
[31] Cai R, Nakamoto T, Kawazoe N, Chen G. Influence of stepwise chondrogenesis-mimicking 3D extracellular matrix on chondrogenic differentiation of mesenchymal stem cells. Biomaterials 2015;52:199-207.
[32] Pina S, Oliveira JM, Reis RL. Natural-Based Nanocomposites for Bone Tissue Engineering and Regenerative Medicine: A Review. Adv. Mater. 2015;27:1143-69.
[33] Meinel L, Karageorgiou V, Fajardo R, Snyder B, Shinde-Patil V, Zichner L, Kaplan D, Langer R, Vunjak-Novakovic G. Bone tissue engineering using human mesenchymal stem cells: effects of scaffold material and medium flow. Ann. Biomed. Eng. 2004;32:112-22.
[34] Zhou C, Deng C, Chen X, Zhao X, Chen Y, Fan Y, Zhang X. Mechanical and biological properties of the micro-/nano-grain functionally graded hydroxyapatite bioceramics for bone tissue engineering. J. Mech. Behav. Biomed. Mater. 2015;48:1-11.
[35] Zhang Q, Lu H, Kawazoe N, Chen G. Preparation of collagen scaffolds with controlled pore structures and improved mechanical property for cartilage tissue engineering. J. Bioact. Compat. Polym. 2013;28:426-38.
[36] Lee SJ, Lee D, Yoon TR, Kim HK, Jo HH, Park JS, Lee JH, Kim WD, Kwon IK, Park SA. Surface modification of 3D-printed porous scaffolds via mussel-inspired polydopamine and effective immobilization of rhBMP-2 to promote osteogenic differentiation for bone tissue engineering. Acta Biomater. 2016;40:182-91.
[37] Chen G, Ushida T, Tateishi T. Scaffold design for tissue engineering. Macromol. Biosci. 2002;2:67-77.
[38] Wang X, Xu S, Zhou S, Xu W, Leary M, Choong P, Qian M, Brandt M, Xie YM. Topological design and additive manufacturing of porous metals for bone scaffolds and orthopaedic implants: a review. Biomaterials. 2016;83:127-41.
[39] Luo Y, Lode A, Wu C, Chang J, Gelinsky M. Alginate/nanohydroxyapatite scaffolds with designed core/shell structures fabricated by 3D plotting and in situ mineralization for bone tissue engineering. ACS Appl. Mater. Interfaces. 2015;7:6541-9.
[40] Zhao C, Xia L, Zhai D, Zhang N, Liu J, Fang B, Chang J, Lin K. Designing ordered micropatterned hydroxyapatite bioceramics to promote the growth and osteogenic differentiation of bone marrow stromal cells. J. Mater. Chem. B. 2015;3:968-76.
[41] Ramay HR, Zhang M. Biphasic calcium phosphate nanocomposite porous scaffolds for load-bearing bone tissue engineering. Biomaterials. 2004;25:5171-80.
[42] Chen F-M, Zhang M, Wu Z-F. Toward delivery of multiple growth factors in tissue engineering. Biomaterials. 2010;31:6279-308.
[43] Higuchi A, Ling Q-D, Hsu S-T, Umezawa A. Biomimetic cell culture proteins as extracellular matrices for stem cell differentiation. Chem. Rev. 2012;112:4507-40.
[44] Kanczler J, Oreffo R. Osteogenesis and angiogenesis: the potential for engineering bone. Eur. Cells Mater. 2008;15:100-14.

[45] Li H, Chang J. Stimulation of proangiogenesis by calcium silicate bioactive ceramic. Acta Biomater. 2013;9:5379-89.
[46] Wei G, Ma PX. Structure and properties of nano-hydroxyapatite/polymer composite scaffolds for bone tissue engineering. Biomaterials 2004;25:4749-57.
[47] Wang H, Li Y, Zuo Y, Li J, Ma S, Cheng L. Biocompatibility and osteogenesis of biomimetic nano-hydroxyapatite/polyamide composite scaffolds for bone tissue engineering. Biomaterials 2007;28:3338-48.
[48] Kim S-S, Park MS, Jeon O, Choi CY, Kim B-S. Poly (lactide-co-glycolide)/hydroxyapatite composite scaffolds for bone tissue engineering. Biomaterials 2006;27:1399-409.

Chapter 4

Promoted angiogenesis and osteogenesis by dexamethasone-loaded calcium phosphate nanoparticles/collagen composite scaffolds with microgroove network

4.1 Summary

Reconstruction of large bone defects remains a significant clinical challenge as current approaches involving surgery or bone grafting often do not yield satisfactory outcomes. For the artificial bone substitutes used for bone grafting, angiogenesis plays a pivotal role directly leading to the final success of newly regenerated bone. In this part, dexamethasone-loaded biphasic calcium phosphate nanoparticles/collagen (DEX@BCP/Col) composite scaffolds with several types of concave microgrooves were prepared for simultaneous promotion of angiogenesis and osteogenesis. The microgrooves in the composite scaffolds were supposed to guide assembly of HUVECs into well aligned tubular structures, thus promoting rapid angiogenesis. The scaffolds were used for co-culture of HUVECs and hMSCs. Subcutaneous implantation in mice showed that more blood vessels and newly formed bone were observed in the microgrooved composite scaffolds than the control scaffold without microgrooves. The composite scaffolds bearing parallel microgrooves with a concave width of 290 μm and a convex ridge width of 352 μm had the highest promotion effect on angiogenesis and osteogenesis among the parallelly microgrooved composite scaffolds. The microgroove network had further superior effect than the parallel microgrooves. The results suggested that microgrooves in the composite scaffolds facilitated angiogenesis and stimulated new bone formation. The microgrooved composite scaffolds should be useful for repair of large bone defects.

4.2 Introduction

Although bone is one of the regenerative tissues, further intervention is needed when the bone defect beyond a certain critical size [1]. Nowadays, the use of autografts and allografts remains to be the gold standard in reparation of large bone defects. However, they have some drawbacks including limited sources, risk of infection and complications, immunological rejection and donor site morbidity [2]. Consequently, more and more attention has been drawn to design artificial bone substitutes with desirable biological properties for large bone defects. Healing of bone defects is a complicated process resulting from the

reciprocal actions of multiple cellular, molecular, biochemical and biomechanical cues, among which angiogenesis of the bone substitutes plays a pivotal role directly leading to the final success of newly regenerated bone [3]. Presence of functional vascular network within the implants is essential for the timely furnishing of oxygen, nutrients and signal molecules, as well as taking metabolic waste and carbon dioxide away [4]. Blood vessel invasion happens once the engineered tissue or material is implanted, but the vascular growth is too slow and almost negligible in providing sufficient blood supply, giving rise to osteonecrosis and trauma non-union, which is believed to be caused by cell death in the regions far from the capillaries [5]. Considering diffusion limit of oxygen and nutrients, generally any reconstructed tissue thicker than 400 μm must be vascularized to survive [6]. Therefore, a desirable scaffold for bone tissue engineering should have the functions to facilitate both angiogenesis and osteogenesis during bone regeneration process.

Incorporation of biological and pharmaceutical factors such as vascular endothelial growth factor (VEGF) and fibroblast growth factor in tissue engineering scaffolds has been generally used for promotion of angiogenesis [7, 8], which has achieved only limited success. Concerns about the usage of these growth factors or cytokines still remain, such as instability, uncontrollable dose, high cost, short half-life and increased risk for tumor. Thus, development of an alternative strategy to effectively induce angiogenesis of the bone substitutes hence to achieve a better bone regeneration in the large bone defects is strongly desirable.

Except for angiogenetic function, bone tissue engineering scaffolds should also have osteoinductive and osteoconductive functions to enhance regeneration of large size bone defects. Protein growth factors such as transform growth factor- β and bone morphogenetic protein-2 (BMP-2) have been frequently incorporated in scaffolds to increase their osteogenesis-promoting effects [9, 10]. Nevertheless, use of protein growth factors to promote bone regeneration has the same problems as mentioned above. Dexamethasone (DEX), which is an osteogenic inducer with low molecular weight, high potency and long-acting properties, has been used to substitute protein growth factors for promotion of osteogenesis. DEX has been incorporated into biphasic calcium phosphate nanoparticles (BCP NPs) to combine the synergistically osteogenic effects of DEX as well as the calcium and phosphorous ions released from the BCP NPs [11].

Therefore, in the present study, composite scaffolds with microgroove network were prepared for simultaneous promotion of angiogenesis and osteogenesis. DEX-loaded BCP NPs were hybridized with collagen to prepare DEX-BCP-Col composite scaffolds. During preparation of the composite scaffolds, pre-fabricated ice particulates were used as a pore-forming agent to control the pore size and increase pore interconnectivity. Furthermore, concave microgrooves were introduced in the composite scaffolds by using micropatterned ice lines or ice network. The combination of DEX, BCP NPs and collagen should have synergistic effects on osteogenic differentiation of stem cells. The microgrooves in the composite scaffolds were supposed to guide assembly of human umbilical vascular endothelial cells (HUVECs) into well aligned tubular structures thus promoting rapid angiogenesis. The composite scaffolds were used for co-culture of HUVECs and human bone marrow-derived mesenchymal stem cells (hMSCs). Effects of the scaffolds on angiogenesis and osteogenesis were investigated by *in vitro* cell culture and *in vivo* implantation.

4.3 Materials and methods

4.3.1 Preparation of DEX@BCP NPs

Gelatin DEX-loaded biphasic calcium phosphate nanoparticles (DEX-BCP NPs) were synthesized by incorporation of DEX during the formation of BCP NPs [11]. 4.5 mg of DEX ($C_{22}H_{29}FO_5$, Sigma-Aldrich)

was dissolved in 2 mL of ethanol and then added into the 48 mL of 0.52 M calcium nitrate tetrahydrate ($Ca(NO_3)_2 \cdot 4H_2O$, Sigma-Aldrich) aqueous solution. The mixture solution was added dropwise to 33.4 mL of 0.5 M diammonium phosphate ($(NH_4)_2HPO_4$, Sigma-Aldrich) solution by a syringe pump (KD Scientific Inc.). The reaction was conducted under magnetic stirring (700 rpm) in a 55 °C water bath. Throughout the reaction, ammonium hydroxide solution (NH_4OH, Sigma-Aldrich) was added dropwise into the reaction solution to maintain the pH at 9.5. After the reaction was maintained for 30 minutes, the slurry was aged for 36 hours at room temperature (RT) to form the DEX-BCP NPs. The prepared DEX-BCP NPs were washed by dispersing them in 20 mL ethanol and shaking at 200 rpm and RT for 20 minutes followed with centrifugation at 8000 rpm. The washing with ethanol was repeated for 3 times to remove DEX adsorbed on surface of DEX-BCP NPs.

4.3.2 Preparation of microgrooved DEX-BCP-Col composite scaffolds

The microgrooved DEX-BCP-Col composite scaffolds were prepared by generation of parallel microgrooves or microgroove network in DEX-BCP-Col composite scaffolds which were prepared by applying pre-fabricated ice particulates as a pore-forming agent. Pure water was spayed into liquid nitrogen to prepare the ice particulates. The ice particulates sizing between 425 and 500 μm were obtained by using two sieves sizing of 425 and 500 μm [12]. Porcine type I collagen (Nitta Gelatin Inc.) was dissolving in 10% (v/v) ethanol aqueous solution to prepare 2.5% and 1.0% (w/v) collagen aqueous solutions. The DEX-BCP NPs were dispersed in 10% (v/v) ethanol aqueous solution to prepare their dispersion solution at a concentration of 93 mg/mL. The ice particulates, 2.5% collagen solution and DEX-BCP NPs dispersion solution were retained in a cooling chamber (Espec Corp.) at -5 ℃ for 4 hours to balance their temperature to -5 ℃. After temperature balance, 3 mL of the pre-cooled DEX-BCP NPs dispersion solution was added dropwise to 11 mL of the pre-cooled 2.5% collagen solution at -5 ℃ and mixed well. The mass ratio of NPs and collagen was 1: 1 (w/w). Then, ice particulates were blended into the collagen/NPs mixture solution at a ratio of 1: 1 (w/v) at -5 ℃. The components were mixed carefully to allow the ice particulates being homogeneously distributed in the mixture solution without air bubble and then poured into silicone mold 1 (9.5 cm in length, 6.5 cm in width and 3 mm in thickness) which were placed on a copper plate wrapped by perfluoroalkoxy film (PFA film, Universal Co., Ltd.). The surface of the collagen/NPs/ice particulates mixture was platted with a spatula and a second silicone mold (9.5 cm in length, 6.5 cm in width, and 0.5 mm in thickness) was settled exactly on mold 1 and the pre-cooled 1.0 % collagen solution were filled into the second mold.

Micropatterned ice templates bearing parallel ice lines or ice cross network were prepared by a jet dispenser (MJET-3-CTR, Musashi Engineering Inc.). Dispensing nozzle of the dispenser was manipulated by a SHOT mini 200α (Musashi Engineering Inc.). PFA film-wrapped copper plate was cooled by liquid nitrogen. The jet dispenser moved back and forth upon the pre-cooled copper plate and ejected water droplets onto the plate. Water droplets instantly freeze to form parallel ice lines or ice cross network. The size of water droplets and hence the width of each line of the micropatterns were controlled by pumping pressure in the syringe and the type of nozzle. The intervals between lines were controlled by CAD programs. 4 types of parallel ice line templates and 1 type of ice line network template were prepared. The micropatterned ice templates were balanced at -5 ºC for 20 minutes and then covered on the above-mentioned second silicon mold. The whole construct was then frozen at -80 ℃ for 8 hours and lyophilized in a freeze dryer (Wizard 2.0, SP scientific). The constructs were then cross-linked with 20 mM N-hydroxysuccimide (NHS, Wako Pure Chemical Industries, Ltd.) and 50 mM 1-ethyl-3-(3-dimethylaminopropyl) carbodiimide (EDC, Peptide Institute Inc.) in an 80% (v/v) ethanol aqueous solution at RT under gentle shaking (~ 20 rpm) for 8 hours.

After cross-linking, the constructs were washed 3 times with Milli-Q water. Glycine aqueous solution (0.1 M) was used to block the unreacted NHS residues. Then, the constructs were rinsed 6 times with water and lyophilized for usage of following experiments. 5 types of microgrooved DEX-BCP-Col composite scaffolds were prepared by using the 5 types of ice templates. They were 4 types of composite scaffolds with varied parallel microgrooves, and 1 type of composite scaffolds with microgroove network. The DEX-BCP-Col composite scaffold without microgrooves was prepared by the same procedure excepting usage of micropatterned template and used as a control.

4.3.3 Characterization of NPs and scaffolds

The morphology features of DEX-BCP NPs was visualized by a transmission electron microscope (TEM, JEOL 2100F). Aqueous solution containing 10 μL of DEX-BCP NPs was dropped on a carbon-coated copper grid to prepare the samples for TEM. The top layers and cross-sections of the microgrooved DEX-BCP-Col composite scaffolds and control composite scaffold were observed by a scanning electron microscope (SEM, JSM-5610, JEOL) at an acceleration voltage of 10 kV. All SEM images were inputted to an ImageJ software (ImageJ2, NIH) to quantify the concave width and convex ridge width of the microgrooves in the composite scaffolds. For each kind of samples, 4 images were used and every 5 microgrooves from each image were analyzed to calculate the means and standard deviations.

4.3.4 *In vitro* cell culture

The composite scaffolds were punched into cylindrical discs (Φ12 mm × H1.5 mm) for cell culture. The samples were sterilized with ethylene oxide gas for 5 hours. The sterilized samples were put in 12-well cell culture plate and conditioned in Dulbecco's Modified Eagle Medium (DMEM, Sigma-Aldrich) at 37 °C for 4 hours. The hMSCs (passage 2, Lonza) were sub-cultured using MSCBM medium (Lonza). The HUVECs (C2519A, Lonza) were sub-cultured using endothelial cell growth medium (EGM2, CC-3162, Lonza) that contained 2% FBS and vascular endothelial growth factor (VEGF). The cells were harvested using conventional trypsin/EDTA after reaching confluence and re-suspended in DMEM to prepare cell suspension solution of 2×10^6 cells/mL for cell seeding. 170 μL of the hMSCs suspension solution was dropped on the basal side (the side without microgrooves) of the scaffold discs. After being cultured for 3 hours, the scaffold discs were turned upside down and encircled by glass rings (inner diameter: 12 mm). 2 mL of the mixture medium (1: 1 MSCBM/EGM2) was added in each well and 200 μL of the HUVECs suspension solution was dropped on the top side (the side with microgrooves) of the scaffold discs. After culture for 6 hours in a humidified incubator at 37 °C and 5% CO_2, the glass rings were removed and the medium was changed to the mixture medium supplemented with 10 mM β-glycerophosphate.

4.3.5 Analysis of cell adhesion in the composite scaffolds

SEM was used to investigate cell adhesion and distribution in the composite scaffolds. After 1 day culture, the cell-seeded composite scaffold discs were rinsed 3 times with PBS. The samples were then fixed with glutaraldehyde (2.5%) at RT for 1 hour. After being rinsed for 3 times with PBS and water respectively, the fixed samples were freeze-dried and their top layers and cross-sections were observed by SEM.

4.3.6 Measurement of HUVECs assembly

The cells/scaffold constructs after 3 days culture were rinsed 3 times with PBS. The samples were then fixed by immersing in paraformaldehyde (4%) at RT for 15 minutes. The samples were washed with PBS, treated with Triton X-100 (0.2%) for at RT 1 hour and blocked in bovine serum albumin (BSA, 1%) at RT for 30 minutes on a rocker. Monoclonal mouse anti-human CD31 antibody (Clone JC70A, Dako) as the primary antibody was diluted in BSA (1%) at 1:40 dilution. The samples were immersed into the primary antibody-contained solution and incubated overnight at 4 °C. After being washed with PBS, the samples were then incubated with goat anti-mouse IgG secondary antibody conjugated with Alexa Fluor 594 secondary antibody (Life Technologies) at 1:500 dilution at RT for 1 hour. The cell nuclei were counterstained by DAPI solution at RT for 10 minutes. The stained samples were washed with PBS and observed by a fluorescence microscope (Olympus) or a confocal microscope (Zeiss LSM 510 Meta).

4.3.7 *In vivo* implantation of composite scaffolds

Animal experiment was approved by the Animal Experiments Committee of National Institute for Materials Science. The surgeries were carried out according to the committee guidelines. For *in vivo* implantation, the cells/scaffold constructs were prepared under the same condition as those used for *in vitro* cell culture. After 3 days of *in vitro* culture, every two same cells/scaffold constructs were stacked into one implant and subcutaneously implanted in the back of the 6-week-old athymic nude mice (Fig. 4.1). Every mouse was implanted with two implants. The mice were sacrificed to retrieve the implants after 8 weeks of implantation. Gross appearance of the harvested implants was observed with a light microscope (DP22, Olympus Corp.).

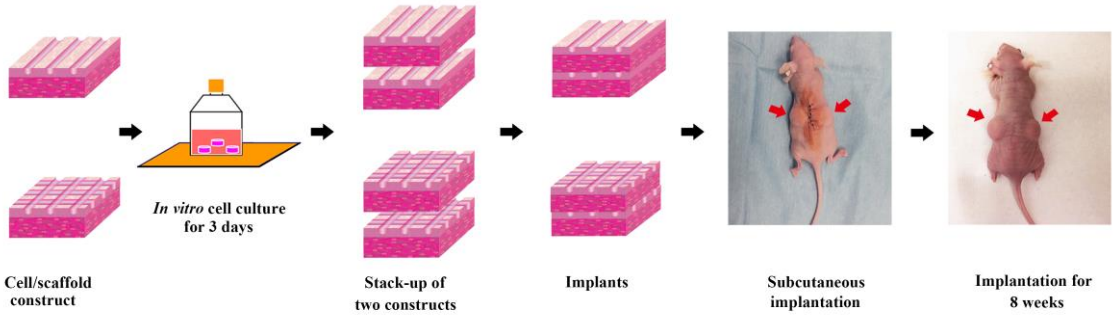

Fig. 4.1. A schematic of *in vitro* cell culture and *in vivo* implantation of the microgrooved DEX-BCP/Col composite scaffolds.

4.3.8 Histological and immunohistochemical evaluations of *in vivo* implants

The harvested implants were rinsed 3 times with PBS and fixed in neutral-buffered formalin solution (10%) at RT for 48 hours. The samples were then decalcified using decalcifying solution B (Wako Pure Chemical Industries, Ltd.) for 48 hours and dehydrated in serial dilutions of ethanol. The samples were then embedded in paraffin, cross-sectioned at thickness of 7 μm and deparaffinized. The cross-sections were stained with hematoxylin and eosin (H&E, MUTO Pure Chemicals CO., Ltd.) solution and observed under a light microscope.

The cross-sections were also immunohistochemically stained for von Willebrand factor (vWF), VEGF and osteocalcin (OCN). For staining of vWF and VEGF, the deparaffinized cross-sections were performed heat-mediated antigen retrieval with citrate buffer (pH 6.0) for 15 minutes. For staining of OCN, the deparaffinized cross-sections were incubated with proteinase K for antigen retrieval for 10 minutes. Then all

the cross-sections were incubated with peroxidase blocking solution 5 minutes and goat serum solution (10%) 30 minutes. Subsequently, the cross-sections were respectively incubated with primary antibodies of rabbit monoclonal anti-human von Willebrand factor (working concentration, 1: 100; Abcam), rabbit monoclonal anti-human VEGFA (prediluted; Abcam) and rabbit polyclonal anti-human osteocalcin (working concentration, 5 μg/mL; Abcam) for 2 hours. After washing with PBS for three times, the cross-sections were incubated with peroxidase-labeled polymer-conjugated secondary antibodies (Cytomation EnVision+, Dako) for 1 hour, followed by incubation with 3,3'-diaminobenzidine (DAB; Liquid DAB+ Substrate Chromogen System, Dako) for 10 minutes for color development. Hematoxylin was used to counterstain the nuclei. All procedures were carried out at RT. The stained samples were observed under a light microscope.

4.3.9 Evaluation of microvessel density (MVD)

Microvessel density (MVD) has been widely performed to evaluate angiogenesis level in tumor models and pathological specimens using endothelial cell markers such as vWF or CD34 [13]. Quantification of MVD was performed for the cross-sections after immunohistochemical staining of vWF. Photomicrographs at a magnification of 200× from 5 randomly selected regions of the stained cross-sections were used to calculate the microvessels in each of these regions using an Image-Pro Plus software (Media Cybernetics, Inc.). The brown-stained lumen-like structures were counted as individual microvessels. The data were then processed for statistical analysis. The average value from the 5 regions was regarded as the MVD level of each cross-section. 4 samples and every 4 cross-sections of each sample were used for the analysis.

4.3.10 PCR assay for *in vivo* implants

Expression of angiogenesis-related and osteogenesis-related genes encoding human-VEGF, KDR (a receptor of VEGF), bone morphogenetic protein-2 (BMP-2) and bone sialoprotein 2 (IBSP) was analyzed by real-time PCR (RT-PCR). After 8 weeks of implantation, the surrounding soft tissue of the harvested implants was cleaned. The implants were then rinsed 3 times with PBS and frozen in liquid nitrogen, followed by crushing into powder and dissolving in Sepasol solution (Nacalai Tesque, Inc.) to isolate RNA from the cells. A first stand cDNA synthesis kit (Applied Biosystems) was used to convert RNA to cDNA. The RT-PCR was performed on a 7500 Real-Time PCR system (Applied Biosystems) [14]. Expression of GAPDH was used as an endogenous standard. Relative gene expression was detected by using the formula $2^{-\Delta\Delta Ct}$. The gene expression of cells in the DEX-BCP-Col composite scaffold without microgrooves was used as a reference. Each experiment was carried out in quadruplicate. Primers and probes are listed in Table 4.1.

Table 4.1. The primers and probes for real-time PCR.

mRNA	Oligonucleotide
GAPDH	Hs99999905_m1
VEGF	Hs00900054_m1
KDR	Hs00911705_g1
IBSP	Forward 5'-TGCCTTGAGCCTGCTTCC-3' Reverse 5'-GCAAAATTAAAGCAGTCTTCATTTTG-3' Probe 5'-CTCCAGGACTGCCAGAGGAAGCAATCA-3'
BMP-2	Hs00154192_m1

4.3.11 Statistics analysis

All quantitative data expressed as the mean ± standard deviation (SD) were analyzed using Kyplot software (version 2.0 beta 15). One-way ANOVA statistical analysis was performed to evaluate the significance of the experimental data, followed by a Tukey's post hoc test for pairwise comparison. When the p-value was less than 0.05, the difference was considered as significant. The data were indicated by * $p < 0.05$, ** $p < 0.01$ and *** $p < 0.001$.

4.4 Results

4.4.1 Preparation and characterization of NPs and microgrooved composite scaffolds

DEX@BCP NPs were prepared by reacting DEX-contained $Ca(NO_3)_2 \cdot 4H_2O$ aqueous solution with $(NH_4)_2HPO_4$ aqueous solution. TEM observation showed the DEX-BCP NPs were short rod-like and had a dimension of 5-25 nm in width and 20-80 nm in length (Fig. 4.2a). The microgrooved DEX@BCP/Col composite scaffolds were manufactured by mixing DEX-BCP NPs, collagen aqueous solution and ice particulates and placing micropatterned templates on the top of the mixture. The constructs were freeze-dried and cross-linked to obtain the composite scaffolds. Parallel ice lines or ice network with different dimensions and intervals were used as templates to introduce the microgrooves into the scaffolds (Fig. 4.3a and c). The flat template without ice lines or ice network was used to prepare a control composite scaffold without microgrooves. Scaffolds with 5 types of microgrooves were prepared by using the respective templates (Fig. 4.3b and d).

SEM observation showed that the basal layers of the composite scaffolds were composed of porous DEX-BCP-Col composites and the top layers were composed of microgrooved collagen thin sheets. For basal layer of each scaffold, they all had abundant spherical large pores, most of which were interconnected by small pores (Fig. 4.3b and d, vertical; Fig. 4.2b and c). Dimension of the spherical large pores was almost equal to the dimension of the pre-prepared ice particulates used as a pore-forming agent. The small pores provided good interconnections among the large pores. The good interconnectivity should be beneficial for migration and spatial distribution of the cells. The surface of the large pores was rough and the DEX-BCP NPs were homogeneously embedded in the collagen matrices (Fig. 4.2d). The top layer had different types of microgrooves. The composite scaffolds had parallel microgrooves with a same concave width of 290 ± 21 μm and a different convex ridge width of 47 ± 8, 153 ± 15 and 352 ± 23 μm were designated as W1G1, W1G2 and W1G3, respectively. The composite scaffolds had parallel microgrooves with a concave width of 493 ± 30 μm and a convex ridge width of 357 ± 14 μm was designated as W2G3. The composite scaffolds had networked microgrooves with a concave width of 297 ± 17 μm and a convex ridge width of 346 ± 11 μm was designated as Network. The microgrooves in cross-sections showed a semicircular shape, which was replicated from the ice lines. The control scaffold that was designated as Flat had a relatively smooth top surface.

4.4.2 Cell adhesion and distribution in composite scaffolds

Cell adhesion in the Flat, W1G1, W1G2, W1G3, W2G3 and Network composite scaffolds after 1 day culture was investigated by SEM (Fig. 4.4a). The hMSCs well adhered on the spherical large pores of the

composite scaffolds. HUVECs well adhered on the convex ridges as well as the concave microgrooves of the microgrooved composite scaffolds. HUVECs randomly adhered on flat surface of the control composite scaffold. All the cells spread widely with many filopodia. The adhesion and morphology of the cells in the composite scaffolds indicated that the scaffolds supported cell adhesion and spreading. Assembly of HUVECs on the microgrooves of the composite scaffolds was observed by DAPI staining and immunofluorescent staining of human-CD 31 after *in vitro* culture for 3 days (Fig. 4.4b and c). HUVECs on the Flat composite scaffold showed a random distribution. For the microgrooved composite scaffolds, HUVECs distributed predominantly in the concave microgrooves and fewer cells were observed on the convex ridges. HUVECs assembled and formed cell bands along the direction of the microgrooves.

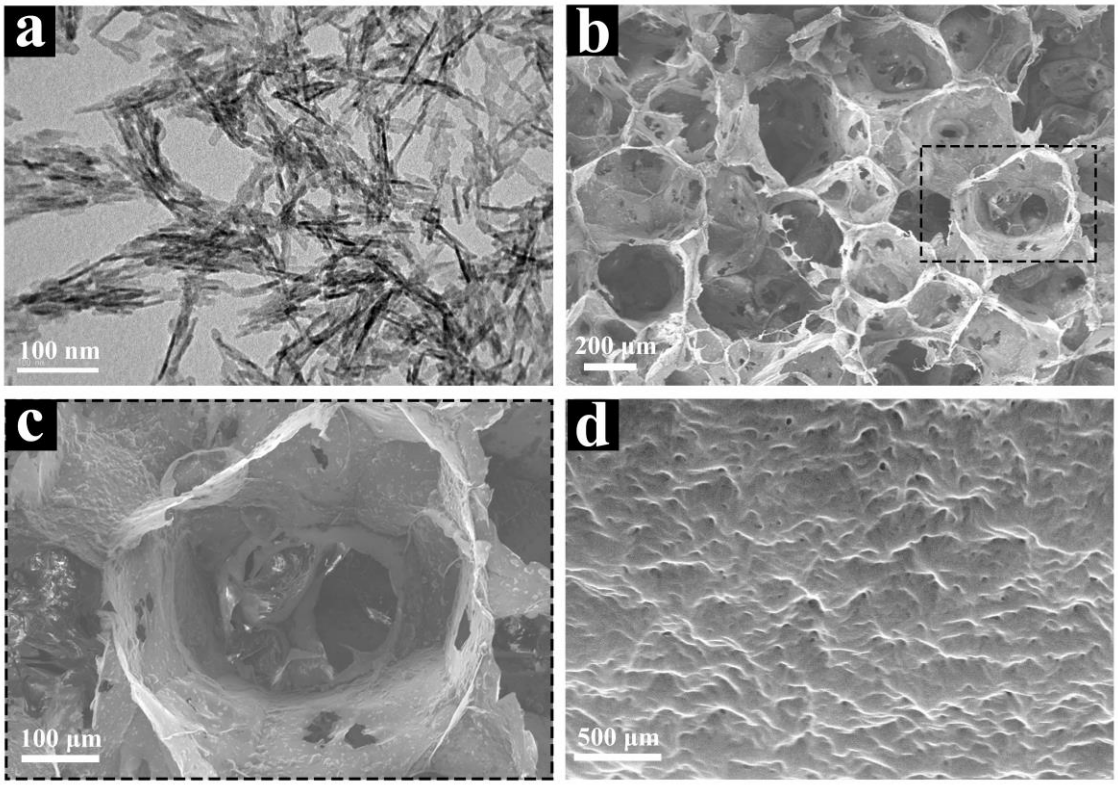

Fig. 4.2. Morphology of DEX-BCP NPs and microporous structure of DEX-BCP/Col composite scaffolds. (a) Morphology of the prepared DEX-BCP NPs. (b) and (c) SEM images of the cross-sections of the basal layer of W1G3 scaffold at low and high magnifications. (d) SEM image of the pore surface of W1G3 scaffold.

4.4.3 Gross appearance and histological analysis of *in vivo* implants

Every two same cells/scaffold constructs were stacked into one implant and subcutaneously implanted into dorsa of nude mice for 8 weeks. No obvious inflammation was observed during the implantation. Gross appearance of the implants is shown in Fig. 4.5a. The two stacked composite scaffolds were connected tightly with each other and no obvious malposition was found. There was no evident change of the shape for all the implants. All implants showed reddish color, which should be due to the formation of blood vessels within the scaffolds.

H&E staining showed uniform cell and matrix distribution throughout all the implants (Fig. 4.5b). After 8 weeks, the new blood vessels that were recognized by existence of lining endothelial cells and red blood

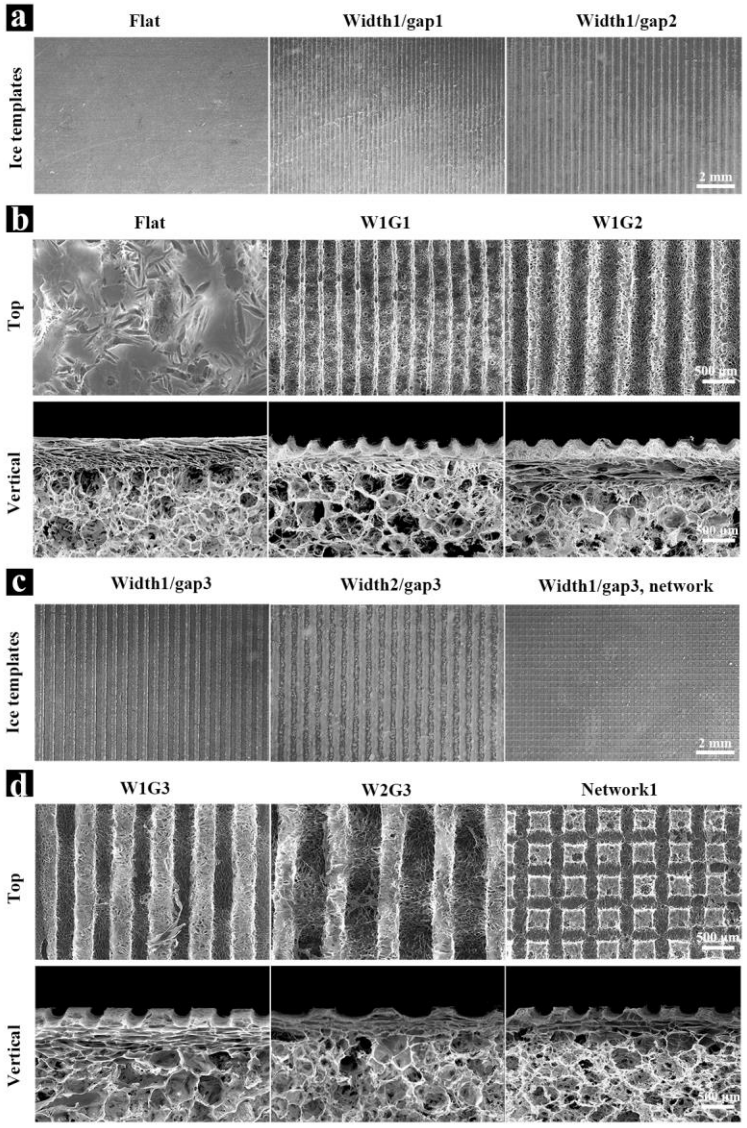

Fig. 4.3. Preparation of microgrooved DEX-BCP-Col composite scaffolds. (a) and (c) Images of ice line templates with different dimensions and intervals prepared from water dispensing. (b) and (d) SEM images of microgrooved DEX-BCP-Col composite scaffolds. Flat: control DEX-BCP-Col composite scaffold without microgrooves. W1G1, W1G2 and W1G3: DEX-BCP-Col composite scaffolds bearing parallel microgrooves with a same concave width of 290 ± 21 μm and a different convex ridge width of 47 ± 8, 153 ± 15 and 352 ± 23 μm. W2G3: DEX-BCP-Col composite scaffolds bearing parallel microgrooves with a concave width of 493 ± 30 μm and a convex ridge width of 357 ± 14 μm. Network: DEX-BCP-Col composite scaffold bearing cross network of microgrooves with a concave width of 297 ± 17 μm and a convex ridge width of 346 ± 11 μm. For (b) and (d), upper images show the top view and lower images show the vertical cross-sectional view of different scaffolds.

cells, were observed in all the groups (yellow triangles in Fig. 4.5b). The new blood vessels were observed through all the regions in the microgrooved scaffold implants, while they were observed only at the peripheral regions of the control scaffold. Among the 5 types of implants bearing microgrooves, angiogenesis appeared to be more evident in the W1G3 and Network scaffolds. At a high magnification, blood vessels with different sizes were observed (Fig. 4.6). Some of the blood vessels in the central regions of the implants were as large as 220 μm. Meanwhile, new bone formation was also observed in all the implants (green

triangles in Fig. 4.5b). The newly formed bone was only in peripheral regions of the Flat composite scaffold, while distributed in whole regions of the microgrooved composite scaffolds. In accordance with the degree of angiogenesis, the degree of osteogenesis appeared to be higher in the Network and W1G3 scaffolds than did in other scaffolds. When compared to the W1G3 scaffold, the angiogenesis level and area of newly formed bone in the Network scaffold were even higher (Fig. 4.5b, Fig. 4.11).

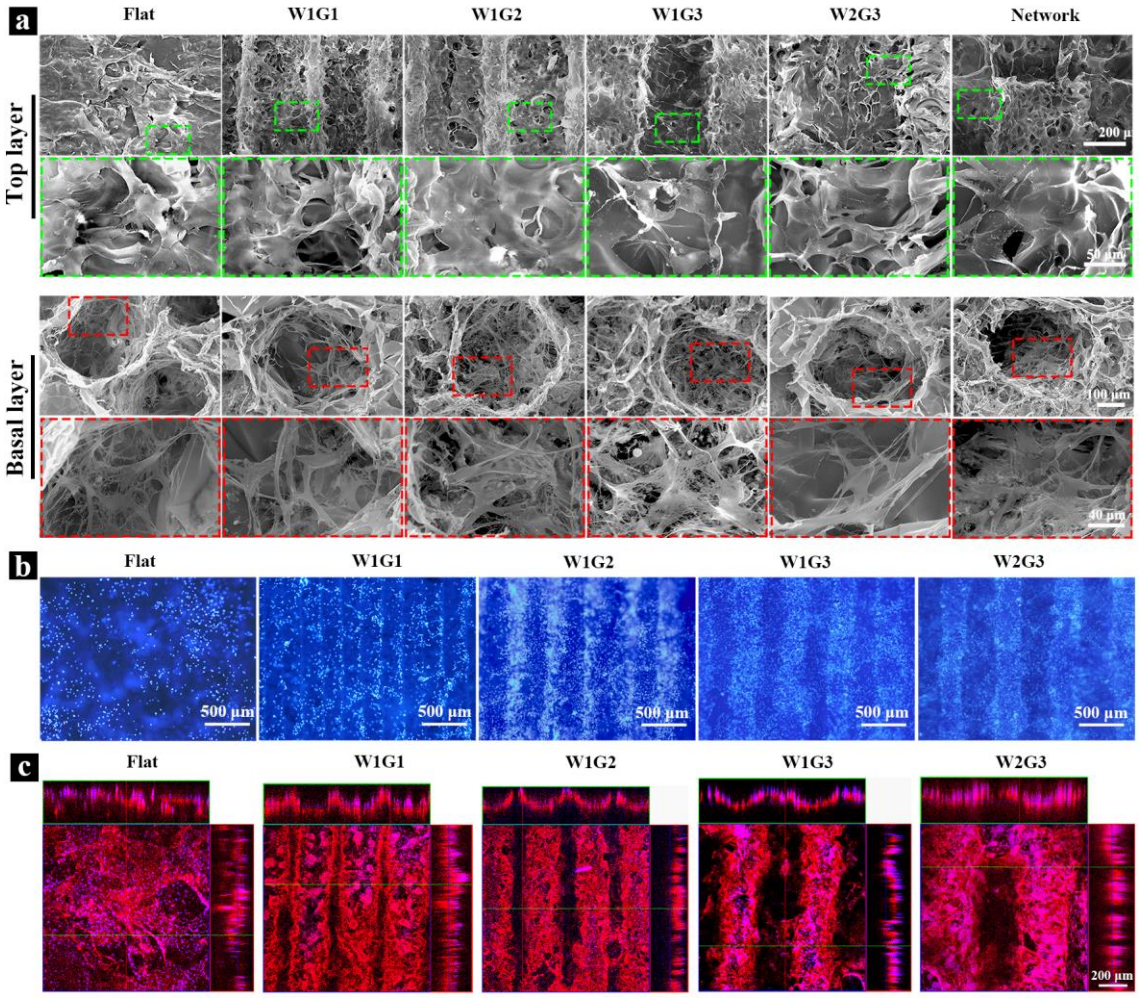

Fig. 4.4. Cell adhesion and distribution in the scaffolds. (a) SEM images of the composite scaffolds after 1 day *in vitro* culture. Cells in the top layer and basal layer of the scaffolds are shown at low and high magnifications. (b) Distribution of HUVECs after 3 days culture. Blue fluorescence: cell nuclei labelled by DAPI. (c) Assembly of HUVECs in the microgrooves after 3 days culture. Red fluorescence: HUVECs labelled by human-CD 31. Blue fluorescence: cell nuclei labelled by DAPI.

4.4.4 MVD of the implants

To further visualize the newly formed blood vessels within the implants, the histological sections of the implants were immunohistochemically stained with vWF, which is one kind of the endothelial cell markers (Fig. 4.7a). The brown-stained lumen-like structures were considered as individual vessels. The newly formed blood vessels were observed in both peripheral regions and central regions of the microgrooved scaffolds. However, they were only observed in the peripheral regions of the control scaffold. The MVD

within the implants was then quantified and the results demonstrated that the dimension of microgrooves influenced the density of the newly formed blood vessels (Fig. 4.7b). The MVD of W1G1, W1G2, W1G3 and Network scaffolds was significantly higher than that of Flat scaffold. For the 5 types of microgrooved composite scaffolds, angiogenesis degree was also different. The Network and W1G3 composite scaffolds showed higher level of MVD, suggesting the concave width and convex ridge width of W1G3 and Network scaffolds were most suitable for the assembly of HUVECs to promote regeneration of blood vessels.

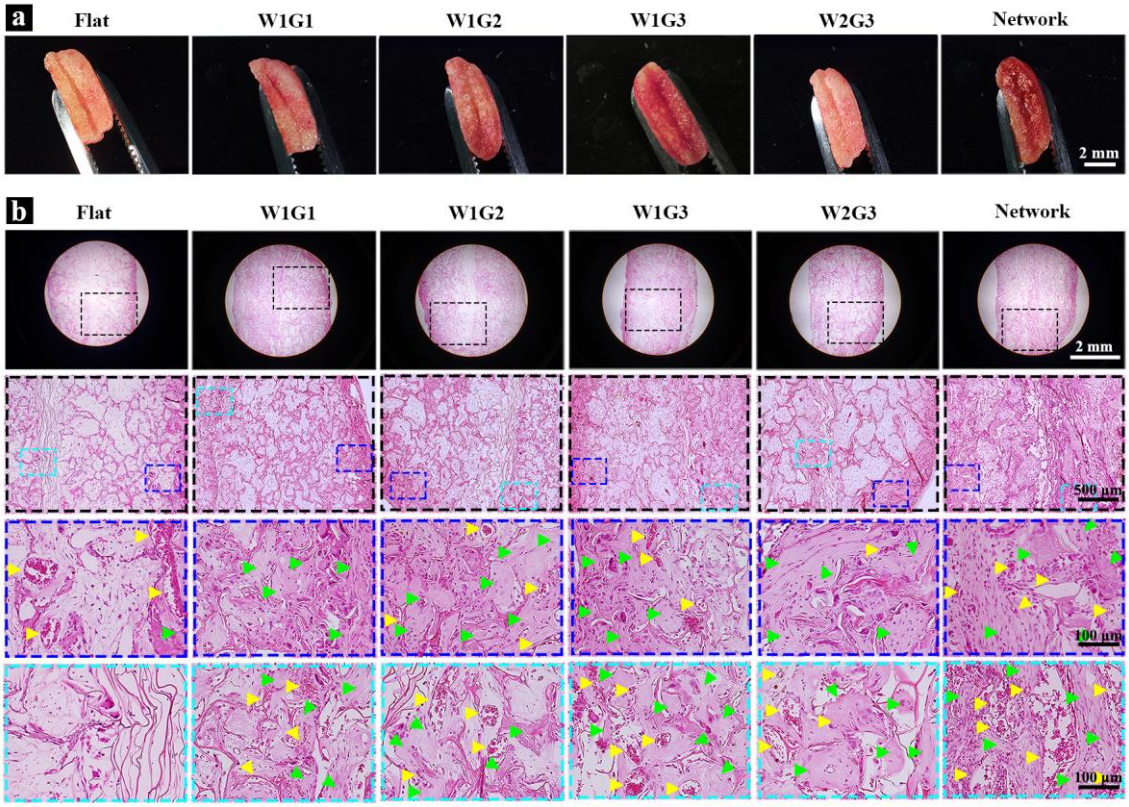

Fig. 4.5. Gross appearance and histological analysis of the implants. (a) Gross appearance of the implants after *in vivo* implantation for 8 weeks. (b) Photomicrographs of H&E staining of the decalcified cross-sections of the implants. The photomicrographs in the second line are the magnified ones of the first line. The photomicrographs in the third and fourth lines are the magnified ones at peripheral and central regions of the photomicrographs shown in the second line. Yellow triangles indicate new blood vessels. Green triangles indicate new bone formation.

4.4.5 Immunohistochemical staining of angiogenesis- and osteogenesis-related proteins

To detect the presence of angiogenesis- and osteogenesis-related proteins, immunohistochemical staining of VEGF and OCN was carried out for the implants. As a typical angiogenic growth factor, VEGF can induce the migration and proliferation of endothelial cells, leading to the formation of tubular structure [15]. The VEGF protein was detected in all the implants at different levels (Fig. 4.8). Expression of VEGF in the microgrooved scaffold implants was much higher than that in the Flat scaffold implant. VEGF showed the highest expression in the Network and W1G3 scaffolds. In comparison to the Flat scaffold, VEGF showed more homogeneous distribution pattern throughout all the regions of the microgrooved scaffolds. Expression of VEGF was most homogenous in the Network and W1G3 scaffolds. OCN is secreted

exclusively by osteoblasts and is involved in bone mineralization and calcium ion homeostasis [16]. OCN was also expressed in all the implants at different levels (Fig. 4.9). Expression of OCN was detected only at the very edge of the Flat scaffold, while was detected throughout the whole construct of all the microgrooved composite scaffolds. Especially, similar to the expression of VEGF, the expression of OCN was higher and more uniform in the Network and W1G3 scaffolds. The results of immunohistochemical staining of VEGF and OCN indicated that both angiogenesis and osteogenesis degree were up-regulated by the microgrooves in the composite scaffolds, among which the Network scaffold showed the highest angiogenesis and osteogenesis degree, followed with the second highest degree of W1G3 scaffold.

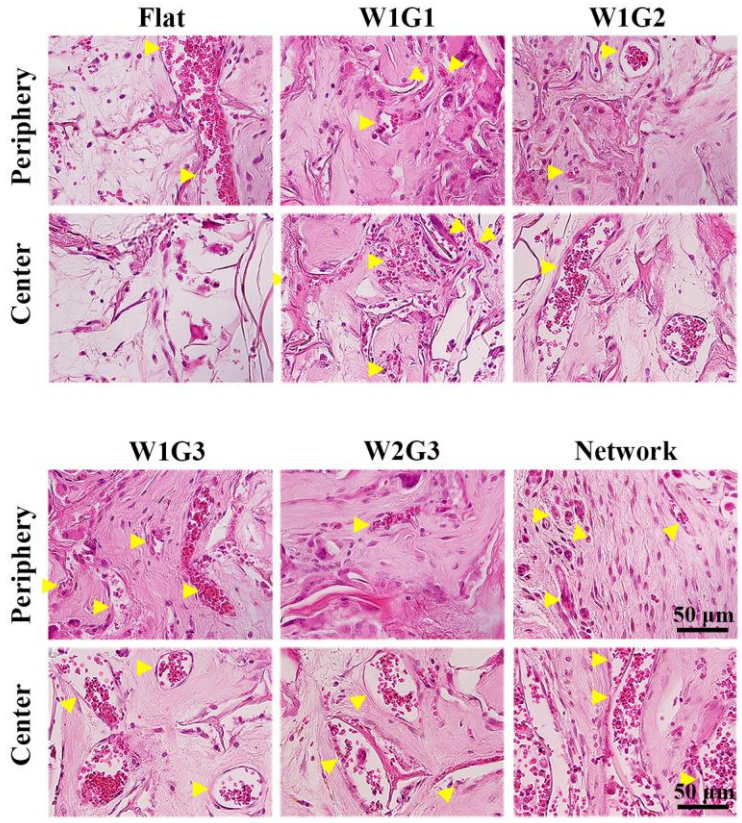

Fig. 4.6. Photomicrographs of H&E staining of the decalcified cross-sections of the 8 weeks implants at a high magnification of the peripheral and central regions. Yellow triangles indicate new formed blood vessels.

4.4.6 Expression of angiogenesis- and osteogenesis-related genes

Expression of angiogenic and osteogenic marker genes after *in vivo* implantation for 8 weeks was analyzed by RT-PCR (Fig. 4.10). Expression of VEGF was significantly up-regulated in all microgrooved scaffold implants in comparison with the Flat scaffold implant. Expression of KDR was significantly up-regulated by the Network scaffold. Expression of IBSP was significantly up-regulated by the W1G2, W1G3 and Network scaffolds. Expression of BMP-2 was significantly up-regulated by the W1G3 and Network scaffolds. For the 5 types of microgrooved scaffolds, up-regulation of the angiogenic and osteogenic genes were shown at different level, among which the Network scaffold showed the highest level and the W1G3 scaffold was the second highest.

4.5 Discussion

Bone defect is one of the most common diseases that threaten public health. In recent decades, instead of allografts and autografts, more and more studies have been focused on artificial bone substitutes with suitable biological properties for repair of large size bone defects. However, the current bone substitutes are facing with some challenges, among which the two most crucial issues are the deficiency of mature vascular networks within the bone substitutes to transport nutrients, oxygen and signal molecules for the rapid osteogenesis [17], and the sustained and prolonged release of valid osteogenic cues to promote and implement the long-term bone regeneration. In the present study, microgrooved DEX-BCP-Col composite scaffolds were prepared to overcome the two problems mentioned above. Compared to the Flat scaffold without microgrooves, the composite scaffolds bearing parallel microgrooves or microgroove network showed promoted effects on the angiogenesis and osteogenesis. The microgrooves together with released DEX, Ca^{2+} and PO_4^{3-} were beneficial for simultaneous angiogenesis and osteogenesis. Vascular endothelial cells (VECs) are polarized cells that have an apical surface that excludes adhesion to ECM proteins and a basal surface that adheres to the underlying basement membrane proteins [18]. The cell polarity can make VECs to assemble into capillary-like networks when they are cultured on ECM matrix such as collagen [19]. In the preset study, the microgrooves could induce the assembly of HUVECs along the microgrooves and therefore stimulate the regeneration of blood vessels. Regeneration of blood vessels could improve the supply of nutrients and removal of metabolic wastes and therefore promote migration, proliferation and osteogenic differentiation of hMSCs. The synergistic effects from microgrooves and released DEX, Ca^{2+} and PO_4^{3-} further promoted bone tissue regeneration after implantation.

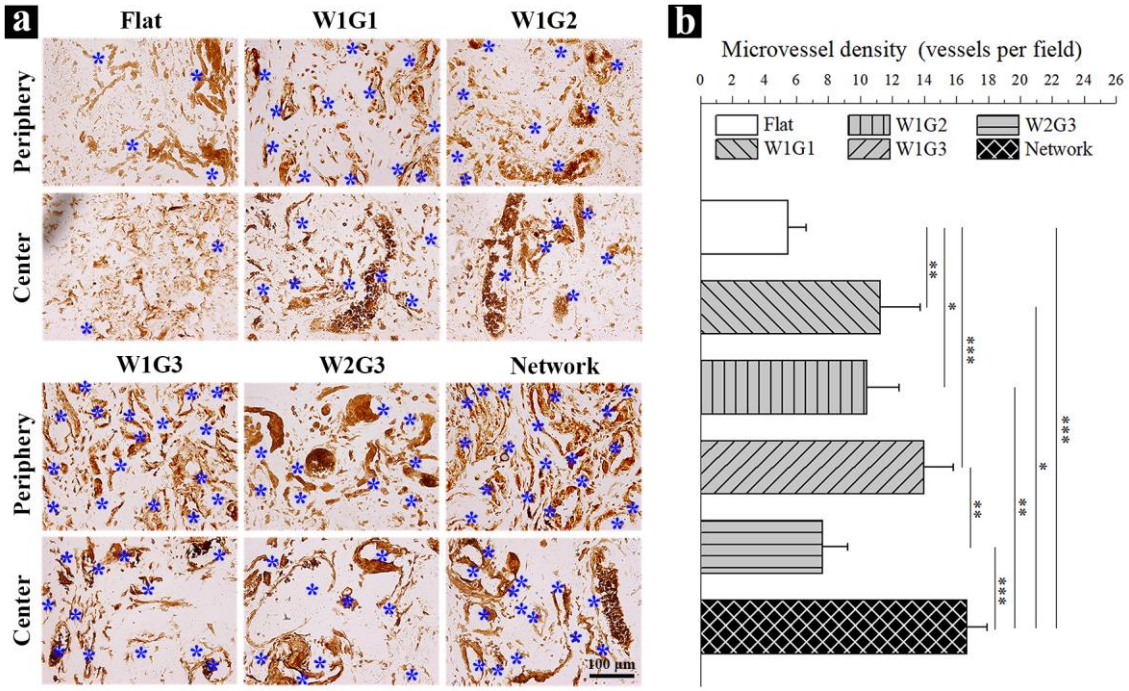

Fig. 4.7. Quantification of the newly formed blood vessels in the implants. (a) Immunohistochemical staining of vWF in the peripheral and central regions of the implants. The brown signals show the presence of vWF. (b) The microvessel density (MVD) within the implants. The MVD was quantified by using the cross-sections immunohistochemically stained for vWF. Data represent mean ± SD, N = 4. Significant difference: * $p < 0.05$; ** $p < 0.01$; *** $p < 0.001$.

To investigate the effect of microgroove structure on angiogenesis, microgrooves having different concave widths or convex ridge widths or cross network were designed and used for a comparison. At first,

the effect of microgroove convex ridge width was compared by keeping the concave widths of the microgrooves at the same level. The W1G1, W1G2 and W1G3 scaffolds bearing microgrooves of the same concave width (290 μm) but different convex ridge widths (47 ± 8, 153 ± 15 and 352 ± 23 μm) were prepared and used for 3D cell culture and implantation. HUVECs well adhered and assembled along the microgrooves in the W1G1, W1G2, and W1G3 scaffolds. The W1G3 scaffold had better promotion effect on the angiogenesis than did the W1G1 and W1G2 scaffolds. A wider convex ridge width (352 ± 23 μm) was better for angiogenesis. The convex ridge widths reflected the gaps between the microgrooves. The large gaps between the microgrooves (W1G3) could isolate the assembled cells in the microgrooves to facilitate formation of microtubular structures. On the other hand, the small gap (W1G1) could not maintain the integration of the assembled cells in the microgrooves and therefore might result in large cell sheets.

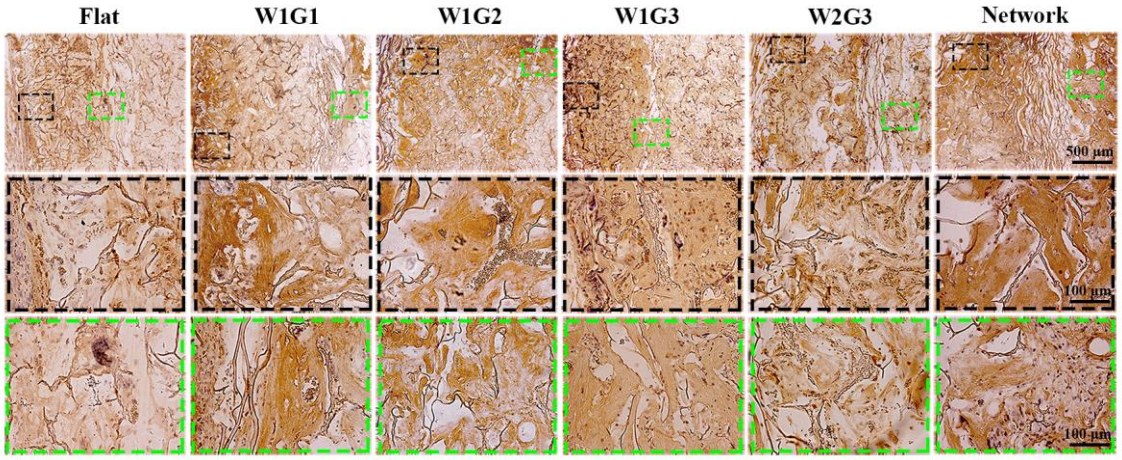

Fig. 4.8. Immunohistochemical staining of VEGF. The brown signals show the presence of VEGF in the cross-sections of the implants. The photomicrographs in the second and third lanes are the magnified ones at peripheral and central regions of the implants.

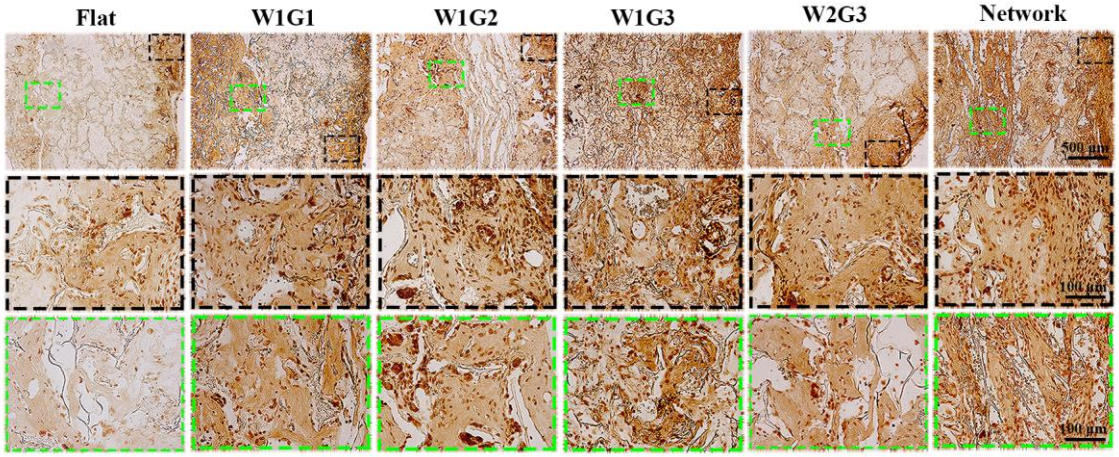

Fig. 4.9. Immunohistochemical staining of OCN. The brown signals show the presence of OCN in the cross-sections of the implants. The photomicrographs in the second and third lanes are the magnified ones at peripheral and central regions of the implants.

The effect of concave widths of the microgrooves was compared by changing the concave width from 290 ± 21 μm (W1G3) to 493 ± 30 μm (W2G3) while keeping the convex ridge width of microgrooves at the same level (W1G3: 352 ± 23 μm; W2G3: 357 ± 14 μm). W2G3 scaffold had lower promotion effect on

angiogenesis than did the W1G3 scaffold. Angiogenesis in W2G3 scaffold was even lower than that of W1G1 and W1G2 scaffolds. The results indicated that the concave width of the microgrooves had very evident effect on angiogenesis. The concave widths of the microgrooves reflected curvature of the semi-spherical microgrooves. Lower concave width resulted in larger curvature. It has been demonstrated that curvature could affect cell-cell interaction thus to play a role for tissue alignment [20]. High curvature is favorable for the formation of functional multicellular structures and large-scale highly organized and aligned tissues [21]. Concave microgrooves could guide the assembly of HUVECs in a contractile stress dependent manner [22]. Initially, upon HUVECs spreading on the microgrooves, they aligned along the main axis of the microgrooves. And then, the cells spread to contact the adjacent cells, formed cell-cell junctions and, due to the geometric constraints within them, exerted 3D traction forces along the direction of the microgrooves [23]. The cell-cell junctions between endothelial cells plays a critical role in transmitting contraction stresses [24] and generation of a mechanically balanced structure (i.e., bundles) [25]. The smaller width of the concave microgrooves hence the higher curvature in W1G3 scaffold could increase cell-cell interaction to strongly stimulate cell assembly along the long axis of the microgrooves to facilitate regeneration of blood vessels. The cross network of microgrooves in Network scaffold had the same concave width and convex ridge width as those of the W1G3 scaffold. The promotion effect on angiogenesis by Network scaffold was the highest among the 5 types of microgrooved scaffolds. The superiority of Network scaffold to W1G3 and the other scaffolds should be due to the microgroove network in Network that could provide more opportunity for the HUVECs to assemble to network structure for promotion of angiogenesis.

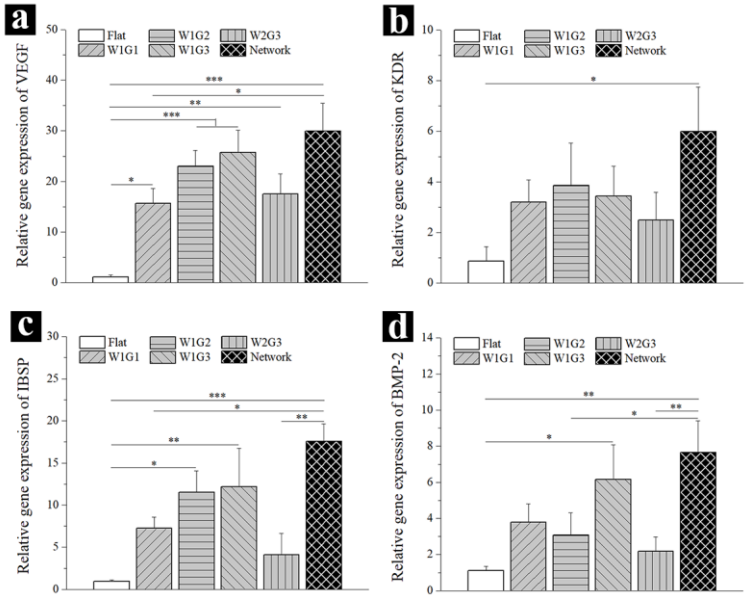

Fig. 4.10. Gene expression of human VEGF (a), KDR (b), IBSP (c) and BMP-2 (d) of the cells in the implants. Data represent mean ± SD, N = 4. Significant difference: * $p < 0.05$; ** $p < 0.01$; *** $p < 0.001$.

It has been widely established that angiogenesis can promote osteogenesis [26, 27]. The osteogenesis promotion effect of the microgrooved composite scaffolds and control scaffold was in a good accordance with their promotion effect on angiogenesis. The Network scaffold showed the best effect on angiogenesis and osteogenesis, followed by W1G3 scaffold. Besides the promotion effect from the microgrooves, release of DEX, Ca^{2+} and PO_4^{3-} from the composite scaffolds should also have stimulative effect on osteogenic differentiation of hMSCs and new bone tissue formation. Degradation of DEX-BCP NPs in the composite scaffolds resulted in the sustained release of DEX, Ca^{2+} and PO_4^{3-}, which could function synergistically to up-regulate the expression of osteogenic genes and proteins [11], leading to the osteogenic differentiation of

hMSCs and the final osteogenesis of the whole constructs. It's noticeable that the ultimately effective blood vessel formation and new bone regeneration in the composite scaffolds should be contributed to the close association and interaction between angiogenesis and osteogenesis. In one aspect, most osteogenic factors involved in osteogenesis, such as BMP-2, can stimulate angiogenesis either directly or indirectly, by generating angiogenic molecules such as VEGF, which is involved in angiogenesis [28]. On the other hand, VEGF stimulates osteoblast differentiation and inhibits osteoblast apoptosis [29]. Mutual promotion of angiogenesis and osteogenesis by the microgrooved DEX-BCP-Col composite scaffolds accomplished the rapid ectopic new bone formation.

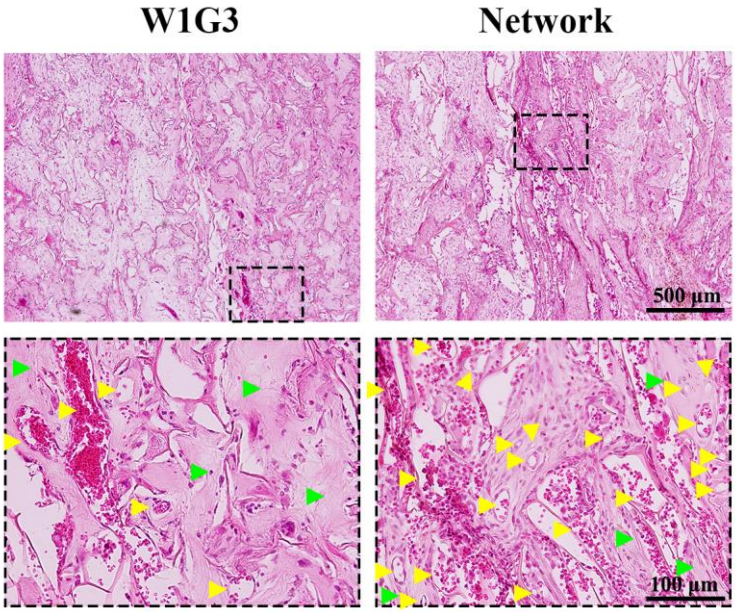

Fig. 4.11. Photomicrographs of H&E staining of the decalcified cross-sections of the W1G3 and Network implants after 8 weeks implantation at low and high magnifications. Yellow triangles indicate new blood vessels. Green triangles indicate new bone formation.

Although some approaches have been explored to enhance the angiogenesis and osteogenesis of the scaffolds for bone tissue engineering, the strategy declaimed in the present study exhibited obvious advantages. Currently, most of the scaffolds designed to control the cell orientation are prepared partially or completely from non-bioactive materials. Microgrooved substrates have been made from silicon [30], silicone rubber [31], titanium [32], quartz [33], acrylic [34], epoxy resin [35], polystyrene [36], and poly-lactic acid and its derivatives [37]. Whereas, in this study, the microgrooved scaffolds were prepared from a natural biological material, i.e., type I collagen. Collagen has many advantages such as high bioactivity, good integration of healing tissues, lowest immune and foreign-body responses, non-cytotoxicity and good biodegradation [38]. It can provide biological cues to regulate cell migration, proliferation and vascular morphogenesis of vascular endothelial cells [39]. Moreover, in our work, the pre-prepared ice lines were used as the templates to prepare the microgrooves. This method did not require conjugation of angiogenic factors and cell adhesion ligands within the scaffolds. The microfabrication technique was a simple and mild process without usage of any toxic solvent. In addition, the microgrooved DEX-BCP-Col composite scaffolds prepared in our work successfully integrated angiogenesis and osteogenesis in the 3D scaffolds, which should provide useful guide for design of the scaffolds for bone tissue engineering.

4.6 Conclusions

Four types of DEX-BCP-Col composite scaffolds bearing parallel microgrooves with different concave width and convex ridge width and one type of DEX-BCP-Col composite scaffold bearing microgroove cross network were prepared by using pre-fabricated ice lines as templates. The DEX-BCP-Col composite scaffolds were used for co-culture of HUVECs and hMSCs for simultaneous promotion of angiogenesis and osteogenesis. HUVECs well assembled along the microgrooves. Subcutaneous implantation in nude mice showed more angiogenesis and bone formation were observed in the microgrooved composite scaffolds than those in the control composite scaffold without microgrooves. The composite scaffolds bearing parallel microgrooves with a concave width of 290 μm and a convex ridge width of 352 μm had the highest promotion effect among the parallelly microgrooved composite scaffolds. The scaffold bearing microgroove cross network surpassed all parallelly microgrooved composite scaffolds. The results suggested that microgrooves in the composite scaffolds stimulated angiogenesis and osteogenesis. The microgrooved DEX-BCP-Col composite scaffolds should be useful for large bone tissue regeneration.

4.7 References

[1] Behzadi S, Luther GA, Harris MB, Farokhzad OC, Mahmoudi M. Nanomedicine for safe healing of bone trauma: Opportunities and challenges. Biomaterials 2017;146:168-82.

[2] Mitra D, Whitehead J, Yasui OW, Leach JK. Bioreactor culture duration of engineered constructs influences bone formation by mesenchymal stem cells. Biomaterials 2017;146:29-39.

[3] Liu WC, Chen S, Zheng L, Qin L. Angiogenesis Assays for the Evaluation of Angiogenic Properties of Orthopaedic Biomaterials–A General Review. Adv. Healthcare Mater. 2017.

[4] Mercado-Pagán ÁE, Stahl AM, Shanjani Y, Yang Y. Vascularization in bone tissue engineering constructs. Ann. Biomed. Eng. 2015;43:718-29.

[5] Novosel EC, Kleinhans C, Kluger PJ. Vascularization is the key challenge in tissue engineering. Adv. Drug Delivery Rev. 2011;63:300-11.

[6] Jain RK, Au P, Tam J, Duda DG, Fukumura D. Engineering vascularized tissue. Nat. Biotechnol. 2005;23:821-3.

[7] Phelps EA, García AJ. Engineering more than a cell: vascularization strategies in tissue engineering. Curr. Opin. Biotechnol. 2010;21:704-9.

[8] Perets A, Baruch Y, Weisbuch F, Shoshany G, Neufeld G, Cohen S. Enhancing the vascularization of three-dimensional porous alginate scaffolds by incorporating controlled release basic fibroblast growth factor microspheres. J. Biomed. Mater. Res., Part A 2003;65:489-97.

[9] Simmons CA, Alsberg E, Hsiong S, Kim WJ, Mooney DJ. Dual growth factor delivery and controlled scaffold degradation enhance in vivo bone formation by transplanted bone marrow stromal cells. Bone 2004;35:562-9.

[10] Vehof JW, Fisher JP, Dean D, van der Waerden JP, Spauwen PH, Mikos AG, Jansen JA. Bone formation in transforming growth factor β-1-coated porous poly (propylene fumarate) scaffolds. J. Biomed. Mater. Res., Part A 2002;60:241-51.

[11] Chen Y, Li J, Kawazoe N, Chen G. Preparation of dexamethasone-loaded calcium phosphate nanoparticles for the osteogenic differentiation of human mesenchymal stem cells. J. Mater. Chem. B 2017;5:6801-10.

[12] Zhang Q, Lu H, Kawazoe N, Chen G. Pore size effect of collagen scaffolds on cartilage regeneration. Acta Biomater 2014;10:2005-13.

[13] Bhatti SS, Kumar L, Dinda AK, Dawar R. Prognostic value of bone marrow angiogenesis in multiple

myeloma: use of light microscopy as well as computerized image analyzer in the assessment of microvessel density and total vascular area in multiple myeloma and its correlation with various clinical, histological, and laboratory parameters. Am. J. Hematol. 2006;81:649-56.
[14] Cai R, Nakamoto T, Kawazoe N, Chen G. Influence of stepwise chondrogenesis-mimicking 3D extracellular matrix on chondrogenic differentiation of mesenchymal stem cells. Biomaterials 2015;52:199-207.
[15] Chen Y, Wang J, Zhu X, Fan Y, Zhang X. Adsorption and release behaviors of vascular endothelial growth factor on porous hydroxyapatite ceramic under competitive conditions. J. Biomater. Tissue Eng. 2014;4:155-61.
[16] Lee NK, Sowa H, Hinoi E, Ferron M, Ahn JD, Confavreux C, Dacquin R, Mee PJ, McKee MD, Jung DY. Endocrine regulation of energy metabolism by the skeleton. Cell 2007;130:456-69.
[17] Levenberg S, Rouwkema J, Macdonald M, Garfein ES, Kohane DS, Darland DC, Marini R, Van Blitterswijk CA, Mulligan RC, D'Amore PA. Engineering vascularized skeletal muscle tissue. Nat. Biotechnol. 2005;23:879-84.
[18] Kramer RH. Extracellular matrix interactions with the apical surface of vascular endothelial cells. J. Cell Sci. 1985;76:1-16.
[19] Montesano R, Orci L, Vassalli P. In vitro rapid organization of endothelial cells into capillary-like networks is promoted by collagen matrices. J. Cell. Biol. 1983;97:1648-52.
[20] Sanz-Herrera JA, Moreo P, García-Aznar JM, Doblaré M. On the effect of substrate curvature on cell mechanics. Biomaterials 2009;30:6674-86.
[21] Hosseini V, Kollmannsberger P, Ahadian S, Ostrovidov S, Kaji H, Vogel V, Khademhosseini A. Fiber-Assisted Molding (FAM) of Surfaces with Tunable Curvature to Guide Cell Alignment and Complex Tissue Architecture. Small 2014;10:4851-7.
[22] Lehoux S, Tedgui A. Cellular mechanics and gene expression in blood vessels. J. Biomech. 2003;36:631-43.
[23] Krams R, Wentzel J, Oomen J, Vinke R, Schuurbiers J, De Feyter P, Serruys P, Slager C. Evaluation of endothelial shear stress and 3D geometry as factors determining the development of atherosclerosis and remodeling in human coronary arteries in vivo. Arterioscler., Thromb., Vasc. Biol. 1997;17:2061-5.
[24] Gjorevski N, Nelson CM. Endogenous patterns of mechanical stress are required for branching morphogenesis. Integr. Biol. 2010;2:424-34.
[25] Nikkhah M, Eshak N, Zorlutuna P, Annabi N, Castello M, Kim K, Dolatshahi-Pirouz A, Edalat F, Bae H, Yang Y. Directed endothelial cell morphogenesis in micropatterned gelatin methacrylate hydrogels. Biomaterials 2012;33:9009-18.
[26] Tsigkou O, Pomerantseva I, Spencer JA, Redondo PA, Hart AR, O'Doherty E, Lin Y, Friedrich CC, Daheron L, Lin CP. Engineered vascularized bone grafts. Proc. Natl. Acad. Sci. USA 2010;107:3311-6.
[27] Kusumbe AP, Ramasamy SK, Adams RH. Coupling of angiogenesis and osteogenesis by a specific vessel subtype in bone. Nature 2014;507:323-8.
[28] Carano RA, Filvaroff EH. Angiogenesis and bone repair. Drug discovery today 2003;8:980-9.
[29] Street J, Lenehan B. Vascular endothelial growth factor regulates osteoblast survival–evidence for an autocrine feedback mechanism. Journal of orthopaedic surgery and research 2009;4:19.
[30] Chen S, Chinnathambi S, Shi X, Osaka A, Zhu Y, Hanagata N. Fabrication of novel collagen-silica hybrid membranes with tailored biodegradation and strong cell contact guidance ability. J. Mater. Chem. 2012;22:21885-92.
[31] Lei Z-y, Liu T, Li W-j, Shi X-h, Fan D-l. Biofunctionalization of silicone rubber with

microgroove-patterned surface and carbon-ion implantation to enhance biocompatibility and reduce capsule formation. Int. J. Nanomed. 2016;11:5563.
[32] Lee M-H, Oh N, Lee S-W, Leesungbok R, Kim S-E, Yun Y-P, Kang J-H. Factors influencing osteoblast maturation on microgrooved titanium substrata. Biomaterials 2010;31:3804-15.
[33] Lee MH, Kang JH, Lee SW. The significance of differential expression of genes and proteins in human primary cells caused by microgrooved biomaterial substrata. Biomaterials 2012;33:3216-34.
[34] Shin SY, Han DH. Influence of a microgrooved collar design on soft and hard tissue healing of immediate implantation in fresh extraction sites in dogs. Clin Oral Implants Res 2010;21:804-14.
[35] Kuo C-C, Wang Y-J. Development of a micro-hot-embossing mold with high replication fidelity using surface modification. Mater. Manuf. Processes 2014;29:1101-10.
[36] Lamers E, Walboomers XF, Domanski M, te Riet J, van Delft FC, Luttge R, Winnubst LA, Gardeniers HJ, Jansen JA. The influence of nanoscale grooved substrates on osteoblast behavior and extracellular matrix deposition. Biomaterials 2010;31:3307-16.
[37] Chen Y, Wang J, Shen B, Chan CW, Wang C, Zhao Y, Chan HN, Tian Q, Chen Y, Yao C. Engineering a Freestanding Biomimetic Cardiac Patch Using Biodegradable Poly (lactic-co-glycolic acid)(PLGA) and Human Embryonic Stem Cell-derived Ventricular Cardiomyocytes (hESC-VCMs). Macromol. Biosci. 2015;15:426-36.
[38] Vernon RB, Gooden MD, Lara SL, Wight TN. Microgrooved fibrillar collagen membranes as scaffolds for cell support and alignment. Biomaterials 2005;26:3131-40.
[39] Whelan MC, Senger DR. Collagen I initiates endothelial cell morphogenesis by inducing actin polymerization through suppression of cyclic AMP and protein kinase A. J. Biol. Chem. 2003;278:327-34.

Chapter 5

Concluding remarks

The research focused on the development of dexamethasone-loaded biphasic calcium phosphate nanoparticles (DEX@BCP NPs) and their composite scaffolds with collagen and exploring their applications in bone tissue engineering. DEX was loaded in BCP NPs either during BCP formation or after BCP NPs formation. The optimized DEX@BCP NPs were hybridized with collagen sponges to prepare their composite scaffolds (DEX@BCP/Col). The composite scaffolds were used for culture of human bone marrow-derived MSCs (hMSCs) to investigate their effects on osteogenic differentiation of hMSCs and bone regeneration. To further enhance the osteogenesis and angiogenesis of the DEX@BCP/Col, microgrooved networks were introduced in the scaffolds. The microgrooved scaffolds were seeded with HUVECs and hMSCs then subcutaneously implanted in nude mice. The formation of the new bone and blood vessels within the scaffolds was checked after 8 weeks' implantation.

Chapter 1 introduces and summarizes the composition and function of natural bone and the commonly used methods for bone defect repair. Among all the methods, more emphasis is placed on the bone tissue engineering. The three fundamental principles for bone tissue engineering are then given, i.e., the scaffolds, the cells and the bioactive molecules. Afterwards, the up-to-date strategies used in bone tissue engineering are highlighted. Design and preparation of biomimetic multiple-functional scaffolds for bone tissue engineering is then motivated.

Chapter 2 summarizes the design and preparation of DEX-loaded BCP NPs. DEX-loaded BCP NPs were prepared by two methods: (1) immersion of BCP NPs in a DEX solution (defined as DEX/BCP NPs), (2) DEX incorporation during BCP NPs formation in a calcifying solution (defined as DEX@BCP NPs). The DEX@BCP NPs showed higher DEX loading amount and more sustainable DEX release than did the DEX/BCP NPs. The DEX@BCP NPs were used for culture of hMSCs and showed a promotive effect on proliferation of hMSCs. Furthermore, the DEX@BCP NPs significantly increased the alkaline phosphatase (ALP) activity, calcium deposition and gene expressions of osteogenic markers of hMSCs when compared to BCP NPs without DEX loading. The results demonstrated BCP NPs are a good carrier for DEX and the DEX@BCP NPs should have potential applications in bone tissue engineering.

Chapter 3 summaries the preparation of DEX@BCP NPs/collagen composite scaffolds and their effects on bone tissue engineering. The DEX@BCP NPs were introduced into the porous composite scaffolds of collagen. The obtained DEX@BCP NPs/collagen scaffold (DEX@BCP/Col) showed high mechanical strength, a controlled and sustained release nature of DEX, as well as a controlled pore structures resulting from using ice particulates as a porogen material. The composite scaffolds showed good biocompatibility and promoted osteogenic differentiation of hMSCs when used for three-dimensional culture of hMSCs. Subcutaneous implantation of the DEX@BCP/Col composite scaffolds at the dorsa of athymic nude mice demonstrated that the composite scaffolds facilitated ectopic bone tissue regeneration.

Chapter 4 summarizes the preparation and application of the DEX@BCP/Col composite scaffolds having several types of concave microgrooves to the scaffolds in aim of simultaneously enhancing angiogenesis and osteogenesis of the scaffolds. The microgrooves in the composite scaffolds were supposed to guide assembly of HUVECs into well aligned tubular structures, thus promoting rapid angiogenesis. The scaffolds were used for co-culture of HUVECs and hMSCs. Subcutaneous implantation in mice showed that more blood vessels and newly formed bone were observed in the microgrooved composite scaffolds than the control scaffold without microgrooves. The composite scaffolds bearing parallel microgrooves with a concave width of 290 μm and a convex ridge width of 352 μm had the highest promotion effect on angiogenesis and osteogenesis among the parallelly microgrooved composite scaffolds. The microgroove network had further superior effect than the parallel microgrooves. The results suggested that microgrooves in the composite scaffolds facilitated angiogenesis and stimulated new bone formation.

In summary, in the research the DEX@BCP NPs with a sustained release profile were prepared and their influence on osteogenic differentiation of the hMSCs was confirmed by in vitro culture of hMSCs. Then, the prepared DEX@BCP NPs were hybridized into porous collagen scaffolds and their potential for bone tissue engineering was investigated. The excellent pore structure, enhanced mechanical property of the DEX@BCP/Col composite scaffolds, as well as the sustained release of DEX from them synergistically facilitated the osteogenic differentiation of hMSCs and new bone tissue regeneration during in vitro culture and *in vivo* implantation. The DEX@BCP/Col composite scaffold with the highest DEX loading amount showed the most promising potential for bone tissue engineering. Afterwards, to further enhance the angiogenesis and osteogenesis, DEX@BCP/Col composite scaffolds with microgroove network were designed and prepared. The results suggest that microgrooves in the composite scaffolds facilitated angiogenesis and promoted new bone formation. The composite scaffolds with the microgroove network showed the highest effects. The DEX@BCP NPs/collagen porous composite scaffolds should be useful for three-dimensional culture of stem cells for osteogenic differentiation and bone tissue engineering.

List of publications

1. Ying Chen, Jingchao Li, Naoki Kawazoe and Guoping Chen. Preparation of dexamethasone-loaded calcium phosphate nanoparticles for the osteogenic differentiation of human mesenchymal stem cells. Journal of Materials Chemistry B 5, 33 (2017): 6801-6810.

2. Ying Chen, Naoki Kawazoe and Guoping Chen. Preparation of dexamethasone-loaded biphasic calcium phosphate nanoparticles/collagen porous composite scaffolds for bone tissue engineering. Acta. Biomaterialia. In press.

3. Ying Chen, Naoki Kawazoe and Guoping Chen. Promoted Angiogenesis and Osteogenesis by Dexamethasone-loaded Calcium Phosphate Nanoparticles/Collagen Composite Scaffolds with Microgroove Network. Under review.

4. Jingchao Li, Ying Chen, Naoki Kawazoe and Guoping Chen. Ligand density-dependent influence of arginine–glycine–aspartate functionalized gold nanoparticles on osteogenic and adipogenic differentiation of mesenchymal stem cells. Nano Research: 1-15.

5. Xiaomeng Li, Ying Chen, Naoki Kawazoe and Guoping Chen. Influence of microporous gelatin hydrogels on chondrocyte functions. Journal of Materials Chemistry B 2017, 5, 5753-5762.

6. Jingchao Li, Ying Chen, Naoki Kawazoe and Guoping Chen. Sub-10 nm gold nanoparticles promote adipogenesis and inhibit osteogenesis of mesenchymal stem cells. Journal of Materials Chemistry B, 5(7), 1353-1362.

7. Jingchao Li, Jing Zhang, Ying Chen, Naoki Kawazoe and Guoping Chen. TEMPO Conjugated Gold Nanoparticles for Reactive Oxygen Species Scavenging and Regulation of Stem Cell Differentiation. ACS Applied Materials & Interfaces, 2017, 9 (41), pp 35683–35692.

Acknowledgements

First and foremost, I would like to express my sincerely gratitude to my supervisor, Professor Guoping Chen, for his continuous kind guidance and help during the last three years of my PhD course. Professor Chen helped me choose the research topics, solve the problems occurring in my experiments and revise my publications and dissertation very carefully. Professor Chen also helped me with my job hunting, during which he gave me many useful suggestions and a kind recommendation. With a far-sighted vision and a rigorous attitude to do research, he set up a gorgeous model for me and all the students. His advice and spirit in scientific research will continue guiding me in my future career and life. It is my great honor to have the chance to be a PhD student of Professor Chen and do research in Professor Chen's group.

Special thanks also should be given to Dr. Naoki Kawazoe, for his kind help and warm encouragement during my research. We have had many discussions about my research during the three years, from which I really learned a lot. His wide scope of knowledge, modest character and optimistic attitude impressed me very well. It is a great pleasure to work with and learn from him.

I really appreciate the valuable suggestion and assistance from Dr. Hongxu Lu, Dr. Qin Zhang, Dr. Rong Cai, Dr. Shangwu Chen, Dr. Jingchao Li and Mrs. Akemi Tateno, Mrs. Fusako Hidaka and Mrs. Akiyama Haruyo. Dr. Hongxu Lu, Dr. Qing Zhang, Dr. Rong Cai, Dr. Shangwu Chen and Dr. Jingchao Li gave me many advices on my research and taught me many skills on my experiments. Mrs. Akemi Tateno, Mrs. Fusako Hidaka and Mrs. Akiyama Haruyo helped me a lot for the matters and procedures involved in University of Tsukuba and NIMS. Moreover, I would like to give my thanks to all my colleagues in Tissue Regeneration Materials Unit for their cooperation in managing of our lab and the supporting of my daily life. They are Dr. Ida Dulinska Molak, Dr. Jasmine Lee, Dr. Jianming Yang, Professor Gang Wu, Dr. Shujun Dong, Dr. Xinlong Wang, Dr. Xiaohong Hu, Dr. Jing Zhang, Dr. Xiaomeng Li, Ms. Xiuhui Wang, Mr. Yingjun Yang, Mr. Yazhou Chen, Mr. Kubybee Lee and Ms. Nur Rofiqoh Eviana Putri.

Beside my supervisor, I would like to give my sincere thanks to the rest of my thesis committee, Professor Yukio Nagasaki, Professor Mitsuhiro Ebara and Professor Tetsushi Taguchi, for their insightful comments, encouragement and kind suggestions during my PhD defense.

I would like to give my most sincere thanks to my father Guo Chen, my mother Xiangyuan Wu, my father-in-law Bangjun Huang, my mother-in-law Enxiang Tian, my husband Zhao Huang and my younger sister Yu Chen, as well as all the friends who have been supporting, encouraging and helping me during my three-year PhD course.

This work was performed at Tissue Regeneration Materials Unit, National Institute for Materials Science and Graduate School of Pure and Applied Science of University of Tsukuba. I appreciate the financial support from NIMS (Junior Research Assistantship) during my 3-year research in NIMS.